Lactoferrin against Inflammatory and Iron Disorders in Different Infection Models

XXXIII Ciclo del Dottorato di Ricerca in Malattie Infettive, Microbiologia e Sanità Pubblica

Dottorando
Luigi Rosa

Relatore
Prof.ssa Maria Pia Conte

Correlatore
Prof.ssa Piera Valenti

SAPIENZA
UNIVERSITÀ DI ROMA

INDEX

1. Introduction

In biology, the term homeostasis is the state of steady internal, physical, and chemical conditions maintained by living systems. This is the condition of optimal functioning for the organism and includes many molecular mechanisms that orchestrate the healthy condition.

Here, I present the role of lactoferrin, an iron-binding multifunctional cationic glycoprotein of the host innate immune defense, as a regulator of iron and inflammatory homeostasis in different infection models.

1.1 Iron homeostasis

In all living cells, iron is necessary for pivotal metabolic processes such as energy production, DNA synthesis/repair/transcription, oxygen transport/storage and drug detoxification. These biological processes rely on iron's ability to accept/donate electrons by redox-fluctuation between divalent ferrous (Fe^{2+}) and trivalent ferric (Fe^{3+}) ions, which in intracellular habitat constitute the iron pool (IP). Of note, Fe^{3+} is less soluble than Fe^{2+} and the precise cytosolic quantization of Fe^{3+} with respect to Fe^{2+} (Fe^{3+}/Fe^{2+} ratio) is still unknown [Ma et al. 2015]. However, free available not bound-Fe^{3+} is very reactive and potentially toxic due to the induction of reactive oxygen species (ROS) formation via the Fenton and Haber-Weiss reactions [Andrews 2000]. ROS formation, causative of damages to lipids, nucleic acids and proteins, is involved in the cell, tissue and organ oxidative stress. The injury by ROS leads to the activation of acute or chronic inflammatory processes implicated in multiple degenerative clinical conditions including the development of cancer, obesity, diabetes and aging. Inflammation is a defensive mechanism addressed to eradicate unsafe stimuli, thus contributing to the repair of damaged cells or tissues. In particular, acute inflammation occurs promptly after the injury and it is characterized by local vasodilatation and increased vessel permeability to ameliorate molecules and cells delivery to help damaged parenchyma repair. However, acute inflammation can converge into the chronic state if the injury persists or the individual's immune system is impaired. Differently, chronic inflammation involves the cycling of destructing and healing processes in tissues suffering from persistent and recurring damages.

To counteract iron chemical reactivity, all organisms have evolved highly specialized systems to bind and transport the metal avoiding the formation of either ROS or insoluble precipitates due to free available iron [Valenti and Antonini 2005]. Moreover, several enzymes belonging to oxidases and reductases family control iron oxidative state [Bonaccorsi di Patti et al. 2018].

Systemic iron homeostasis, the control of iron balance throughout the body, requires mechanisms for regulating iron entry into and mobilization from stores, for meeting erythropoietic needs, and for

scavenging previously used iron. As there is no efficient pathway for iron excretion, intestinal absorption must be modulated to provide enough (but not too much) iron to keep stores replete and erythroid demands met. There must be effective communication between cells that consume iron (primarily erythroid precursors) and cells that acquire and store iron (duodenal enterocytes, hepatocytes, tissue macrophages) [Hentze et al. 2004]. Transfer between tissues must be orchestrated to maintain homeostasis (Figure 1).

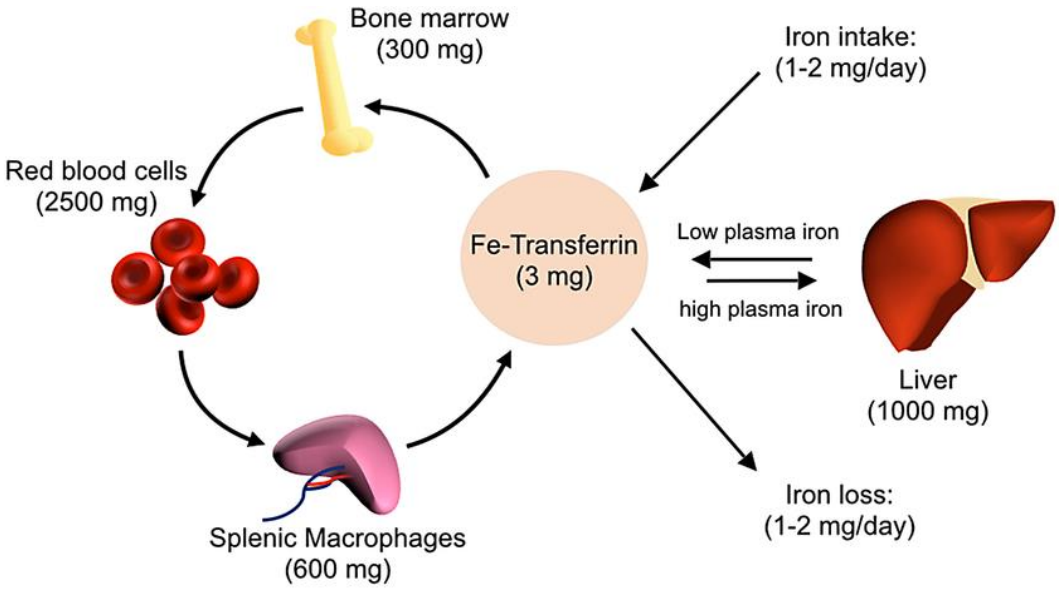

Figure 1. Overview of host iron homeostasis. Since there is no specific excretory system for iron in mammals, the correct balance of this metal between tissues/secretions and blood is mainly regulated by two different pathways: dietary iron absorption from the enterocytes (1–2 mg) and iron recycling from the lysis of senescent erythrocytes by macrophages (about 20 mg/day). Iron is absorbed from the diet by duodenal enterocytes and transported into the bloodstream, where it is bound by transferrin. Most iron is incorporated into erythrocytes for heme synthesis. Splenic macrophages recover iron from senescent erythrocytes and release iron into circulation via ferroportin. Smaller amounts of iron are imported into other tissues as needed. Iron loss is not directly regulated and occurs through minor bleeding and shedding of duodenal enterocytes. Approximate iron content of adult human tissues is represented in parentheses. The Figure was taken from Michels et al. [2015].

Enterocyte iron absorption is primarily carried out through an apical reductase, the duodenal cytochrome b (DCYTB). The resulting ferrous iron is internalized by apical divalent metal transporter 1 (DMT1). In the cytoplasm, ferrous ions belonging to IP are sequestered by ferritin (Ftn). Ftn, the major iron storage protein, composed by 24 subunits, possesses ferroxidase activity and a large cavity where up to 4,500 ferric ions, as oxy-hydroxide micelles, are sequestered. According to the body's request, iron is newly reduced inside Ftn and ferrous ions are exported. On the basolateral side of enterocytes, ferroportin (Fpn), the sole protein able to export iron from cells to blood, found also in macrophages, hepatocytes and placental cells [Donovan et al. 2005], releases Fe^{2+} to hephaestin (Heph), which, in turn, oxidizes iron to allow Fe^{3+} binding to transferrin (Tf) in the blood. Tf is a glycoprotein able to bind two ferric ions per molecule. Iron transport from blood

to cells occurs through the binding between Fe-Tf and its receptor 1 (TfR1), leading to endosome formation. Of note, when Tf saturations exceed 75%, specialized cells, including macrophages and hepatocytes, can uptake iron by non-Tf-bound iron (NTBI), hemoglobin, and heme. NTBI is acquired by the cells via ZRT/IRT-like protein-14 (ZIP14), a transmembrane metal-ion transporter originally identified as a zinc transporter, but subsequently also defined as an iron transporter [Liuzzi et al. 2006].

In the acidified endosome, iron is released from Tf and translocated, after the reduction by six-transmembrane epithelial antigen of the prostate 3 (STEAP3), via DMT1 into the cytoplasm where it can be utilized for cell metabolism [Brissot et al. 2019] or sequestered by Ftn. In circulating macrophages, the iron import also occurs through the binding between Fe-Tf and TfR1. Inside the macrophages, iron, deriving from both Tf-mediated import and lysis of senescent erythrocytes, is sequestered by Ftn and then, according to the request, exported by Fpn acting in partnership with ceruloplasmin (Cp), another ferroxidase similar to Heph [Bonaccorsi di Patti et al. 2018]. Of note, ferroxidase activity by Cp has been demonstrated to be crucial for the stabilization of Fpn on the plasma membrane [Bonaccorsi di Patti et al. 2018]. In fact, some pathological conditions, characterized by the absence of Cp activity (i.e., aceruloplasminemia), show a prominent induction of Fpn internalization and degradation, with consequent accumulation of intracellular iron and promotion of ROS production [Kono et al. 2010; Persichini et al. 2012; Bonaccorsi di Patti et al. 2018].

The main regulator of iron homeostasis is hepcidin, a 25 amino acid cationic peptide hormone, found in plasma [Krause et al. 2000] and urine [Park et al. 2001; Hunter et al. 2002]. The bioactive hepcidin, a cationic peptide hormone of 25 amino acids mainly synthesized by hepatocytes, derives from the proteolytic cleavage of an 84-amino acid precursor. Hepcidin is controlled by several factors. In particular, it is transcriptionally feedback-regulated by iron stores [Coffey and Ganz 2017]. This mechanism involves multiple pathways through which hepatocytes directly sense systemic iron levels [Zumerle et al. 2014; Coffey and Ganz 2017]. Hepcidin synthesis is involved in the internalization and degradation of Fpn [Qiao et al. 2012]. Consequently, high hepcidin levels, hindering iron export by Fpn, lead to intracellular iron overload as well as to a decrease of the iron import systems as Dcytb, DMT1 and TfR1 [Fisher and Nemeth 2007]. Conversely, hepcidin low levels, unable to trigger Fpn degradation, restore iron export and import [Ganz 2018; Casu et al. 2018] A schematic representation of iron uptake, cycling and distribution within the body is reported in Figure 2.

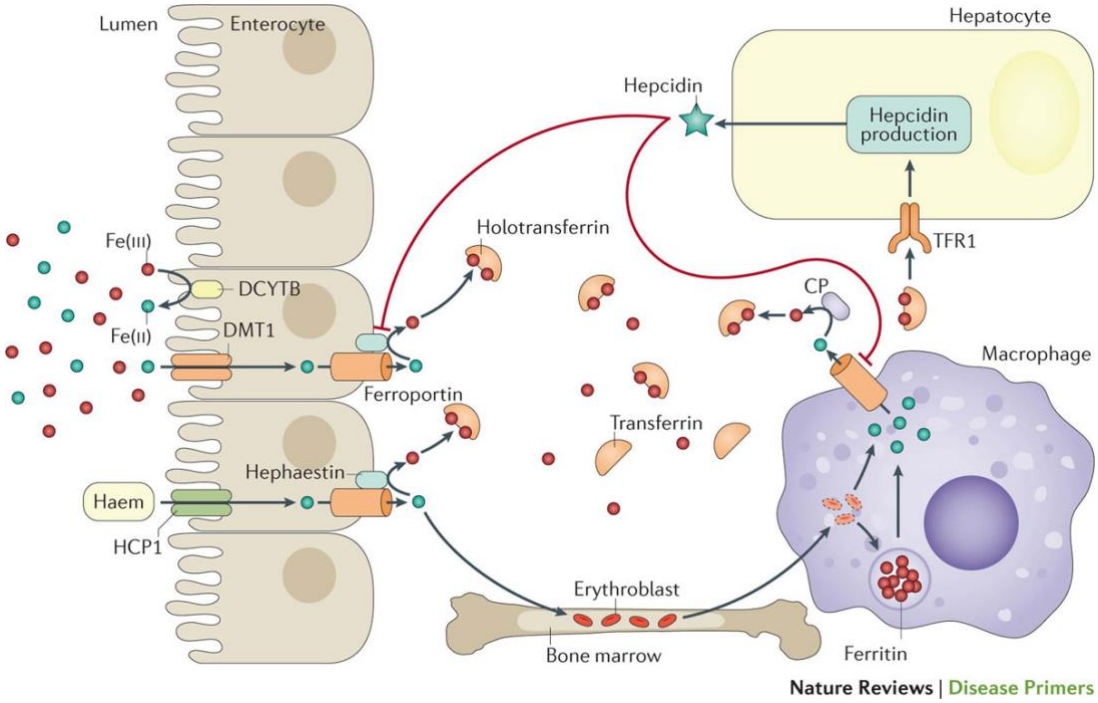

Figure 2. Iron uptake, cycling and distribution within the body. The main sources of plasma iron are enterocytes and macrophages. Non-hem iron is absorbed through divalent metal transporter 1 (DMT1), which is found on the apical surface of enterocytes after conversion of iron from its ferric to its ferrous form by a reduction process that can involve the duodenal cytochrome b reductase 1 (Dcytb). The mechanism of hem iron uptake by enterocytes is not fully elucidated. By contrast, macrophages acquire iron from erythrophagocytosis (whereby erythrocytes are degraded and the contained iron is recycled). Iron is released from enterocytes and macrophages into plasma through ferroportin. Iron is then oxidized by ceruloplasmin (Cp) which circulates in plasma and hephaestin which is anchored to enterocytes and binds to transferrin (to form holo-transferrin). Cp has a role in the control of iron export from reticuloendothelial cells, and both hephaestin and CP might have a role in cell iron metabolism in other tissues. Holo-transferrin delivers iron to every cell type, although erythroblasts (immature erythrocytes) are the main consumers. Holo-transferrin levels are also sensed by hepatocytes that take up iron through transferrin receptor 1 (TfR1). In response to high levels of holo-transferrin, hepcidin — which induces the degradation of ferroportin — is secreted into plasma to control the iron export. The Figure was taken from Brissot et al. [2018].

In inflammatory status where high levels of pro-inflammatory cytokines, as interleukin (IL)-1α, IL-1β and IL-6 are detected, iron export is significantly impaired by hepcidin up-expression [Nemeth and Ganz 2014; Coffey and Ganz 2017] and Fpn down-regulation [Cutone et al. 2014; Cutone et al. 2017]. However, it cannot be excluded that the down-regulation of Fpn might be mediated by IL-6 also in a hepcidin-independent way [Weinstein et al. 2002; Ludwiczek et al. 2003] as demonstrated in beta-thalassemic pregnant and non-pregnant women [Lepanto et al. 2018].

Overall, iron homeostasis disorders are so closely connected to inflammatory disorders, that it is difficult to distinguish which is the cause and which is the effect. Inflammation arises in the absence of infection as a natural response following tissue's damage or excessive cell death [McDonald et al. 2010]. In addition, inflammation can take place in the presence of the infection, where high levels of free available iron favor bacterial and viral growth thus causing severity of infection. As

matter of fact, iron is also essential for the life and multiplication of pathogenic microorganisms except for some commensal bacteria as *Lactobacillus* is able to grow without this metal.

The tissue injuries unrelated or related to infections generate a strong immune response resulting in the release of pro-inflammatory bioactive compounds leading to the consequent development of systemic diseases such as systemic inflammatory response syndrome or sepsis. The cytokines and chemokines are the primary immune-mediators depending on the recruitment of neutrophils, macrophages and dendritic cells, while secondary mediators, as complement system, are activated consequently. Several connections among immune cells, primary and secondary mediators defend host against systemic infections or pathological destructive inflammation thus supporting damaged tissue repair [Kruzel et al. 2017]. In the subsequent paragraphs, I highlight the iron and inflammatory homeostasis disorders unrelated or related to infections.

1.2 Iron and inflammatory homeostasis disorders unrelated to infections

During inflammatory process unrelated to infections, also called aseptic inflammation, the Fpn down-regulation caused by IL-6 or its degradation caused by the binding with hepcidin provokes a significant decrease of iron export from cells into plasma. Consequently, at the cellular level, iron overload in the host cells including enterocytes and macrophages is established, while at the systemic level, iron deficiency (ID), ID anemia (IDA) and anemia of inflammation (AI) have been found [Frazer and Anderson 2003; Miller 2012]. ID, IDA and AI are the most widespread iron disorders with over 30% of the world's population affected by anemia, with the cause of anemia primarily due to iron deficiency [Miller 2012]. In ID without anemia, total serum iron (TSI) concentration and serum Ftn (sFtn) are very low, while hemoglobin (Hb) levels remain normal. ID may be classified according to sFtn and TSI concentrations (<24 ng/mL and <30 mg/dL, respectively) as mild (sFtn = 12–24 ng/mL) or severe ID (sFtn <12 ng/mL). In IDA, the iron stores are low or absent, resulting in severe low Hb and red blood cell (RBC) levels. IDA is usually classified in line with the number of RBCs ($<4\times10^6$ cells/mL) and Hb concentration (<11 g/dL,) as mild (Hb 7–10.9 g/dL) or severe IDA (Hb <7 g/dL). In AI, in addition to the low hematological parameters, normal-to-elevated sFtn and high levels of IL-6 and other pro-inflammatory cytokines are observed. The most common intervention programs for ID and IDA are based on the classical preconception that oral iron administration or the consumption of iron-rich foods increases hematological parameters, thus reducing the prevalence of anemia. However, although most of these programs designed by governments and international agencies are easy to perform at low cost, they are ineffective in preventing and curing ID and IDA. Several studies highlighted how ferrous iron supplementation often fails to restore iron homeostasis disorders in patients suffering from ID and IDA, causing frequent adverse effects, such as gastrointestinal discomfort, nausea, vomiting,

diarrhea and constipation [Paesano et al. 2006; Palacios 2011; Rizvi and Schoen 2011; Ortiz et al. 2012; Zaim et al. 2012; Lepanto et al. 2018]. Moreover, in vivo studies in rats fed with an iron-enriched diet showed a higher production of ROS [Kadiiska et al. 1995] and a more severe progression of the colitis inflammatory status [Reifen et al. 2000]. AI, the most severe iron homeostasis disorder, is difficult to prevent and cure because it is associated with high levels of IL-6, which in turn induce the deregulation of the main proteins involved in iron homeostasis: hepcidin, Fpn, Tf, TfRs, Cp and Heph [De Domenico et al. 2008]. Therefore AI, characterized by hypoferremia in the blood despite suitable iron stores [Nemeth and Ganz 2006], is very difficult to cure in the absence of a contemporary decreasing of serum IL-6 levels. Since AI is a secondary manifestation of inflammatory disorders, anti-inflammatory therapeutic approaches should be mainly addressed to restore physiological iron homeostasis. So far, other than classical iron supplementation, almost all therapeutic strategies, principally based on erythropoiesis-stimulating agents and erythrocyte transfusions, are not fully efficient against AI [Pettersson et al. 1993; Kato et al. 1994; Peeters et al. 1996]. Among the innovative therapies, it has been proposed the use of Fpn agonists or hepcidin antagonists [Wessling-Resnick 2010; Casu et al. 2018].

In addition, many studies have explored the relationship between inflammation and pregnancy [Behnia et al. 2016; Nadeau-Vallée 2016]. Pregnancy adverse outcomes, such as miscarriage, abortion and preterm delivery (PTD), are strictly associated with inflammatory processes and, in particular, to cytokine imbalance, and in this respect, IL-6 seems to play a key role as activator of acute phase immune response [Hurst et al. 2001]. Indeed, in physiological pregnancies, the balance between T helper cells 1 (Th1) and Th2 is strongly shifted toward Th2, playing a defensive role in the fetal-maternal relationship [Saito et al. 2010]. This balance is perturbed by inflammatory processes causing a shift toward Th1 predominance, characterized by pro-inflammatory cytokines synthesis involved in the stimulation of cervical prostaglandin secretion, uterine contractility, PTD [Paesano et al. 2012], intrauterine growth restriction, low birth-weight and inferior neonatal health [Scholl 2005] as well as in the establishing of iron homeostasis disorders as anemia, often occurring during pregnancy [Paesano et al. 2010; Paesano et al. 2012; Rosa et al. 2017]. Furthermore, high IL-6 levels in amniotic fluid (AF) have been associated with subsequent pregnancy loss [Wenstrom et al. 1996] as well as to PTD and fetal growth restriction [Bogavac et al. 2012; Xiao et al. 2012] thus suggesting that the primary efforts to prevent and counteract all these adverse outcomes should be addressed to counteract the underneath inflammatory disorders. Several interventions, such as cervical cerclage and bed rest, as well as common therapies, such as beta mimetics, atosiban and calcium channel blockers were mostly ineffective in preventing PTD [Locci et al. 2006; Berghella et al. 2011].

Overall, the best way to block systemic inflammatory processes leading to iron homeostasis disorders would be achieved with a therapeutic approach able to restore both inflammatory processes and iron homeostasis dysregulations.

1.3 Iron and inflammatory homeostasis disorders related bacterial and viral infections

AI has been considered, for a long time, as a host defense mechanism against extracellular pathogens, limiting iron availability in the blood [De Domenico et al. 2008; Nemeth and Ganz 2006; MacKenzie et al. 2008]. This concept should be deeply reviewed in light of the capability of some pathogens to enter and survive inside cells, such as macrophages. Intracellular iron retention could be an inducer of the growth of facultative and obligate intracellular pathogens inside epithelial cells and macrophages, thus increasing infection severity [Ajello et al 2002; Sessa et al. 2017]. In this respect, the recent discovery of the tight correlation between iron and inflammatory homeostasis must take into account that infectious processes by intracellular bacteria are favored and enhanced by intracellular iron overload, making imperative a strong revision of the classical iron therapy.

Intracellular pathogens compete for iron sequestered in host proteins, often by intercepting or interrupting mammalian iron trafficking pathways. Iron acquisition follows a general paradigm in intracellular pathogens: iron, in one form or another, is recognized by the bacteria and translocated across the bacterial membrane(s), generally by a permease system, where it can then be utilized. There are three predominant mechanisms by which this occurs: the biosynthesis of siderophores, receptor mediated endocytosis of the main iron-binding molecules (lactoferrin, Tf, hemopexin, haptoglobin, Hb and heme) or passive transport mediated by bacterial reductase (Figure 3).

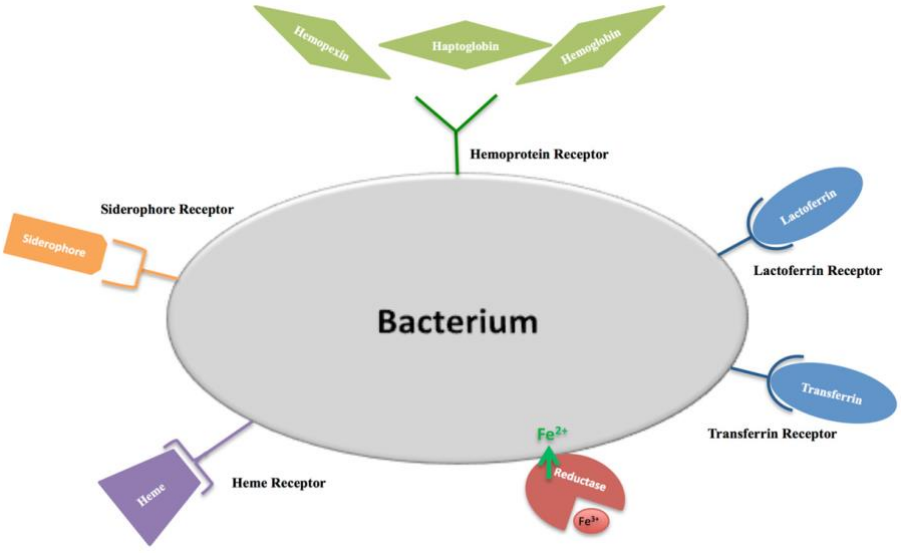

Figure 3. The bacterial iron transport mechanisms: (i) synthesis of high affinity ferric ion chelators, siderophores; (ii) receptor mediated endocytosis of the main iron-binding molecules (lactoferrin, transferrin, hemopexin, haptoglobin, hemoglobin and heme); (iii) passive transport mediated by bacterial reductase.

The biosynthesis of small iron-chelating molecules, known as siderophores, represent a primary mechanism of ferric iron acquisition among bacteria. Model siderophores, such as enterobactin, have a notably high affinity for Fe^{3+} ($Ka = 10^{51}$), which allows them to directly chelate iron bound in host proteins such as Tf [Carrano and Raymond 1979]. Siderophores are then transported across the outer membrane by a TonB-dependent receptor protein, bound in the periplasm by a siderophore-binding protein and trafficked through an inner membrane permease system where the siderophore can then be dissociated from Fe^{3+} to facilitate reduction to Fe^{2+}.

The serum Tf is abundant in mammalian blood, and represents an iron resource for extracellular pathogens. As reported, Tf is endocytosed by mammalian cells, via holo-Tf recognition by the TfR [Harding et al., 1983]. Upon endocytosis, TfR-holo-Tf vacuoles are trafficked through the endocytic recycling pathways. This pathway provides an opportunity for intracellular pathogens to obtain holo-Tf and thus iron. *Neisseria* species possess sophisticated mechanisms for the acquisition of Tf. *Neisseria meningitidis* access host Tf by manipulating Tf trafficking in the cell, redirecting it to sites of bacterial colonization [Barrile et al., 2015]. Tf can then be acquired by *Neisseria* via fusion of Tf-containing endosomes with the pathogen-containing vacuole.

Most iron in the mammalian body is sequestered in heme molecules. Due to the cytotoxicity of free heme, most heme is bound in hemoproteins such as Hb. Hemoproteins are ubiquitously expressed in mammalian cells, as they play crucial functions in metabolism (e.g., electron transport chain). Thus, hemoproteins and heme represent an ample pool of iron to intracellular pathogens. The acquisition of heme from the host is well-characterized in *Yersinia* species, and is representative of systems found in other pathogens such as *Neisseria* and *Bartonella* [Rohde and Dyer 2004; Parrow et al. 2009].

In addition to siderophore-mediated acquisition of ferric iron, many Gram-negatives possess mechanisms for the acquisition of ferrous iron, which is presumed to freely flow through the outer membrane, possibly via porins. This strategy is dependent upon ferrireductase activity, which is thought to be either cell-associated or translocated into the extracellular space. Several bacteria have been shown to display ferrireductase activity, but few ferrireductases have been directly identified.

Other that bacterial infections, iron homeostasis is also perturbed during viral infections, leading to iron disorders [Weinberg 1996], which are worsened by the action of pro-inflammatory cytokines [Ganz et al. 2013]. Viral infections need active cell metabolism and, therefore, a significant viral replication requires a high iron availability [Drakesmith Prentice 2008]. As a general rule, intracellular iron overload, induced by up-expression of hepcidin, promotes the progression of viral infections, as demonstrated for the human immunodeficiency virus (HIV) [Schmidt 2020]. Conversely, hepatitis C virus (HCV) infections represent a peculiar exception, presenting the down-

regulation of hepcidin, which is then up-regulated following antiviral therapy [Armitage et al. 2014]. Intracellular iron overload damages HCV particles.

Since viral infections are directly promoted by intracellular iron overload, other than the contribution of the iron export system, the involvement of the iron uptake system, Tf/TfR1, in the establishment and maintenance of intracellular iron dysregulation, cannot be neglected. TfR1 is a homodimeric type II membrane glycoprotein (~95 kDa) characterized by an apical, a helical, and a protease-like domain [Lawrence et al. 1999; Hentze et al. 2004]. In particular, the N-lobe of Tf interacts with the protease-like domain, while the C-lobe interacts with the receptor's helical domain. Interestingly, the apical domain of TfR1 is an attractive target for viral particles [Giannetti et al. 2003]. The canine parvovirus (CPV) and the feline panleukopenia virus (FPV) have been reported to infect host cells through TfR1 [Parker et al. 2005] as well as the mink enteritis virus [Park et al. 2005] and the New World hemorrhagic fever arenaviruses [Radoshitzky et al. 2007; Sarute and Ross 2017]. HCV also interacts with TfR1 for its internalization in endosomal compartments [Fillebeen and Pantopoulos 2013]. Therefore, similar to the mechanism described for Tf, upon the binding of viral particles, TfR1 undergoes endocytosis, thus translocating viruses into intracellular compartments. Of note, the interaction between the virus and TfR1 does not interfere with iron delivery [Wessling-Resnick 2010]. Recently, the effect of HCV infection on TfR1 recycling has been deepened [Haberger et al. 2020]. In particular, HCV-infected cells showed decreased levels of α-taxilin, an essential factor for the TfR1 recycling, thus resulting in lower levels of TfR1 active protein and consequently in reduced Tf binding, internalization, recycling, and intracellular iron level [Haberger et al. 2020]. Overall, while iron homeostasis disorders associated to several bacterial infections have been well defined, the relationship between iron homeostasis and viral infection is still not well understood [Wessling-Resnick 2010].

In the following sections I discuss the role of *Chlamydia trachomatis*, *Pseudomonas aeruginosa*, as obligate and facultative intracellular bacteria prototypes, and SARS-CoV-2, as viral prototype, infections on the inflammatory processes as well as on the iron homeostasis disorders.

1.3.1 Iron and inflammatory homeostasis disorders related to Chlamydia trachomatis infection

Chlamydia trachomatis is responsible for the most common sexually-transmitted bacterial disease worldwide. The vagina of healthy childbearing age women is a complex ecosystem composed by several microbial species that establish a mutualistic relationship with the host. These microorganisms compose the vaginal microbiota (VM) and co-participate to preserve the healthy status of the vagina as well as the maintenance of acidic pH (pH < 4.5) [Larsen and Monif 2001; Oakley et al. 2008; Russo et al. 2018].

Vaginitis is an inflammatory condition that causes vaginal discharges, itching, irritation, burning and odor. Bacterial vaginosis, trichomoniasis and vulvovaginal candidiasis are the most common infectious causes of vaginitis [Anderson et al. 2004; Farage et al. 2008; Hainer and Gibson 2011].

Bacterial vaginosis (BV) is a pathologic condition characterized by dysbiosis of VM where a marked drop or disappearance of lactobacilli, the main components of commensal flora in the healthy vagina, is observed. In addition, an overgrowth of anaerobes, responsible for the activation of pro-inflammatory processes, including the release of pro-inflammatory mediators, such as IL-1β, IL-6, and IL-8 has been found [Russo et al. 2018; Hainer and Gibson 2011; Hedges et al. 2006; Beigi et al. 2007; Rampersauda et al. 2012; Valenti et al. 2018].

BV represents a risk factor for tubal factor infertility, pelvic inflammatory disease, obstetrical complications and high susceptibility to sexually transmitted pathogens as *Chlamydia trachomatis*, *Neisseria gonorrhoeae* and *Trichomonas vaginalis* [Peipert et al. 2007; Brotman et al 2010]. In particular, BV causes endometritis, cervical inflammation, infiltration of neutrophils and localized erythema. Furthermore, women affected by BV, as well as those with sexually transmitted bacterial infections (STBIs), in vaginal fluid (VF) present higher concentrations of IL-1β, IL-6 and IL-8 [Hedges et al. 2006; Beigi et al. 2007; Valenti et al. 2018; Sawada et al. 2006].

C. trachomatis infection is asymptomatic in about 80% of women and causes acute and chronic infections. Unlike acute infections, which can be cured with antibiotics, chronic infections are difficult to eradicate and need prolonged therapies, thus increasing the risk of developing antibiotic resistance [Mitchell et al. 1991]. Even if novel alternative therapies are needed, the difficulty in finding new agents against *C. trachomatis* resides in the complex biphasic developmental life-cycle of this peculiar pathogen: extracellular infectious bodies (elementary bodies, EBs) metabolically inactive, and the intracellular non-infectious bodies (reticulate bodies, RBs), metabolically active (Figure 4). The EBs adhesion and entry into mucosal epithelial cells initiate a signal transduction cascade of the host cell, leading to the recruitment and reorganization of the actin cytoskeleton at the site of attachment (Figure 4). Following the fusion of EB-containing endosomes, EBs develop into larger, metabolically active but noninfectious RBs (Figure 4). Using ATP and nutrients from the host cell, RBs grow and divide by binary fission within a membrane-bound vacuole, termed inclusion. Subsequently, the RBs asynchronously transform into EBs, which are released, after approximately 48 h, from the host cell by lysis [Wyrick 2010; Bastidas et al. 2013] (Figure 4).

In recent years, it has been demonstrated that *C. trachomatis* can generate a persistent form during its developmental cycle as a consequence of several stress-inducing factors [Wyrick 2010; Di Pietro et al. 2013] (Figure 4). As a result, normal RBs transform into enlarged and morphologically aberrant RBs, thus stopping the production of infectious EBs [Hogan et al. 2004; Wyrick 2010].

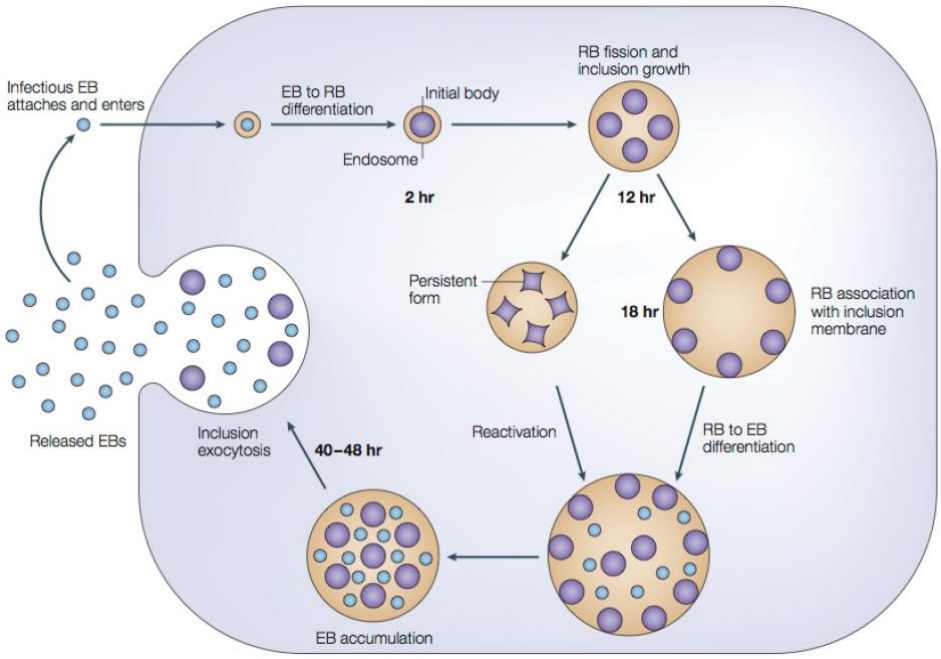

Figure 4. The developmental cycle of *Chlamydia trachomatis*. An infectious elementary body (EB) attaches and enters a eukaryotic host cell. The EB is surrounded by an endosomal membrane to form an inclusion. Within the inclusion, the EB differentiates into an active reticulate body (RB), which then divides by binary fission. Within 40–48 h the RBs transform back into infective EBs which are released to infect neighboring cells. If growth inhibitors are present during this process, intracellular *C. trachomatis* bacteria develop a non-replicating persistent form, which reverts to an infectious form upon removal of the inhibitor. The Figure was taken from Potroz and Cho [2015].

In particular, *C. trachomatis* enters into the persistence state in the presence of iron-chelating drugs, which inhibit the developmental cycle and, hence, show its dependence on iron for the achievement of infectious cycle [Raulston 1997; Thompson and Carabeo 2011]. In fact, it is well-documented in the literature that the Chlamydiaceae are strictly iron-dependent [Raulston 1997; Al-Younes et al. 2001; Freidank et al. 2001] but the long-standing genetic intractability of the organism has rendered many benchmark approaches to iron biology ineffectual in past chlamydial research. Consequently, our understanding of this fundamental biological process is incomplete in Chlamydiae. In this regard, iron limitation in host cells has been shown to be of the utmost importance for the growth and survival of *Chlamydia* spp. [Raulston 1997; Al-Younes et al. 2001].

Following *C. trachomatis* infection, cervical epithelial cells produce several pro-inflammatory cytokines including TNF-α, IL-1α, IL-6, and IL-8 that augment the cell inflammatory response, thus inducing direct damage to genital tissues. In this respect, the expression major proteins involved in iron homeostasis could be perturbed due to the massive synthesis of these pro-inflammatory cytokines, principally IL-6 and IL-1α. As reported by Vardhan et al. [2009], in *C. trachomatis* infected HeLa-299 cells, the expression of TfR is downregulated, whereas expression of Ftn is upregulated, thus suggesting that iron homeostasis is modulated in *C. trachomatis*-infected HeLa cells at the interface of acquisition of iron [Vardhan et al. 2009]. Furthermore, IL-8, in turn, recruits

innate immune cells, which are abundant in the genital mucosa and are able to further worsen chronic inflammation and tissue-damage of the reproductive system [Redgrove and McLaughlin 2014].

1.3.2 Iron and inflammatory homeostasis disorders related to Pseudomonas aeruginosa lung infection

Cystic fibrosis (CF) is a genetic disorder affecting several organs and reducing expectancy and quality of life. The most relevant damages are observed in the airways that are inherently prone to infection. Airway infections begin in early life [Ranganathan et al. 2011] and by adulthood, they became chronic. Even though the microbial epidemiology has changed in the last years, it is well established that the chronic airway infections are often sustained by *Pseudomonas aeruginosa* [Lipuma 2010; Salsgiver et al. 2016]. *P. aeruginosa*, a facultative intracellular gram-negative bacterium, is a leading cause of hospital-acquired infections and the main bacterial pathogen responsible for severe lung deterioration in CF patients. Among hospital-acquired *P. aeruginosa* infections, ventilator-associated pneumonia is a major clinical entity, with about 20% prevalence and dramatically high mortality and monetary costs [Fujitani et al. 2011; Kollef et al. 2014]. Other common syndromes associated with *P. aeruginosa* lung infection are those occurring in patients with chronic lung disease, such as chronic obstructive pulmonary disease and CF [Döring et al. 2011]. All CF patients experience *P. aeruginosa* lung infection during their lifetime, and more than 80% of them become chronically infected in the adult years [Döring et al. 2011; Folkesson et al. 2012]. Lifelong *P. aeruginosa* infection causes decreases in lung function and poor clinical scores for CF patients, ultimately resulting in a fatal prognosis [Ciofu et al. 2013].

During CF-induced airway infection progress, *P. aeruginosa* gradually shifts from the virulent pathogen form of early infection to the host-adapted pathogen form typical of the chronic phase, characterized by biofilm lifestyle and antibiotic resistance [Hogardt and Heesemann 2013], thus increasing the rate of lung function decline, morbidity, and mortality [Emerson et al. 2002].

Airways inflammation is a hallmark of CF, being present even before bacterial colonization and detectable infection, as demonstrated by high levels of interleukin (IL)-8 and accumulation of neutrophils in bronchoalveolar lavage fluid (BALF), and in general to activation of numerous pro-inflammatory genes dependent from nuclear factor kappa-light-chain-enhancer of activated B cells (NF-κB) and activator protein (AP)-1 pathways [Dakin et al. 2002; Verhaeghe et al. 2007; Bragonzi et al. 2017]. Inflammation is related to the prolonged inflammatory response in the lung that persists even after the inflammatory stimulus is over [Nichols et al. 2008]. As a matter of fact, the massive recruitment of leukocytes into the lung airways gives rise to a self-enhancing loop, where the infiltrated neutrophils undergo necrosis and release proteases and chemoattractant molecules, thus

leading to tissue damage and to the further recruitment of leukocytes. Furthermore, neutrophils are highly activated because of the genetic defect thus increasing lung damage [Cockx et al. 2018].

In addition to infection and inflammation, a dysbalance of iron homeostasis is observed in CF airways and high levels of iron (up to >100 μM) in airway secretions can be recorded [Reid et al. 2002; Reid et al 2004; Reid et al. 2007]. Iron loss into the sputum negatively correlates with cell lung functionality, while it positively correlates with cell and tissue damage and disease severity [Reid et al. 2002; Ward and Kaplan 2012]. Iron excess can derive from the altered expression of the main proteins involved in iron homeostasis. In particular, an increased expression of both Fpn and Ftn in lung tissue of CF patients has been observed [Ghio et al. 2013]. Moreover, elevated concentrations of both Ftn and Tf in the lung lavage of CF patients were found [Ghio et al. 2013]. Overall, all the changes in Fpn, Ftn and Tf expression converge in high rates of iron accumulation in the lower respiratory tract of CF subjects [Reid et al. 2007]. Of note, conversely to gastrointestinal ephitelium, where Fpn is localized to the basolateral membrane of the cells, in airway ephitelium is mainly present in the apical membrane of the cells [Yang et al. 2005]. This disparity in localization of Fpn supports the tissue-specific role for this protein with release of iron to either the airways or the alveoli rather than to the blood for systemic distribution. Fpn may therefore play a key role in iron absorption/recycling and iron detoxification in different tissues and cells [Ghio 2009] (Figure 5).

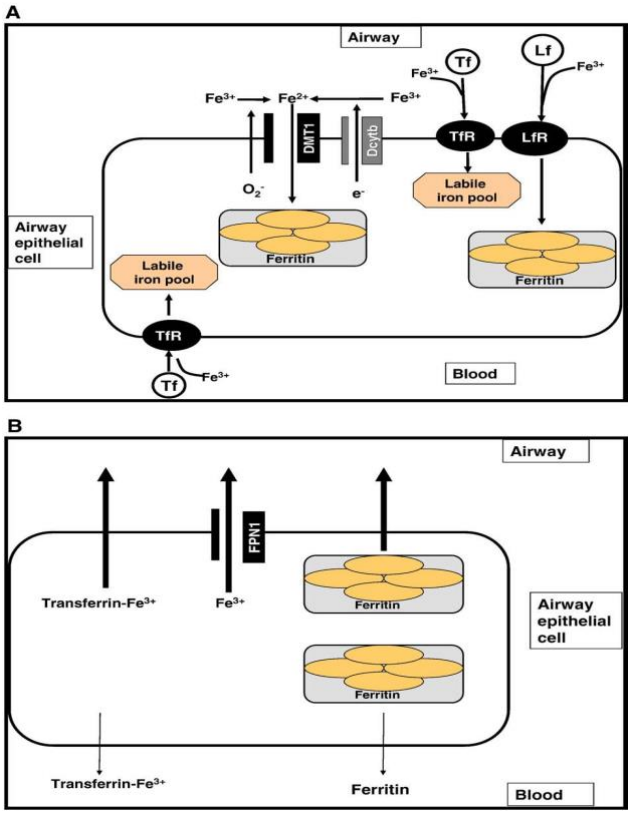

Figure 5. Schematics for iron import (A) and iron export (B) by airway epithelial cells

The iron overload in CF airways favors the growth and the biofilm lifestyle of *P. aeruginosa*, thus worsening the inflammatory status and host damage [Hogardt and Heesemann 2013; Reid et al. 2004; Singh et al. 2002; Berlutti et al. 2005; Gomez et al. 2007; Gifford et al. 2012]. Bacterial biofilm invades CF airway epithelial cells that respond by activating a strong inflammatory response [Valenti et al. 2011; Frioni et al. 2014]. Therefore, infection, inflammation and iron disorders reinforce each other, establishing an unsafe vicious circle difficult to counteract and solve in vivo.

Despite the improvement of infection therapy based on aerosolized antibiotics [Waters and Smyth 2015], chronic *P. aeruginosa* infections remain very difficult to treat [Gibson et al. 2003; Vidya et al. 2016]. Aggressive antibiotic and anti-inflammatory treatments may ameliorate CF patient symptoms in the short-term, but they do not consistently reduce inflammation and bacterial load, which may be related to persistently elevated iron concentrations in the airway [Reid et al. 2007]. So far, it has not been established whether iron dyshomeostasis in lung is a cause or a consequence of *P. aeruginosa* infection in CF, while it is known that decreasing available iron generally ameliorates lung injury associated to inflammation states [Louie et al. 1993; Ghio et al. 1994]. Therefore, since inflammation is a hallmark also in CF, iron is likely to be a major actor in the maintenance of this disease.

1.3.3 Iron and inflammatory homeostasis disorders related to SARS-CoV-2 infection

Recently, the world has been dealing with a devastating global pandemic coronavirus infection, with more than 60 million infected worldwide and over 1.5 million deaths as of December 1st 2020, related to a novel coronavirus, namely severe acute respiratory syndrome coronavirus 2 (SARS-CoV-2), characterized by a spherical morphology and identified through next-generation sequencing. The genetic sequence of SARS-CoV-2 shows more than 80% identity to SARS-CoV and 50% to the MERS-CoV [Tian et al. 2020; Lu et al. 2020]. Of note, SARS-CoV-2 possesses a higher transmissibility from human to human and lower pathogenicity in respect to SARS-CoV [Li et al. 2020].

Coronavirus belongs to the family of Coronaviridae, subfamily Coronavirinae, order Nidovirales and this subfamily includes four genera: *Alphacoronavirus*, *Betacoronavirus*, *Gammacoronavirus*, and *Deltacoronavirus* [Chen and Zhong 2020]. Coronavirus possesses a single-strand, positive-sense RNA genome ranging from 26 to 32 kilobases in length [Su et al. 2020]. The first open reading frame represents the majority of the viral genome and encodes 16 non-structural proteins, while the other open reading frames encode structural and accessory proteins [Cui et al. 2018; Guo et al. 2020]. The residual viral genome is responsible for the expression of four essential structural proteins: spike glycoprotein, small envelope protein, matrix protein, and nucleocapsid protein. In

particular, spike (S) glycoprotein is composed of two subunits (S1 and S2) [Cui et al. 2018]. Homotrimers of S proteins on the viral surface are responsible for binding to host receptors (S1) and membrane fusion (S2) [Li et al. 2016; Lu et al. 2020]. Noteworthy, S1 subunit, like in other Beta-coronaviruses, is composed of a core and an external subdomain and represents only a 40% amino acid identity with other SARS-CoVs. However, in SARS-CoV-2, the S2 subunit, which contains a fusion peptide, a transmembrane domain and a cytoplasmic domain, is highly conserved. Of note, in in silico study by Ehsani [2020], a purposeful and restricted protein sequence search revealed a potential sequence similarity between the relatively less-studied cysteine-rich cytoplasmic domain of coronavirus spike proteins and the vertebrate hepcidin protein.

S1 directly interacts with angiotensin-converting enzyme 2 (ACE2), the functional receptor expressed on the surface of pulmonary, cardiac, renal, intestinal and endothelial host cells [Lu et al. 2020]. In particular, alveolar epithelial parenchymal type II cells express ACE2. Notably, nasal epithelial cells, comprising two clusters of goblet cells and one cluster of ciliated cells, show the highest expression among all investigated cells in the respiratory tree [Qi et al. 2020]. As the virus can be detected in upper respiratory tract samples, the nasofarinx can be involved as a site of replication. Furthermore, SARS-CoV-2 is also able to infect T lymphocytes, despite their very low expression levels of ACE2, leading researchers to hypothesize the presence of an alternative receptor allowing viral entry into these cells [Wang et al. 2020]. In this respect, in a paper by Tang et al. [2020], the Authors show that SARS-CoV-2 infected ACE2 knockout cells, suggesting the presence of another receptor for SARS-CoV-2 entry. In this respect, TfR directly binds to S protein of SARS-CoV-2 with a binding affinity very similar to that observed between ACE2 and SARS-CoV-2 [Tang et al. 2020]. In addition, TfR directly interacted with ACE2. In virus-infected cells, TfR-ACE2-virus and TfR-virus complex was found on the cell membranes and in the cytoplasm, respectively. No ACE2-virus complex was observed in the cytoplasm, thus suggesting TfR-mediated transport of SARS-CoV-2 from cell membranes to cytoplasm [Tang et al. 2020]. Furthermore, studies have shown that the serine protease TMPRSS2 can prime S protein, thus allowing spike protein cleavage and regulating the entire mechanism of viral entry [Hoffmann et al. 2020]. Other proteases can also be involved [Hoffmann et al. 2020]. The schematic representation of SARS-CoV-2 life cycle is reported in Figure 6.

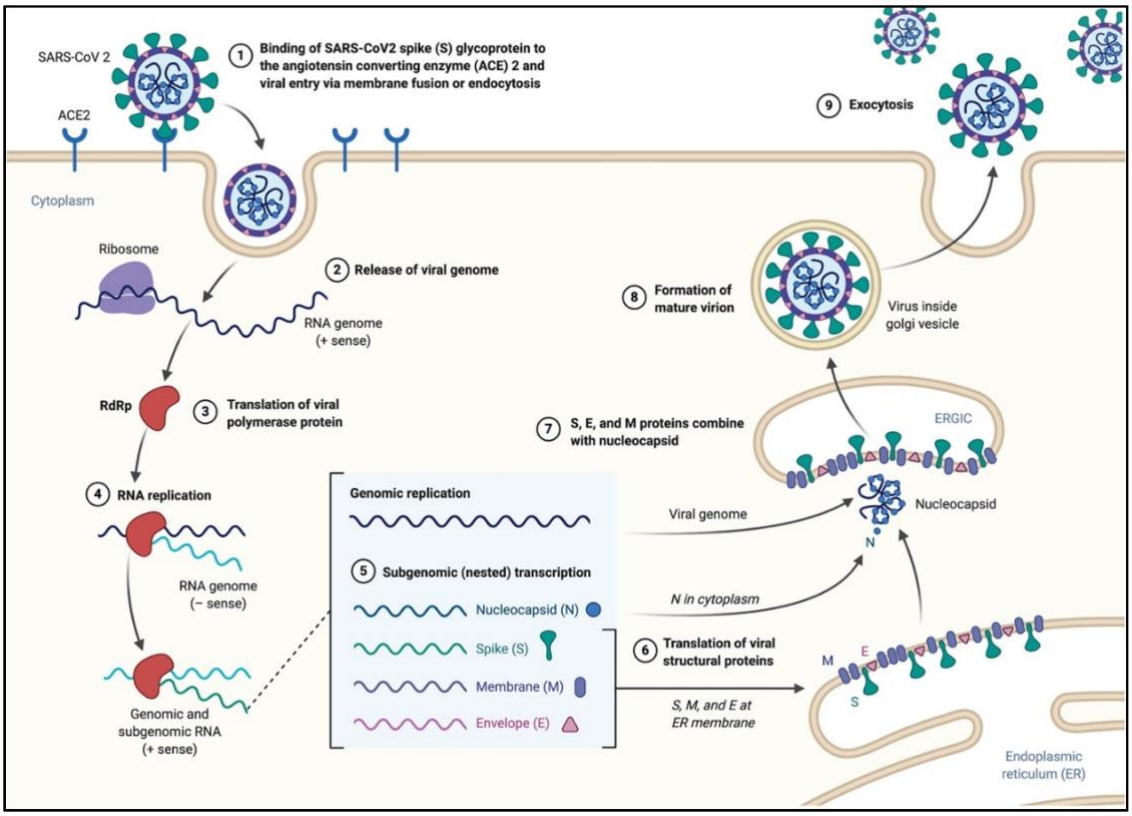

Figure 6. The life cycle of SARS-CoV-2 in the host cells. The S glycoproteins of the virion bind to the cellular receptor angiotensin-converting enzyme 2 (ACE2) and enters target cells through an endosomal pathway. Following the entry of the virus into the host cell, the viral RNA is unveiled in the cytoplasm. ORF1a and ORF1ab are translated to produce pp1a and pp1ab polyproteins, which are cleaved by the proteases of the RTC. During replication, RTC drives the production full length (−) RNA copies of the genome and used as templates for full-length (+) RNA genomes. During transcription, a nested set of sub-genomic RNAs (sgRNAs), is produced in a manner of discontinuous transcription (fragmented transcription). Even though these sgRNAs may have several open reading frames (ORFs), only the closest ORF (to the 5′ end) will be translated. Following the production of SARS-CoV-2 structural proteins, nucleocapsids are assembled in the cytoplasm and followed by budding into the lumen of the endoplasmic reticulum (ER)–Golgi intermediate compartment. Virions are then released from the infected cell through exocytosis. The Figure was taken from Alanagreh et al. [2020].

The serine protease TMPRSS2 and cathepsin B/L, expressed by salivary glands, lung, small intestine, liver, kidney, and heart endothelial cells, could lead as a consequence to systemic vasculitis, thromboembolism and disseminated intravascular coagulation [Carnevale et al. 2020]. Further hypothetical targets could consider other viral components such as ORF3b, not homologous with that of SARS-CoVs, and a secreted protein (encoded by ORF8), structurally different from those of SARS-CoV [Chen and Zhong 2020].

Although the respiratory tract is the primary portal of entry of SARS-CoV-2, gastrointestinal involvement associated with nausea, vomiting and diarrhea and persistence of viral particles may also occur [Chen and Zhong 2020; Wang et al. 2020]. Early studies found a low incidence (1–3.5%) of gastrointestinal or hepatic manifestations, but more recent studies reported a higher rate of affection (11.4–24.2%). Moreover, in subjects suffering from SARS-CoV-2, transaminases may

range from mild to elevated levels [Agarwal et al. 2020], probably related to the presence of ACE2 receptors on enterocytes in the ileum and colon [Burgueño et al. 2020], cholangiocytes, and hepatocytes [Chen et al. 2020; Liang et al. 2020; Ong et al. 2020]. ACE2 seems to mediate inflammatory processes and, consequently, the occurrence of diarrhea [Zhang et al. 2020]. As several studies indicated a possible fecal–oral transmission, SARS-CoV-2 RNA should be detected in the stool of patients affected by coronavirus disease-19 (COVID-19) [Wu et al. 2020]. However, it is unclear whether SARS-CoV-2 replicates in human intestine and contributes to possible fecal–oral transmission [Zhang et al. 2020] or the intestine is a potential site of SARS-CoV-2 replication, thus contributing to local and systemic illness and overall disease progression [Wang et al. 2020]. Gut dysbiosis secondary to gastrointestinal inflammation is known to possibly interfere with distant disorders [Dhar and Mohanty 2020]. In light of this view, a gut–lung axis, bidirectionally acting, has been hypothesized: endotoxins and microbial metabolites synthesized by gut microbiota can influence the lung through the circulation, while lung inflammation can affect the gut microbiota [Dumas et al. 2018]. Therefore, gut microbiota could participate in the pathogenesis of acute respiratory distress syndrome and vice versa [Dickson 2016].

Most patients infected with SARS-CoV-2 exhibit mild-to-moderate symptoms, such as sudden anosmia or ageusia, fever, abnormal cough, headache and fatigue, diarrhea, and recover without sequelae. However, around 15% develop severe pneumonia and 5% progress to acute respiratory distress syndrome, septic shock, and/or multiple organ failure, associated with high mortality.

In patients affected by COVID-19, most of the severe cases demonstrated massive systemic levels of infection-related biomarkers and inflammatory cytokines, as IL-6, TNFα and Ftn [Huang et al. 2020]. The excessive release of pro-inflammatory cytokines, referred as a ‘cytokine storm’, has evolved as an important surveillance system that, when triggered, fights infection and eliminates pathogens but may contribute as a principle contributory cause of internal organs or systems impairment as recently hypothesized for cardiovascular, neurological, septic shock or cutaneous sequelae or related risk factors for poor prognosis [Shankar and Prasad 1998; Adams-Chapman and Stoll 2001; Cutone et al. 2014; Dall’Agnola et al. 2018; Conti et al. 2020; Lagunas-Rangel and Chávez-Valencia 2020; Han et al. 2020; Xiong et al. 2020; Li et al. 2020; Zhang et al. 2020].

Therefore, the activation and progression of organs impairment induced by SARS-CoV-2 could be by inflammatory processes and related iron dysregulation.

Few data are available on the possible contribution of altered iron homeostasis on COVID-19 [Xia et al. 2019; Zhao et al. 2020; Shah et al. 2020]. In a retrospective study involving 50 COVID-19 patients, serum iron was found extremely low in most cases and a predictor of mortality [Zhao et al.

2020]. In addition, alterations of iron metabolism were associated with hypoxemia in severe COVID-19 patients in the intensive care unit (ICU) [Shah et al. 2020; Bellmann-Weiler et al. 2020]. Hepcidin may represent the link between iron deficiency and COVID-19 severity. However, the relative contribution of hepcidin upregulation to the disrupted iron homeostasis in COVID-19 remains to be determined.

In a recent study conducted in San Raffaele University Hospital in Milan, 111 Italian COVID-19 patients were analyzed for hepcidin levels other than inflammatory markers such as IL-6 [Nai et al. 2020]. Iron concentration was below normal range in 93.7% of patients. Conversely hepcidin levels were significantly increased in 61.3% of patients. However, considering that hypoferremia suppresses hepcidin expression [Camaschella et al. 2020], even normal hepcidin is inappropriately high in most cases. Interestingly, limiting the analysis to critical patients in ICU, high hepcidin predicts mortality, independently of age, lung function, inflammation and tissue damage.

No drug or vaccine against SARS-CoV-2 has been approved due to the absence of evidence deriving from rigorous clinical trials. Moreover, although some treatments seem to be effective against this virus, they exert several adverse effects. Safe and effective drugs are needed to prevent and cure COVID-19. there is an urgent need to explore alternative methods for treating, without adverse effects, COVID-19 clinically advanced conditions in order to reduce viral infection, replication and spread as well as mortality, and to mitigate the potential future outbreaks, before the set-up of vaccine. At last, but not least, the hypothesis to identify new drugs or natural substances, which, without side effects, are able to inhibit viral infection, to increase the host's local defenses as well as to restore the iron and inflammatory homeostasis disorders, is extremely tempting.

1.4 Lactoferrin

It's just over 80 years since the glycoprotein Lactoferrin (Lf) was first discovered in bovine milk [Sorensen and Sorensen 1939] and later purified as an iron-containing red protein from human milk [Johanson 1960]. This glycoprotein is present in milk from different species such as cow, pig, mouse, horse, rabbit, and dog and its production is species- and lactation stage-dependent [Masson and Heremans 1971; Czosnykowska-Łukacka et al. 2019]. Notably, concentration of Lf in human milk is the highest among the different species, with the maximum peak in colostrum (6.7 g/L) and lower concentrations in transitional (3.7 g/L) and mature milk (2.6 g/L) [Czosnykowska-Łukacka et al. 2019] (Table 1). Despite its name, Lf was subsequently found to be present also in other biological fluids including saliva, tears, mucus, seminal fluid, bronchial secretions, and in secondary granules of neutrophils [Alexander et al. 2012] (Table 1).

Table 1: Lactoferrin concentration in different human fluids and secretion

Biological Fluids	Concentration (mg/ml)
Colostrum	8
Milk	1.5-4
Tears	2
Saliva	0.008
Vaginal secretion	0.008
Seminal fluid	0.112
Cerebrospinal fluid	Undetectable
Plasma	0.0004
Joint fluid	0.001

Lf is functionally and structurally similar to serum Tf (sTf) with 60% sequence identity [Baker et al. 2002]. As a matter of fact, this glycoprotein, also known as lacto-transferrin, is classified as a member of the Tf family, in addition to melano-, ovo-, and sTf [Baker and Lindley 1992]. Tfs are a superfamily of iron-binding proteins constituted by a single polypeptide chain of 650–700 residues with a two-fold internal repeat derived from an earlier gene duplication event, which gives rise to an N-lobe and a C-lobe. The two homologous lobes share about 40% sequence identity and each of them can reversibly bind a ferric ion [Metz-Boutigue et al. 1984]. Both Lf and sTf have high affinities for Fe^{3+} ($Kd = 10^{-20}$ M) [Baker et al. 1994] due to a highly conserved set of ligands for the ferric ion [Baker et al. 1987; Bruns et al. 1997]. However, Lf and sTf differ in some physicochemical properties, in particular Lf has high iron binding stability at low pH, whereas sTf releases iron under such conditions [Baker et al. 2002]. This different feature reflects distinct functions of the considered proteins: indeed, sTf acts as a cargo for iron transport not only into cells [Luck and Mason 2012] but also in the blood, a district that it is usually characterized by pH values in a narrow neutral range (7.2–7.4) [Gomme et al. 2005], while Lf often exerts its role at inflamed and infected sites, where pH can reach acidic values. Indeed, Lf shares its anti-microbial, anti-fungal, anti-viral, and anti-parasitic activities with ovo-Tf [Valenti and Antonini 2005; Giansanti et al. 2012], whereas it possesses unique features as an anti-inflammatory, immunomodulatory, and anti-cancer molecule [Zhang et al. 2014; Legrand 2016; Lepanto et al. 2019; Cutone et al. 2020]. Moreover, it is emerging as a fundamental regulator of cellular and systemic iron homeostasis [Rosa et al. 2017; Bonaccorsi di Patti et al. 2018]. All the activities ascribed to Lf can be dependent or independent of its iron-binding ability.

The Lf primary structure has been characterized in multiple species [Baker et al. 1994]. Human Lf (hLf) shows high similarity with other Lfs isolated from bovine (bLf), horse, and buffalo [Moore et al. 1997; Sharma et al. 1999; Karthikeyan et al. 1999]. It is an 80 kDa single polypeptide chain of 691 amino acids, with the N- (residues 1–333) and C- (residues 345–691) lobes connected by a three-turn-helix peptide (residues 334–344) (Figure 7) [Anderson et al. 1990].

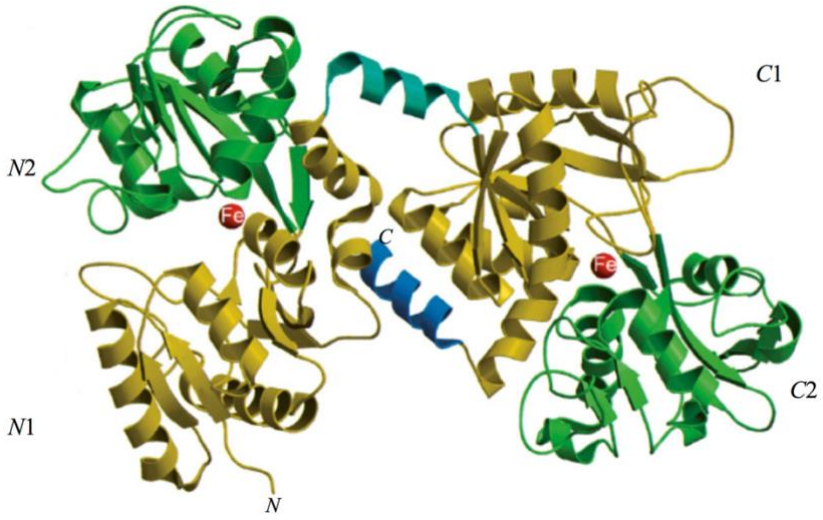

Figure 7. Structure of lactoferrin. The *N*-lobe on the left and the *C*-lobe on the right are divided into four domains, labeled N1, N2, C1, C2. The red spheres represent the two ferric ions in each iron-binding site. The Figure was taken from Rosa et al. [2017].

Ferric ligands are constituted by two tyrosines (Y92 and Y192 for N-lobe and Y433 and Y526 for the C-lobe), a histidine (H253 for N-lobe and H595 for C-lobe) and an aspartic acid (D60 for the N-lobe and D395 for the C-lobe), that, along with two oxygens from a CO_3^{2-} ion, form a binding site with an octahedral geometry [Baker et al. 1999]. Spectroscopic studies and the 3D structure suggest that the CO_3^{2-} anion binds first, thus neutralizing the positive charge of the arginine residue (Arg-121 in the *N*-lobe and Arg-465 in the *C*-lobe) [Baker 1994; Baker et al. 2002]. The participation of the CO_3^{2-} anion in the iron coordination binding appears to be ideal for iron reversible binding [Baker 1994] since the protonation of the CO_3^{2-} anion is a likely first step in the breakup of the iron site at low pH [Moore et al. 1997] (Figure 8).

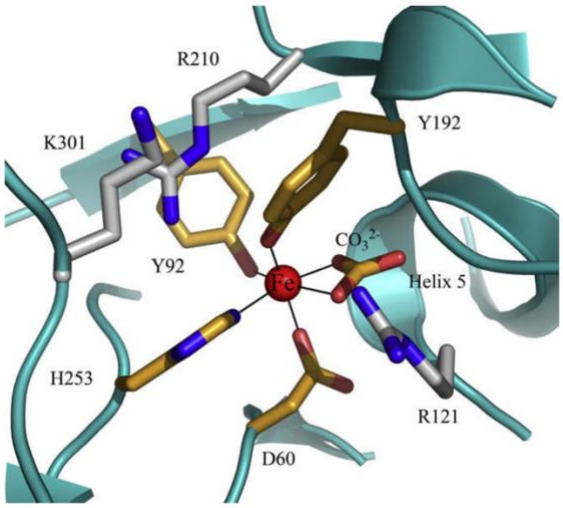

Figure 8. Lactoferrin iron-binding site. Iron-binding site in the *N*-lobe: two tyrosine (Y92 and Y192), one aspartic acid (D60), one histidine (H253) and one carbonate anion together with the arginine residue (R121). Two basic residues behind the iron site, an arginine (R210) and a lysine (K301) help modulate iron release. The Figure was taken from Rosa et al. [2017].

Lf is rich in basic amino acids (isoelectric point ca.9) especially in the N-lobe, which presents two peptide sequences, namely lactoferricin (Lfcin, aa. 1–47 in hLf and 17–41 in bLf) and lactoferrampin (Lfampin, aa. 269–285 in hLf and 268–284 in bLf), which have been described to possess their own biological functions [Bellamy et al. 1992; Van der Kraan et al. 1992]. Both peptides can be generated by Lf tryptic digestion after oral ingestion, thus suggesting their physiological implication in gut homeostasis. Indeed, Lfcin and Lfampin are endowed with potent anti-microbial [Van der Kraan et al. 2004; Gifford et al. 2005], anti-fungal [Fernandes et al. 2017], anti-viral [Berlutti et al. 2011], anti-inflammatory [Drago-Serrano et al. 2018], and anti-cancer properties [Arias et al. 2017]. Most of the functions ascribed to these peptides are due to their high positive charge, which enables them to interact with negatively charged surface of both prokaryotic and eukaryotic cells, thus altering the permeability of membranes and, in case of pathogens, inducing cell lysis and death [Arias et al. 2017; Epand and Vogel 1999].

Depending on its iron content, Lf can assume two opposite conformational states, the open iron-free form (apo-Lf) and the closed iron-binding form (holo-Lf) [Baker and Baker 2012]. The native form of Lf, produced and secreted in physiological conditions, has an iron saturation rate between 10% and 20%, thus leading to the prevalence of apo- and monoferric Lf and a very low content of diferric Lf. On the other hand, in inflammation and/or infection sites, characterized by high levels of free iron, the holo-form is mostly present. Interestingly, the iron content influences the physico-chemical properties of Lf [Rosa et al. 2018]. First of all, holo-Lf is more stable than the unsaturated form, with higher thermal stability and a significant resistance to proteolytic digestion [Rosa et al. 2018]. Some of the functions exerted by Lf can also be affected to its iron-binding status, as it is

able to scavenge free iron in fluids and inflamed and/or infected sites, suppressing free radical-mediated damage and decreasing the availability of the metal to pathogens and cancer cells. In addition, many studies have shown that, depending on the iron-saturation rate, Lf can exert dissimilar functions by activating specific signaling pathways [Jiang and Lönnerdal 2012; Cutone et al. 2020]. It is, therefore, of the utmost importance to consider the iron saturation rate when carrying out in vitro and in vivo experiments.

Lf biological function is also influenced by glycosylation, the most common protein post-translational modification affecting protein folding, immunogenicity, protein solubility, and resistance to proteolysis. Glycosylation is a species-specific and tissue-specific modification, e.g., hLf and recombinant human Lf (rhLf) contains two major glycosylation sites, Asn 138 and Asn 479 [Haridas et al. 1995; Thomassen et al. 2005], but different N-glycan patterns [Le Parc et al. 2014]. Indeed, rLf expressed in cow has a lower content of sialic acid and fucose, showing high mannose-, hybrid-, and complex-type structures, while N-glycans from hLf are comprised entirely of highly branched, highly sialylated, and highly fucosylated complex-type structures [Yu et al. 2011]. Bovine, caprine and ovine Lfs present five potential glycosylation sites (Asn233, 281, 368, 476, and 545) compared to only one in murine Lf (Asn 476) [Baker and Baker 2009]. However, in bLf only four sites are invariably glycated (Asn233, Asn368, Asn476, and Asn545) [Moore et al 1997], whereas Asn281 can selectively undergo glycosylation, giving rise in this case to a higher molecular mass bLf (84kDa vs. 81kDa) [Wei et al. 2000].

1.4.1 Bovine lactoferrin

Despite the structural differences reported above, bLf has been classified as and hLf bioequivalent by virtue of high sequence homology and function sharing and, in addition, it is classified as a "generally recognized as safe" (GRAS) substance by the USA Food and Drug Administration. Therefore, the majority of the in vitro [Sessa et al. 2017; Lepanto et al. 2019] and in vivo studies [Valenti et al. 2017], as well as clinical trials [Paesano et al. 2014; Lepanto et al. 2018] have been conducted by using commercial bLf rather than the highly costing rhLf. However, differences in the primary source of bLf, and in industrial procedures, influencing bLf integrity and purity, have shown great impact on the efficacy of commercial bLf preparations, especially in vivo, where bLf bioavailability can crucially influence the success or the failure of its action [Rosa et al. 2018].

1.4.2 Functions of bovine lactoferrin

All the functions ascribed to bLf can be dependent or independent of bLf-iron-binding ability.

1.4.2.1 Antibacterial and Anti-Biofilm Activity Dependent on Lf Iron-Binding Ability

The first function attributed to Lf was the antimicrobial activity. The bacteriostatic action of Lf is usually iron dependent, as iron supplementation reverts its effect [Weinberg 1993]. The Lf antibacterial activity is counteracted by three main mechanisms put in place by bacterial pathogens: (i) synthesis of high affinity ferric ion chelators, named siderophores, that compete with iron-binding proteins for iron acquisition and delivery into bacteria through specific receptors [Petrik et asl. 2017]; (ii) iron acquisition through Lf or Tf binding mediated by their specific surface receptors [Beddek and Schryvers 2010]; iron acquisition through Hb, haptoglobin and hemopexin binding mediated by surface hemoprotein receptors [Wandersman and Stojiljkovic 2000]; iron acquisition through heme binding mediated by the surface hemophore receptor [Huang and Wilks, 2017]; (iii) iron acquisition through bacterial reductase able to reduce ferric to ferrous ions, thus eliminating the substrate of the Fenton reaction and assimilating ferrous ions that passively enter inside microbial cells [Pilarczyk-Zurek et al. 2016]. The bacterial iron transport mechanisms are discussed in Section 3 and summarized in Figure 3.

Later, in 2002, Singh et al. [2002] demonstrated another important iron-dependent Lf function: inhibition of *P. aeruginosa* biofilm formation in CF by the iron-binding activity of Lf [Singh et al. 2002]. As a matter of fact, CF is associated with alterations in the influx and efflux of chloride and sodium ions, which involves also abnormal high concentrations of iron and Ftn in sputum [Stites et al. 1998]. This increased availability of iron (median value of 6.3×10^{-5} M) induces the generation of ROS, which contributes to lung disorders, as well as to the enhanced growth and colonization of *P. aeruginosa* and *Burkholderia cepacia*, two motile Gram-negative pathogens that are a major source of the morbidity and mortality of CF patients. For both bacteria, biofilm formation is one of the major virulence factors. Peptides and proteins of natural non-immune defenses, including Lf, play a crucial role in combating such infections. A striking Singh et al. [2002] discovery was that apo-Lf, by chelating iron, inhibits *P. aeruginosa* adhesion and biofilm formation through activation of a specialized form of motility, named switching. Like *P. aeruginosa,* also free-living forms of *B. cepacia* show a noticeable motility under iron-limiting conditions. On the other hand, iron availability or the addition of iron-saturated bLf inhibits the motility and induces abundant *P. aeruginosa* and *B. cepacia* growth and aggregates, evolving into biofilm [Berlutti et al. 2005]. In CF patients, however, these protective effects of Lf are compromised by the presence of high iron concentrations and, consequently, by high levels of holo-Lf [Rogan et al. 2004]. Even if the hLf concentration increases in infection and inflammation processes, in sputum of CF patients, free iron concentrations remain higher than in normal subjects [Appelmelk et al. 1994]. The high iron concentration (6.3×10^{-5} M) saturates hLf (1×10^{-5} M), thus preventing hLf from inhibiting biofilm formation.

1.4.2.2 Antibacterial Activity Independent of Lf Iron-Binding Ability

An iron-independent bactericidal action is exerted by Lf direct interaction with the lipopolysaccharide (LPS) of Gram-negative or with the lipoteichoic acid of Gram-positive bacteria [Appelmelk et al. 1994; Brandenburg et al. 2001]. The bactericidal activity of Lf is located in the *N*-terminal region, as its derivative cationic peptide Lfcin, generated by pepsin digestion, is several folds more active than the intact protein in interacting with LPS and in killing Gram-negative bacteria [Tomita et al. 1991; Bellamy et al. 1992]. It is also important to underline that the presence of high calcium concentrations can counteract the release of LPS from Gram-negative bacteria induced by Lf. In fact, the ability of Lf to bind Ca^{2+} through the carboxylate groups of the sialic acid residues present on glycan chains provokes the release of significant amounts of LPS from Gram-negative bacteria, without needing a direct interaction with bacteria [Rossi et al. 2002]. The bactericidal activity towards Gram-positive bacteria appears to be related to the same cationic residues involved in the bactericidal activity against Gram-negative bacteria [Valenti and Antonini 2005].

1.4.2.3 Inhibition of Bacterial Adhesion on Abiotic and Cell Surfaces

Independently from its iron-binding ability, bLf inhibits the bacterial adhesion to host cells through its competitive binding to host cells and/or to microbial surface components [Valenti and Antonini 2005]. Microbial adhesion and subsequent colonization, resulting in biofilm formation on abiotic surfaces, such as catheters, prosthesis and medical devices, represent a serious problem that can lead to illness and death. Efforts to reduce microbial adhesion, using new materials or compounds inhibiting microbial adhesion, have had modest success once applied to the patient. Consequently, it would be very helpful to discover other compounds able to hinder microbial adhesion. In 1989, the ability of Lf, in both apo- and holo-form, to inhibit the adhesion of *Streptococcus mutans* to hydroxyapatite (HA), mimicking the tooth surface, was an interesting disclosure [Visca et al. 1989]. The further demonstration that Lf inhibits the adhesion of *S. mutans* to HA through residues 473–538 of its *C*-lobe confirmed that this activity is unrelated to Lf iron-binding properties [Oho et al. 2002]. The influence of Lf on bacterial adhesion on contact lenses has been also shown through the much lower number of adherent *P. aeruginosa* on hLf-coated lenses compared to that observed on hLf non-coated ones [Williams et al.2003]. The different nature of abiotic surfaces, microbial adhesion mechanisms and in vitro experimental conditions indicate that the inhibition of bacterial adhesion by apo- or holo-Lf can explain the different requirement to exert adhesion: ionic binding to biomaterials, as well as specific binding to bacterial structures, or both.

The ability of microbes to adhere, colonize and form biofilm on host cells is also a crucial step in the development and persistence of infections. The first demonstration of the mucosal protective activity of hLf against injury by adherent *Escherichia coli* HB101 was included in the data reported by Longhi et al. [1993].

Later, it was confirmed that Lf can inhibit the first step for bacterial pathogenesis through the inhibition of bacterial adherence to host cells [Berlutti et al. 2005; Kawasaki et al. 2000; Araujo and Giugliano 2001; Ochoa et al. 2006; Berlutti et al. 2008; Ammendolia et al. 2010; Frioni et al. 2014]. Lf has also been shown to inhibit the adherence of enterotoxigenic *E. coli* (ETEC) to human epithelial cells and to intestinal mucosa of germfree mice [Kawasaki et al. 2000], as well as the adhesion of three adhesive diarrheagenic *E. coli* strains (DAEC), enteroaggregative *E. coli* (EAEC) [Araujo et al. 2000] and enteropathogenic *E. coli* (EPEC) [Araujo and Giugliano 2001].

HLf and bLf, human Lfcin (hLfcin) and bovine Lfcin (bLfcin) are all able to bind to Gram-negative and Gram-positive bacterial surfaces [Dalmastri et al. 1988], as well as to host cells, by binding to glycosaminoglycans (GAGs) [Wu et al. 1995] and specifically to heparan sulfate (HS) [Shimazaki et al. 1998].

However, Lf can prevent adhesion through other mechanisms. The importance of the sugar residues on Lf is suggested by the observation that whereas native hLf inhibits *Shigella* spp. adhesion [Willer Eda et al. 2004], recombinant hLf (rhLf), with different glycosylation, has no effect on *Shigella flexneri* adhesion to epithelial cells [Gomez et al. 2003]. Another paper suggests that hLf, rhLf and bLf inhibit the attachment of *Helicobacter felix* to gastric epithelial cells, probably by interaction between oligomannoside-type glycans of Lf and bacterial adhesins that recognize these residues [Dial and Lichtenberger 2003]. Although inhibition of bacterial adhesion seems generally to be mediated by Lf binding to both bacterial and host cell surfaces, the surprising discovery of hLf proteolytic activity [Qiu et al. 1998] provided an additional mechanism to explain Lf anti-adhesive activity. Thus, inhibition by hLf of the adhesion of EPEC strains [Araujo and Giugliano 2001], which use a type III secretory system to deliver effector proteins into the host cell, was ascribed to hLf-mediated degradation of the secreted proteins, EspA, B, D [Ochoa et al. 2003], as well as hLf inhibition of *H. influenzae* and *Aggregatibacter actinomycetemcomitans* adhesion to the degradation of two colonization factors and of autotransporter proteins, respectively [Plaut et al. 2001; Hendrixson et al. 2003; Rose et al. 2003].

Although the experimental conditions of the studies reported were different, the pre-incubation of Lf with host cells seems never to inhibit Gram-positive and Gram-negative bacterial adhesion, suggesting that Lf binding to GAGs or HS is not crucial. Instead, the inhibition of Gram-positive and Gram- negative bacterial adhesion by Lf seems to require Lf binding to bacteria or a putative

Lf-mediated degradation of the adhesins or proteins of the secretory systems. During the adhesion process, bacteria are unable to stimulate the epithelial cell inflammatory responses at significant levels [Berlutti et al. 2003].

1.4.2.4 Inhibition of Bacterial Entry into Host Cells

Some mucosal pathogenic bacteria are capable not only of adhering, but also of entering into non-professional phagocytes, such as epithelial cells. Inside host cells, bacteria are in a protective niche in which they can replicate and persist, thus avoiding host defenses. In addition, antibiotic therapies are not always effective at eradicating intracellular pathogens [Armstead 2011]. Virulence determinants, such as surface proteins able to bind host cells, play a key role in the entry process inside the host cells. Lf has been shown to inhibit the entry of Gram-negative and Gram-positive facultative intracellular bacteria. The first demonstration of the inhibition of bacterial invasion by bLf involved *E. coli* HB101 (pRI203), a recombinant strain able to enter inside cells owing to the *inv* gene located in pRI203 plasmid [Longhi et al. 1993]. Bacterial entry into host cells is mediated by the binding of bacterial invasin, a product of the *inv* gene, to the host integrin receptor. The effectiveness of apo- and holo-bLf and bLfcin towards *E. coli* strain HB101 (pRI203) invasion is correlated with their ability to bind to both cultured cells and the bacterial outer membrane [Longhi et al. 1993]. Likewise, for *Y. enterocolitica* and *Y. pseudotuberculosis*, grown in conditions allowing maximal invasin synthesis, a 10-fold inhibition of invasion of cultured cells by bLfcin was observed [Di Biase et al. 2004]. It appears that the binding of Lf and Lfcin to integrins through the same domains that are targeted by invasin, and to GAGs and/or HP, can induce a dramatic subversion in bacterial-host cell interaction, thus inhibiting bacterial internalization [Ochoa et al. 2006]. Similar mechanisms apply to the inhibition of the invasion of the Gram-positive bacteria *L. monocytogenes*, *Streptococcus pyogenes* (GAS) and *Staphylococcus aureus*, i.e., apo- or holo-bLf binding to both bacterial adhesins and host cells [Ajello et al. 2002]. The ability of bLf to decrease GAS invasion was also confirmed by an in vivo trial carried out on 12 children suffering from pharyngitis and already scheduled for tonsillectomy [Ajello et al. 2002]. Although all studies, reported above, have been carried out with different facultative intracellular microorganisms in different in vitro models, Lf, in apo- or holo-form, always exerts an inhibiting activity against the microbial internalization [Valenti and Antonini 2005; Berlutti et al. 2008; Berlutti et al. 2010]. In contrast to inhibition of bacterial adhesion, Lf binding to GAGs and/or HP of host cells seems crucial in inhibiting bacterial internalization.

1.4.2.5 Antiviral Activity of Lactoferrin in Apo- and Metal-Saturated Forms

The antiviral activity of hLf was first demonstrated in mice infected with the polycythemia-inducing strain of the Friend virus complex (FVC-P) [Lu et al. 1987]. An antiviral activity of both hLf and bLf against enveloped and naked viruses has been shown [Berlutti et al. 2011; Wakabayashi et al.2014]. In some in vitro studies, bLf in apo- and in metal-saturated forms exerts a similar antiviral activity thus indicating that Lf does not only inhibit viral infection through its iron chelating property but also hinders viral attachment to the target host cells through its competitive binding [Marchetti et al. 1996; Marchetti et al. 1998; Marchetti et al. 1999; Siciliano et al. 1999; Superti et al. 2001; Berlutti et al. 2011]. In particular, Lf can interact with negatively charged compounds such as GAGs, thus inhibiting virus-receptor interaction [El Yazidi-Belkoura et al. 2001]. In addition to interacting with GAGs, Lf prevents viral infections by binding to dendritic cell-specific intercellular adhesion molecule 3-grabbing non-integrin (DC-SIGN) and LDL receptors [Groot et al. 2005; Chien et al. 2008]. Moreover, Lf exerts an antiviral activity against cytomegalovirus (CMV), herpes simplex virus (HSV), HIV, rotavirus, poliovirus (PV), respiratory syncytial virus (RSV), hepatitis B virus (HBV), HCV, parainfluenza virus (PIV), alphavirus, hantavirus, human papillomavirus (HPV), feline calicivirus (FCV), adenovirus, enterovirus 71 (EV71), echovirus 6, influenza A virus, Japanese encephalitis virus, and tomato yellow leaf curl virus (TYLCV) [Berlutti et al. 2011; Wakabayashi et al. 2014]. The authors of these two reviews agree that the antiviral effect of Lf occurs in the early phase of infection, preventing the entry of viral particles into the host cells, either by blocking cellular receptors or by directly binding to the viral particles. Lf exerts its antiviral activity against the majority of the tested viruses by binding to HS, while against few viruses by interacting with surface components of viral particles [Berlutti et al. 2011; Wakabayashi et al. 2014]. In particular, Lf binds to E1 and E2 proteins of HCV [Yi et al. 1997], to F protein of RSV [Sano et al. 2003] and to gp120 protein of HIV [Puddu et al. 1998]. Moreover, Lf interacts against both viral particles and host cells when exerting its antiviral activity against Echovirus 6 [Tinari et al. 2005]. It is important to underline that Lang and Colleagues investigated the role of Lf in the entry of SARS pseudovirus into Myc cells. Their results reveal that Lf was able to block the binding of the spike protein to host cells, indicating that Lf exerted its inhibitory function at the viral attachment stage [Lang et al. 2011]. However, Lf did not block the virus entry by the direct interaction of spike protein with ACE2, the functional receptor of SARS-CoV [Lang et al. 2011]. The current accepted model suggests that Lf could block viral entry by interacting with heparan sulfate proteoglycans (HSPGs), which mediate the transport of extracellular virus particles from the low affinity anchoring sites to the high affinity specific entry as ACE2 [Burckhardt and Greber 2009].

1.4.2.6 Anti-inflammatory activity of lactoferrin

The anti-inflammatory activity exerted by Lf is strictly dependent on its ability to enter inside host cells through receptor-mediated endocytosis and to consequently translocate into the nucleus [Ashida et al. 2004], thus modulating pro-inflammatory gene expression in the host cells [Suzuki et al. 2008; Liao et al. 2012]. In fact, the binding between hLf and its receptors (hLfRs) can activate different intracellular signaling pathways [Jiang et al. 2012] or result in the hLf clathrin-mediated endocytosis and subsequent nuclear translocation [Ashida et al. 2004], thus enabling hLf to act as a regulator or trans regulator of cellular gene expression [Legrand 2016]. It has been also found that hLfRs, which are differentially expressed in different tissues and cell types, are related to multifunctional activities of hLf [Suzuki et al. 2005]. In 1991, the first human intestinal receptor from fetal intestinal brush-border membranes was isolated [Kawakami et al. 1991], while, in 2001, this receptor was cloned and functionally studied [Suzuki et al. 2001]. This receptor is currently known as intelectin-1 (ITLN1) [Akiyama et al. 2013]. ITLN1 is a glycoprotein constituted of three 40 kDa subunits that are cross-linked by disulfide bonds making up a 120 kDa homo-trimer of 295 amino acids and N-linked oligosaccharides [Akiyama et al. 2013]. This receptor is present in the intestinal epithelium [Suzuki et al. 2005], in Paneth and goblet cells [Wrackmeyer et al. 2006], as well as on cholangiocytes [Mancinelli et al. 2018]. ITLN1 is a high affinity Lf receptor (Kd = 10^{-6} M) able to transduce several Lf-mediated functions, ranging from the facilitation of intestinal iron absorption in infants to the strengthening of the immune system [Iigo et al. 1999; Donovan 2016; Demmelmair et al. 2017]. Besides ITLN1, Low Density Lipoprotein (LDL) receptor related protein (LRP1), a low specificity receptor, has been isolated [Herz and Strickland 2001; Jeon and Blacklow 2005; Kuhara et al. 2000]. LRP1 can bind to multiple targets. It is a type I transmembrane receptor of 600 kDa, composed of five subunits [Jeon and Blacklow 2005], which is abundantly expressed in hepatocytes, neurons, smooth muscle cells, fibroblasts, and cholangiocytes [Suzuki et al. 2005; Mancinelli et al. 2018]. In hepatocytes, it is involved in the uptake of lipoproteins containing triglycerides and cholesterol through an endocytic pathway. LRP1 has also been shown to take part in several cellular processes, including cell migration, survival, motility, and differentiation, and it has been proven to play a role in different pathologies such as thrombosis, fibrinolysis, and atherosclerosis [Lin and Hu 2014]. Concerning other hLfRs, CD14 has been exclusively found on monocytes, asialoglycoprotein receptor (ASGPR) in the liver, and nucleolin in lymphocytes [Suzuki et al. 2001]. Interestingly, in addition to ITLN1, the surface nucleolin is involved in the ability of hLf to enter into the nucleus [Ashida et al. 2004; Suzuki et al. 2008; Losfeld et al. 2009]. Therefore, due to receptor specificity, hLf can exert several different functions depending on the cell system it acts upon. Regarding bLf, its interaction with hLfRs was first described by Shin et al. [Shin et al.

2008], and its nuclear localization in human enterocytes was then observed [Paesano et al. 2012], thus strengthening and partially explaining how bLf could act as a potent bioequivalent of the human homologue.

The anti-inflammatory activity of bLf, used in several clinical trials, was demonstrated in pregnant and non-pregnant women affected by IDA or AI [Paesano et al. 2006; Paesano et al. 2009; Paesano et al. 2010; Paesano et al. 2012; Paesano et al. 2014; Lepanto et al. 2018]. The women, receiving 100 mg of bLf, iron saturated at 20–30%, two times a day, acquired about 70–84 μg/day of iron, respectively. Although the amount of the supplemented iron by bLf was very far from the one required daily (1–2 mg), a significant surprising increase of the number of RBCs and the concentration of Hb, TSI and sFtn as well as the percentage of hematocrit was detected already after 30 days of the treatment. From all these evidences, it is very clear that Lf efficacy in curing IDA and AI is not directly associated to iron supplementation, but to a more complex mechanism involving the most important proteins of iron homeostasis: Fpn and hepcidin [Paesano et al. 2012; Rosa et al. 2017; Lepanto et al. 2019]. The significant improvement of hematological parameters is related to a consistent decrease of serum IL-6 levels, which, in turn, modulates the Fpn and hepcidin expression [Paesano et al. 2009, Paesano et al. 2010, Paesano et al. 2012; Paesano et al. 2014; Lepanto et al. 2018].

In addition, it has been demonstrated in in vitro experiments on human inflamed macrophages that bLf treatment determines a macrophagic shift from M1 to M2 phenotype. As matter of fact, following inflammatory stimuli, macrophages polarize into M1 phenotype, characterized by the synthesis of pro-inflammatory cytokines, including IL-6, as well as by the dysregulation of the main iron-related proteins, as the down-regulation of Fpn/Cp axis, TfR1 and the up-regulation of cytosolic Ftn [Corna et al. 2010; Recalcati et al. 2010; Cutone et al. 2017]. All these changes lead to the blockade of iron recycling to blood by macrophages, the major iron source for the body deriving from the lysis of senescent erythrocytes [Cutone et al. 2017]. We have proved that bLf reverts iron disorders induced by inflammatory stimuli by down-regulating IL-6 synthesis and up-regulating Fpn expression, thus restoring the physiological cell-to-blood iron export [Cutone et al. 2017]. Importantly, bLf, other than Fpn expression, is able to modulate all the iron-related proteins, up-regulating TfR1, Cp and down-regulating cytosolic Ftn [Cutone et al. 2017] (Figure 9).

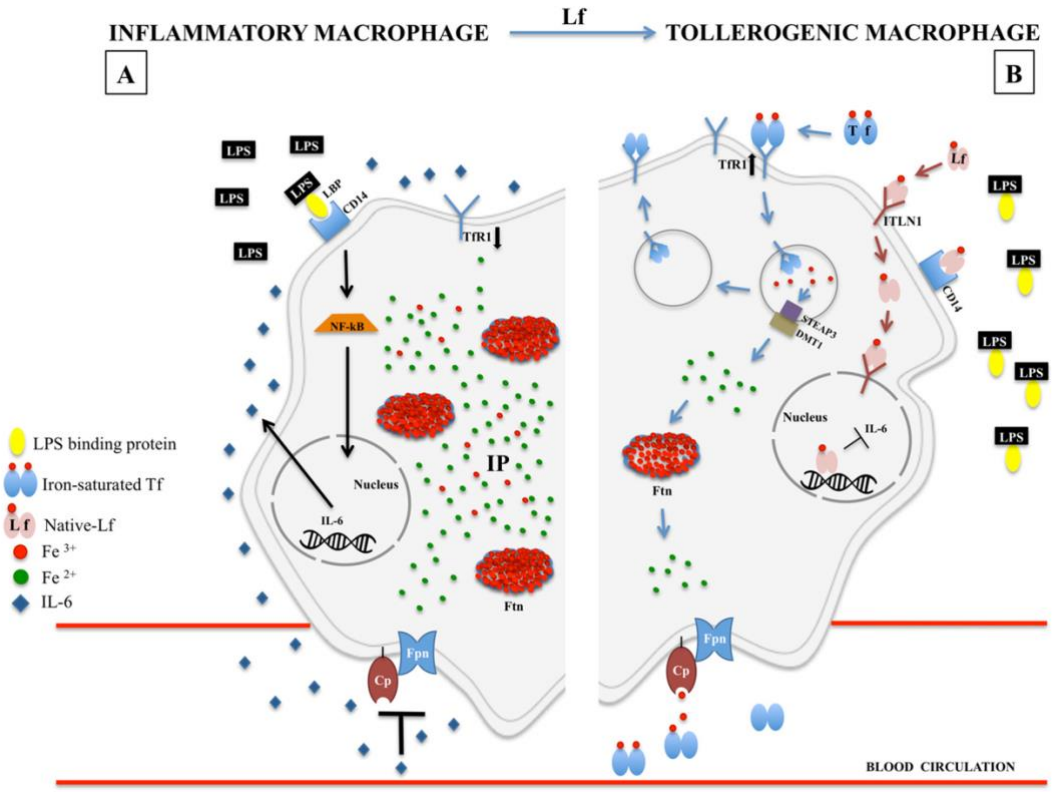

Figure 9. Iron homeostasis in LPS-inflamed macrophages, in the absence (A) or presence (B) of lactoferrin. (A) LPS stimulation, triggered by LPS-binding protein (LBP) and CD-14, induces the nuclear translocation of cytoplasmic NF-κB which in turn induces IL-6 synthesis. Serum IL-6 down-regulates Fpn/Cp axis, inhibiting iron export from the macrophage to blood circulation. Consequently, the increase of intracellular iron pool (IP) triggers the up-regulation of intracellular Ftn and the down-regulation of TfR1 expression thus hindering additional intracellular iron accumulation. (B) Lf-mediated inflammatory-to-tolerogenic macrophagic shift. Lf is internalized by ITLN1-mediated endocytosis and translocated into the nucleus where it inhibits IL-6 synthesis. As a cascade, the inhibition of IL-6 synthesis restores Fpn/Cp-mediated iron export from the macrophage to blood circulation. Consequently, the decrease of intracellular IP triggers either the inhibition of Ftn synthesis and the up-regulation of TfR1, thus restoring the physiological iron balance between reticuloendothelial system and blood. LPS: lipopolysaccharide; LBP: LPS binding protein; NF-κB: nuclear factor-κB; IL-6: interleukin-6; IP: iron pool; Fpn: ferroportin; Cp: ceruloplasmin; Ftn: ferritin; Tf: transferrin; TfR1: transferrin receptor 1; Lf: lactoferrin; ITNL1: intelectin-1; STEAP3: six-transmembrane epithelial antigen of the prostate 3; DMT1: divalent metal transporter 1. The Figure was taken from Lepanto et al. [2019].

2. AIM

As reported in Introduction section, the major proteins involved in iron homeostasis are differently dysregulated by the type of infection (e.g. facultative or obligate intracellular microorganisms) as well as the type of organ affected (e.g. lung or intestine).

Lactoferrin (Lf), a cationic glycoprotein of natural immunity, exerts multiple functions both dependent and independent of its iron-withholding ability and represents one of the most important endogenous anti-microbial constituents of human secretions [Valenti and Antonini 2005; Rosa et al. 2017]. The milk derivative bovine Lf (bLf) shares high sequence homology with the human protein, showing identical properties [Valenti and Antonini 2005]. In particular, unrelated to its iron-withholding function, bLf inhibits the host cell invasion by some intracellular facultative or obligate bacterial pathogens [Frioni et al. 2014; Valenti et al. 2017; Lepanto et al. 2019] as well as inhibits the viral entry into host cells [Berlutti et al. 2011 and reference therein]. Noteworthy, it exerts a potent anti-inflammatory activity, contributing to mucosal protection from inflammation-related damage [Lepanto et al. 2019 and reference therein]. The anti-inflammatory activity exerted by bLf is strictly dependent on its ability to enter inside host cells through receptor-mediated endocytosis and to consequently translocate into the nucleus [Ashida et al. 2004], thus modulating pro-inflammatory gene expression in the host cells [Suzuki et al. 2008; Liao et al. 2012]. Recently, it has been demonstrated that bLf is involved in the modulation of iron homeostasis [Bonaccorsi di Patti et al. 2018]. In particular, in human macrophages stimulated with LPS, bLf was found to be able to modulate the expression of Fpn, Ftn, TfR-1, and membrane-bound Cp [Cutone et al. 2017].

Here, the role of milk derivative bLf in counteracting infection, inflammation and related iron homeostasis disorders in different infection models is discussed.

The first model highlights the in vitro and in vivo role of bLf in counteracting *Chlamydia trachomatis* infection and related inflammatory as well as iron homeostasis disorders induced by this bacterium, prototype of obligate intracellular pathogen. *C. trachomatis* infection is asymptomatic in about 80% of women and causes acute and chronic infections. Unlike acute infections, which can be cured with antibiotics, chronic infections are difficult to eradicate and need prolonged therapies, thus increasing the risk of developing antibiotic resistance [Mitchell et al. 1991]. In addition, following *C. trachomatis* infection, cervical epithelial cells produce several pro-inflammatory cytokines including TNF-α, IL-1β, IL-6, and IL-8 that augment the cell inflammatory response, thus inducing direct damage to genital tissues. Furthermore, IL-8, in turn, recruits innate immune cells, which are abundant in the genital mucosa and are able to further worsen chronic inflammation and tissue-damage of the reproductive system [Redgrove and McLaughlin 2014]. At last, little is known about *C. trachomatis* infection and related iron homeostasis disorders. In

particular, *C. trachomatis* enters into the persistence state in the presence of iron-chelating drugs, which inhibit the developmental cycle and, hence, show its dependence on iron for the achievement of infectious cycle [Raulston 1997; Thompson and Carabeo 2011]. In this regard, iron limitation in host cells has been shown to be of the utmost importance for the growth and survival of *Chlamydia* spp. [Raulston 1997; Al-Younes et al. 2001]. Taken together these evidences, the aim of this part of the study is to evaluate the role of bLf on *C. trachomatis* infection, inflammation and the putative iron homeostasis disorders in in vitro model and the effects of bLf intravaginal treatment on pregnant women affected by *C. trachomatis* infection associated with inflammatory state in in vivo study.

The second model regards the in vivo role of aerosolized bLf in counteracting infection and inflammation as well as iron dysbalance in a CF and WT mouse model affected by chronic *Pseudomonas aeruginosa* lung infection. Recently, it has been investigated the role of aerosolized bLf against infection and inflammation in murine models of acute and chronic *P. aeruginosa* lung infection [Valenti et al. 2017]. Interestingly, it has been found that bLf was efficient in reducing, yet not significantly, bacterial load in both acute and chronic infection, compared to the control groups. Regarding inflammation, bLf-treated mice showed a significant decrease of several pro-inflammatory cytokines as well as of total leukocytes and neutrophils counts in broncho-alveolar lavage fluid for both acute and chronic infection models, compared to saline treated ones [Valenti et al. 2017]. In addition, Frioni et al. [2014] showed in vitro a rebalance of Fpn synthesis after bLf treatment in CF polarized epithelium infected with the *P. aeruginosa* strain. Here, the efficacy of aerosolized bLf in counteracting infection and inflammation as well as iron dysbalance in a CF and WT mouse model affected by chronic *P. aeruginosa* lung infection is explored.

The third and last model regards the role of bLf on SARS-CoV-2 infection. Two promising *in vitro* studies, the first on SARS-CoV [Lang et al. 2011] and the second on SARS-CoV-2 [Mirabelli et al. 2020] have demonstrated that Lf is able to inhibit the early phase of virus infection [Lang et al. 2011] and is efficient against SARS-CoV-2 also in post-infection phase [Mirabelli et al. 2020].

Therefore, based on these evidences, and in order to evaluate the possibility of using bLf in the clinical treatment of COVID-19, we tested the antiviral activity in *in vitro* experiments to verify if its activity was related to the binding to viral particles and/or to host cells similarly to what happens with other viruses [Berlutti et al. 2011; Wakabayashi et al. 2014]. Furthermore, the SARS-CoV-2 Spike trimer structure in prefusion conformation has been used to perform a protein-protein molecular docking analysis with the aim to confirm the hypothesis of a direct interaction between the Spike glycoprotein and the bLf protein. The structure of the Spike S glycoprotein [Wrapp et al. 2020] has been completed using modelling techniques and used to predict Lf interaction sites.

Furthermore, the selected high-score protein-protein complex has been structurally investigated using classical molecular dynamics (MD) simulation and the free energy of interaction between these proteins has been evaluated through the molecular mechanic energies combined with generalized Born and surface area continuum solvation (MM/GBSA) method.

Hence, a clinical trial has been designed to validate the aforementioned assumptions. We conducted a parallel 3 groups clinical trial to investigate effect and tolerability of a liposomal bLf formulation as a supplementary nutraceutical agent in COVID-19 patients. A total of ninety-two COVID-19 patients, twenty-five asymptomatic and sixty-seven mild-to-moderate, were recruited and divided in 3 groups according to the administered regimen: 32/92 COVID-19 patients, fourteen hospitalized and eighteen in home-based isolation, received oral and intranasal liposomal bLf supplement; thirty-two COVID-19 hospitalized patients were treated with hydroxychloroquine, azitromicin and lopinavir/darunavir as standard of care treatment; twenty-eight COVID-19 patients, in home-based isolation did not take any medication against COVID-19. Furthermore, a group of thirty-two healthy subjects with negative COVID-19 rRT-PCR was added as a control group for ancillary analysis.

3. MATERIALS AND METHODS

3.1. Bacterial and viral strains, cell cultures and animal model

3.1.1 Propagation and titration of Chlamydia trachomatis strain and cell culture

Chlamydia trachomatis L2 strain 434/Bu (VR-902B) was obtained from the American Type Culture Collection (ATCC). The human epithelial HeLa-229 cell line from cervix adenocarcinoma (ATCC CCL-2.1) was cultured at 37 °C in Dulbecco's Modified Eagle Medium (DMEM; Euroclone, Milan, Italy), supplemented with 10% fetal bovine serum (FBS; Euroclone, Milan, Italy), in a humidified atmosphere with 5% CO_2.

Elementary body (EB) aliquots of *C. trachomatis* L2 were stored at −80 °C and propagated in HeLa-229 cells, grown in DMEM supplemented with 10% FCS, as previously described by Mastromarino et al. [2014]. The infectious titer was assessed by immunofluorescence assay (IFA). Briefly, HeLa-229 cells grown on glass coverslips in 24-well plates were infected with 10-fold serial dilutions of bacterial stock, incubated for 48 h at 37 °C, fixed with methanol and stained with fluorescein isothiocyanate-conjugated monoclonal (FITC) antibody anti-*C. trachomatis* (MicroTrak, Trinity Biotech). The total number of *C. trachomatis* inclusion forming units (IFUs) was obtained by counting all fields using a fluorescence microscope (100× magnification).

3.1.2 Pseudomonas aeruginosa strain and animals

Pseudomonas aeruginosa MDR-RP73, a clinical strain isolated at the late stage of chronic lung disease from a patient with CF [Jeukens et al. 2013], was checked for purity on trypticase soy agar (TSA) plates (Becton Dickinson, Sparks, Maryland, USA). *P. aeruginosa* strain were grown in tryptic soy broth (TSB) (Becton Dickinson, Sparks, Maryland, USA) to the exponential growth phase. Next, the bacteria were pelleted by centrifugation (2,700 g, 15 min, 4 °C) and washed twice with sterile phosphate-buffered saline (PBS) before infection.

Animals employed in all procedures were 11–14 week-old gut-corrected CFTR-deficient C57BL/6 $Cftr^{tm1UNC}$TgN (FABPCFTR)#Jaw mice (CF mice) and their WT littermates. Mice were originally obtained from Case Western Reserve University and maintained at San Raffaele Scientific Institute (Milan, Italy). Throughout all experimental procedures, in order to maintain definite pathogen-free conditions, mice were retained in sterile ventilated cages. Fluorescent lights were cycled 12 h on, 12 h off, and ambient temperature (23±1 °C) and relative humidity (40–60%) were controlled. Mice were fed with irradiated 5K-52 rodent chow (Safe, Augy, France) and autoclaved tap water. Intraperitoneal injection of 2.5 mg of 2,2,2-tribromethanol (Avertin, Sigma-Aldrich, St. Louis, MO, USA) in saline solution was administered (15 μL/g volume/body weight) to anesthetize mice. A ventral midline incision was carried out to directly visualize and expose the trachea. Mice were

intubated with a sterile and flexible 22-gauge catheter (Becton Dickinson, Madrid, Spain) attached to a 1 mL syringe [Facchini et al. 2014].

Animal studies were conducted according to protocols approved (3 December, 2015) by San Raffaele Scientific Institute (Milan, Italy) Institutional Animal Care and Use Committee (IACUC#733) and adhered strictly to the Italian Ministry of Health guidelines for the use and care of experimental animals.

3.1.3 SARS-CoV-2 strain and cell cultures

SARS-CoV-2 strain was isolated from nasopharyngeal specimen taken from a patient with laboratory confirmed COVID-19.

The African green monkey kidney-derived Vero E6 and human colon carcinoma-derived Caco-2 cells were provided by ATCC. Cells were grown in high-glucose Dulbecco's modified Eagle's medium (DMEM) (Euroclone, Milan, Italy) supplemented with 10% FBS (Euroclone, Milan, Italy) at 37°C in humidified incubators with 5% CO2.

SARS-CoV-2 strain was propagated in Vero E6 cells. Viral titres were determined by 50% tissue culture infectious dose (TCID50) assays in Vero E6 (Spearman-Kärber method) by microscopic scoring. All experiments were performed at the Department of Molecular Medicine, University of Padua, under Biosafety Level 3 (BSL3) protocols, in compliance with laboratory containment procedures approved by the University of Padua.

3.2 Lactoferrin

For in vitro experiments, highly purified bLf was kindly provided by Morinaga Industries (Japan). BLf was checked by SDS-PAGE and silver nitrate staining. Its purity was about 98% and its concentration was confirmed by UV spectroscopy according to an extinction coefficient of 15.1 (280 nm, 1% solution) [Rosa et al. 2018]. The bLf iron saturation was about 10-15% as detected by optical spectroscopy at 468 nm based on an extinction coefficient of 0.54 (100% iron saturation, 1% solution). LPS contamination of bLf, estimated by Limulus Amebocyte assay (Pyrochrome kit, PBI International, Italy), was equal to 0.6 ± 0.05 ng/mg of bLf. Before each in vitro assay, bLf solution was sterilized by filtration using 0.2 µm Millex HV at low protein retention (Millipore Corp., Bedford, MA, USA).

3.3 Infection assays and treatments

3.3.1 Effects of bovine lactoferrin on C. trachomatis elementary bodies infection of HeLa-229 cells

In order to investigate the putative interaction of bLf with bacteria and/or host cells, the following different experimental approaches were performed. To evaluate if bLf can interfere with the *C. trachomatis* infectivity rate by binding bacterial surface components, 25,000 *C. trachomatis* EBs/mL, corresponding to a multiplicity of infection (MOI) of 0.05, were pre-incubated in DMEM with FBS 2% (fresh medium), in the absence or presence of bLf (100 µg/mL), for 1 h or 3 h at 37 °C in humidified atmosphere with 5% CO_2. Subsequently, the *C. trachomatis* EBs suspension was centrifuged at 30,000g for 15 min, and the supernatant was removed. The pellet containing *C. trachomatis* EBs was suspended in fresh medium and used to infect a total of about $1x10^5$ HeLa-229 cells. Briefly, after 1 h, the cells were washed with PBS to remove the non-internalized *C. trachomatis* EBs and newly incubated in fresh medium. After 48 h post infection (hpi) at 37 °C in 5% CO_2, the total number of *C. trachomatis* IFU was determined by IFA. In order to evaluate if bLf interferes with the *C. trachomatis* attachment to host cells, HeLa-229 cells were pre-incubated in fresh medium in the absence or presence of bLf (100 µg/mL). After 1 h or 3 h of incubation at 37 °C in 5% CO_2, bLf was removed by washing the cell monolayers 3 times with PBS. Subsequently, HeLa-229 cells were infected with *C. trachomatis* at a MOI of 0.05 as above described. After 48 hpi at 37 °C in 5% CO_2, the total number of *C. trachomatis* IFU was determined by IFA. To assess if bLf can interfere with both bacterial and host cell components, bLf was added to HeLa-229 cells at the moment of infection. Briefly, HeLa-229 cells were infected with *C. trachomatis* at a MOI of 0.05 in the absence or presence of bLf (100 µg/mL). After 1 h at 37 °C in 5% CO_2, the cells were washed with PBS to remove the non-internalized *C. trachomatis* EBs, and fresh medium was added. After 48 hpi at 37 °C and 5% CO_2, the total number of *C. trachomatis* IFU was determined by IFA. At last, bLf was added to HeLa-229 cells 3 h after *C. trachomatis* infection. HeLa-229 cells were infected with *C. trachomatis* at a MOI of 0.05. After 1 h of incubation at 37 °C in 5% CO_2, the cells were washed with PBS to remove the non-internalized *C. trachomatis* EBs and fresh medium was added. After further 3 h of incubation at 37 °C in 5% CO2, fresh medium, with or without bLf (100 µg/mL), was added to the infected cells. After 48 hpi at 37 °C and 5% CO_2, the total number of *C. trachomatis* IFU was determined by IFA.

3.3.2 Effects of bovine lactoferrin on P. aeruginosa chronic infection of WT and CF mice

To establish the chronic infection, mouse lungs were inoculated with 50 µL of an agar bead suspension containing $1.0\pm0.1 \times 10^6$ CFUs of *P. aeruginosa* MDR-RP73 to mimic biofilm lifestyle

[Facchini et al. 2014; Bianconi et al. 2015; Cigana et al. 2016]. *P. aeruginosa* strain was implanted via the cannula into the lung with both lobes inoculated. 36 CF and 31 WT mice were randomly assigned to the bLf or saline group. Aerosolized treatments with saline (control group) or bLf (200 μg/50 μL of freshly prepared solution) were performed by using the micro-spray aerosol device (MicroSprayer aerosolizer model IA-C and FMJ-250 high-pressure syringe; Penn-Century Inc., Windmoor, PA, USA). Administrations were performed 5 min after infection under anesthesia (5% isoflurane–oxygen, running at 4 L/min) according to established procedures. BLf or saline treatments were repeated daily for seven days. As previously reported [Facchini et al. 2014; van Heeckeren 2012], mice suffered inoculation of agar beads and related procedures with major differences between WT and CF mice. In particular, 42% of CF mice (15 CF) and 80% of WT (25 WT) survived the infection. Thus, the final groups were composed by: 8 CF-vehicle treated, 7 CF-bLf treated and 11 WT-vehicle treated, 14 WT-bLf treated. All mice survived over seven days treatment and were sacrificed six hours after the last treatment.

After the sacrifice of the mice, broncho-alveolar lavage fluid (BALF) and lung homogenates were collected and analyzed. Briefly, a total of 1 mL of RPMI 1640 with protease inhibitors (Complete tablets, Roche Diagnostic, Basel, Switzerland) was used to perform the broncho-alveolar lavage through a 22-gauge venous catheter. The lavages were repeated three times. The obtained BALFs were aliquoted and serially diluted 1:10 in PBS. Aliquots were used to count *P. aeruginosa* CFUs and total cells. To perform neutrophils and macrophages counts, BALF aliquots were centrifuged (330×g for 8 min at 4 °C). The supernatants were collected and stored at −80 °C and the resulting pellets were resuspended in RPMI, containing 10% FBS, in order to obtain a final cell suspension of about 1×10^6 cells/mL. A total of 150 μL of cell suspension was used to determine differential cell count by cytospins stained with Diff Quick (Medion Diagnostic, Düdingen, Switzerland).

Concerning the lung homogenates, lungs were aseptically removed and homogenized in 2 mL PBS with protease inhibitors. PBS serially 1:10 dilutions of lung homogenates were performed to count *P. aeruginosa* as above described. Afterward, lung homogenates were pelleted by centrifugation (16,000×g for 30 min at 4 °C) and the resulting supernatant and the pellet samples were stored at -80 °C and then used to perform cytokine and western blot analysis, respectively.

3.3.3 Effects of bovine lactoferrin on SARS-CoV-2 infection of Vero E6 and Caco-2 cells

For infection assay, Vero E6 cells were seeded in 24-well tissue culture plates at a concentration of $1x10^5$ cells/well for 24h at 37°C in humidified incubators with 5% CO_2, while Caco-2 cells were seeded at a concentration of $2x10^5$ cells/well for 48h at 37°C in humidified incubators with 5% CO_2. In order to assess the putative inhibition of SARS-CoV-2 strain infection on monkey Vero E6 cells, 100 μg/ml of bLf were used. Conversely, the supposed antiviral activity against SARS-CoV-

2 strain on human Caco-2 cells has been investigated using not only 100 but also 500 μg/ml of bLf. In order to investigate the putative interaction of bLf with viral particles and/or host cells, the following different experimental approaches in both Vero E6 and Caco-2 cells were performed. To evaluate if bLf can interfere with the viral infectivity rate by binding viral surface components, SARS-CoV-2 at MOI of 0.1 and 0.01 was pre-incubated with bLf for 1h at 37°C in humidified incubators with 5% CO_2. The cells were then infected with these suspensions for 1h at 37°C in humidified incubators with 5% CO_2. In order to evaluate if bLf interferes with the viral attachment to host cells, the cells were pre-incubated in culture medium without FBS with bLf for 1h at 37°C in humidified incubators with 5% CO_2. The cells were then washed PBS and infected with SARS-CoV-2 at MOI of 0.1 and 0.01 for 1h at 37°C in humidified incubators with 5% CO_2. To assess if bLf can interfere with both viral and host cell components, bLf was added together with SARS-CoV-2 at MOI of 0.1 and 0.01 to cell monolayer for 1h at 37°C in humidified incubators with 5% CO_2. In addition, the pre-incubation of SARS-CoV-2 with bLf for 1h at 37°C was used to infect cell monolayer previously pre-treated with bLf for 1 h at 37°C.

Regarding Vero E6 cells, after each experimental approach, the cells were washed with PBS, overlaid with DMEM containing 0.75% of carboxymethylcellulose and 2% of FBS and incubated for 48h at 37°C in humidified incubators with 5% CO_2. After 48h, the cells were washed, fixed with 5% of formaldehyde for 10 min at room temperature and stained with crystal violet at 1% for 5 min. The number of plaques was determined after extensive washing.

The other infection experiments were carried out with Caco-2 cells. Substantial cell death was not detected up to 7 days on Caco-2 cells after SARS-CoV-2 infection at MOI 0.1 [Chu et al. 2020]. In this respect, after each experimental procedure, the cell monolayers were replaced with DMEM with 2% of FBS and after 6, 24 and 48 hpi the supernatant samples were collected for RNA extraction and quantitative real-time reverse transcription (rRT)-PCR analysis of viral particles. Briefly, we lysed 200 μl of supernatant in an equal volume of NUCLISENS easyMAG lysis buffer (Biomerieux, France). Detection of SARS-CoV-2 RNA was performed by an in-house real-time RT–PCR method, which was developed according the protocol and the primers and probes designed by Corman et al. [2020] that targeted the genes encoding envelope (E) (E_Sarbeco_F, E_Sarbeco_R and E_Sarbeco_P1) of SARS-CoV-2. Quantitative rRT–PCR assays were performed in a final volume of 25 μl, containing 5 μl of purified nucleic acids, using One Step Real Time kit (Thermo Fisher Scientific) and run on ABI 7900HT Fast Sequence Detection Systems (Thermo Fisher Scientific). Cycle threshold (Ct) data from rRT–PCR assays were collected for E genes. Genome equivalent copies per ml were inferred according to linear regression performed on calibration standard curves.

3.4 In silico analysis of interaction between bovine lactoferrin and Spike glycoprotein of SARS-CoV-2

Protein-protein docking methods: the structure of the SARS-CoV-2 spike glycoprotein in prefusion conformation was extracted from a clustering procedure carried out as indicated in a previously published paper [Romeo et al. 2020]. The three-dimensional structure of the diferric forms of bLf and hLf, refined at 2.8 Å and 2.2 resolution respectively, were downloaded from the PDB Database (PDB IDs: 1BFL, [Lang et al. 2011] and 1B0L, [Sun et al. 1999]). The protein-protein docking analysis between the modelled SARS-CoV-2 spike glycoprotein [Romeo et al. 2020] and the Lf structures was carried out using the Frodock docking algorithm [Ramirez-Aportela et al. 2016]. Frodock's approach combines the projection of the interaction terms into 3D grid-based potentials and the binding energy upon complex formation, which is approximated as a correlation function composed of van der Waals, electrostatics and desolvation potential terms. The interaction-energy minima are identified through a fast and exhaustive rotational docking search combined with a simple translational scanning [Garzon et al. 2009]. Both docking procedures were performed using Frodock's (http://frodock.chaconlab.org/) web-server.

Molecular dynamics: topology and coordinate files of the input structures were generated using the tLeap module of the AmberTools 19 package [Salomon-Ferrer et al. 2013]. The spike glycoprotein and Lf were parametrized using the ff19SB force field, and were inserted into a rectangular box of TIP3P water molecules, with a minimum distance of 12.0 Å from the box sides, and after neutralizing the solution with 0.15 mol/L of NaCl ions. To remove unfavorable interactions, all structures underwent four minimization cycles, each composed by 500 steps of steepest descent minimization followed by 1500 steps of conjugated gradient minimization. An initial restraint of 20.0 kcal • mol-1 • Å-2 was imposed on protein atoms and subsequently reduced and removed in the last minimization cycle. Systems were gradually heated from 0 to 300 K in a NVT ensemble over a period of 2.0 ns using the Langevin thermostat, imposing a starting restraint of 0.5 kcal • mol-1 • Å-2 on each atom, which was decreased every 500 ps in order to slowly relax the system. The systems were simulated in an isobaric-isothermal (NPT) ensemble for 2.0 ns, imposing a pressure of 1.0 atm using the Langevin barostat and fixing the temperature at 300 K. Covalent bonds involving hydrogen atoms were constrained using the SHAKE algorithm [Ryckaert et al. 1977]. A production run of 30 ns was performed for with a timestep of 2.0 fs, using the NAMD 2.13 MD package [Ng et al. 2015]. The PME method was used to calculate long-range interactions, while a cut-off of 9.0 Å was set for short-range interactions. System coordinates were saved every 1000 steps.

Trajectory analysis: distance analysis was performed using the distance module of the GROMACS 2019 analysis tools [Abraham et al. 2015], while hydrogen bond persistence was evaluated using the hbonds module coupled to in-house written codes. The hydrophobic contacts were identified using the contact_map and contact_frequency routines of the mdtraj Python library [McGibbon et al. 2015]. Generalized Born and surface area continuum solvation (MM/GBSA) analysis were performed over the last 15 ns of the trajectories, using the MMPBSA.py.MPI program implemented in the AMBER16 software [Case et al. 2016] on 2 nodes of the ENEA HPC cluster CRESCO6 [Ponti et al. 2014]. Pictures of the Spike-Lf and Spike RBD-ACE2 complexes were generated using the UCSF Chimera program [Pettersen et al. 2014].

3.5 Detection of cytokines

3.5.1 Effects of bovine lactoferrin on Chlamydia trachomatis-induced inflammation

Preliminary experiments, carried out with *C. trachomatis* EBs at a MOI of 0.05, showed a very low cytokine expression by infected HeLa-229 cells. Therefore, HeLa-229 cells were infected with *C. trachomatis* EBs at a MOI of 5 to reach a higher expression of IL-6 and IL-8 than that observed at the MOI of 0.05. After 1 h of incubation, the cells were washed with PBS to remove the non-internalized *C. trachomatis* EBs and supplemented with fresh medium. After further 3 h of incubation at 37 °C in 5% CO_2, fresh medium, with or without bLf (100 μg/mL), was added to the infected cells. The cytokine production was determined in cell monolayer supernatants by ELISA using Human ELISA Max Deluxe Set (BioLegend, San Diego, California, USA) after 48 h of incubation at 37 °C in 5% CO_2.

3.5.2 Effects of bovine lactoferrin on Pseudomonas aeruginosa-induced inflammation

After quantification of total protein content with Bradford's assay (Bio-Rad, Hercules, CA, USA), cytokine levels in supernatants of lung homogenates were analyzed using the Bio-Plex Protein Array System (Bio-plex Pro Mouse Cytokine 23-Plex Immunoassay, Bio-Rad, Hercules, CA, USA) according to the manufacturer's instruction. The following inflammatory cytokines and chemokines were detected: IL-1α, IL-1β, IL-2, IL-3, IL-4, IL-5, IL-6, IL-9, IL-10, IL-12(p40), IL-12(p70), IL-13, IL-17, Eotaxin, G-CSF, GM-CSF, IFN-γ, KC, MCP-1, MIP-1α, MIP-1β, RANTES, and TNF-α.

3.6 Detection of protein involved in iron homeostasis

3.6.1 Effects of bovine lactoferrin on Chlamydia trachomatis-induced iron homeostasis disorders

As reported in section 3.5.1, *C. trachomatis* EBs at a MOI of 0.05 showed a very low cytokines expression by infected HeLa-229 cells. Therefore, HeLa-229 cells were infected with *C. trachomatis* EBs at a MOI of 5 in order to induce a massive inflammation that, in turn, induces a dysregulation of the major proteins of iron homeostasis. After 1 h of incubation, the cells were washed with PBS to remove the non-internalized *C. trachomatis* EBs and supplemented with fresh medium. After further 3 h of incubation at 37 °C in 5% CO_2, fresh medium, with or without bLf (100 μg/mL), was added to the infected cells for 48h. After 48h, the adherent cells were scraped in 2 ml of PBS containing 1 mM phenylmethylsulfonyl fluoride (PMSF), pelleted by centrifugation at 2,500×g for 5 min, and stored at −80°C for protein analysis. Pellets of cells were suspended in 300 μL of lysis buffer (25 mM 3-morpholinopropane-1-sulfonic acid pH 7.4/150 mM NaCl/1% Triton containing 1 mM PMSF, 2 μM leupeptin, and pepstatin) and let to solubilize in ice for 1 h. Afterward, samples were centrifuged (20,000×g for 30 min at 4 °C). Total protein content of samples was measured by Bradford assay and a total of 20 μg of protein was used for Sodium Dodecyl Sulphate - PolyAcrylamide Gel Electrophoresis (SDS-PAGE). Prior loading, samples were mixed with SDS sample buffer containing 1,4-dithiothreitol and heat-treated (except for Fpn). Primary antibodies used for Western blots were: monoclonal anti-Tf receptor 1 (anti-TfR) (Santa Cruz, CA, USA) (1:5,000), monoclonal anti-Fpn 31A5, generously provided by T. Arvedson (Amgen, Thousand Oaks, CA, USA) (1:10,000) [Ross et al. 2012], polyclonal anti-Ftn (Santa Cruz, CA, USA) (1:10,000) and monoclonal anti-actin (Santa Cruz, CA, USA) (1:10,000). After proper secondary antibody (Horseradish Peroxidase-conjugated), Enhanced ChemiLuminescence (ECL Prime) (GE Healthcare, Little Chalfont, UK) was used for blot development. Protein levels were normalized on β-actin by using ImageJ program.

3.6.2 Effects of bovine lactoferrin on Pseudomonas aeruginosa-induced iron homeostasis disorders

Pellets of lung homogenates were suspended in 500 μL of lysis buffer (25 mM MOPS pH 7.4/150 mM NaCl/1% Triton and protease inhibitors) and let to solubilize in ice for 1 h. Afterward, samples were centrifuged (20,000×g for 30 min at 4 °C) and supernatants were collected and stored at −80 ◦C). Total protein content of samples was measured by Bradford assay and a total of 20 μg of protein was used for SDS-PAGE. Prior loading, samples were mixed with SDS sample buffer containing 1,4-dithiothreitol and heat-treated (except for Fpn). Primary antibodies used for Western blots were: monoclonal anti-transferrin receptor 1 (anti-TfR) (Santa Cruz, CA, USA) (1:5,000), monoclonal anti-Fpn 31A5 (Amgen, Thousand Oaks, CA, USA) (1:10,000) [Ross et al. 2012], polyclonal anti-Ftn (Santa Cruz, CA, USA) (1:10,000) and monoclonal anti-actin (Santa Cruz, CA, USA) (1:10,000). After proper secondary antibody (Horseradish Peroxidase-conjugated), Enhanced

ChemiLuminescence (ECL Prime) (GE Healthcare, Little Chalfont, UK) was used for blot development. Protein levels were normalized on β-actin by using ImageJ program.

In addition, BALF was used to determine the total iron content. BALF samples (100 μL) were mixed with 100 μL of 10 mM HCl and with 100 μL of a freshly prepared solution consisting of equal volumes of 1.4 M HCl and 4.5% (w/v) $KMnO_4$ in H_2O (iron-releasing reagent). After incubation for 2 h at 60 °C in a fume hood, samples were cooled to room temperature and 30 μL of the iron-detection reagent (6.5 mM ferrozine, 6.5 mM neocuproine, 2.5 M ammonium acetate and 1 M ascorbic acid) was added and incubated for 30 min. Thereafter, a total of 280 μL of each sample was measured at 550 nm in a 96-well plate using a microplate reader. Iron standard curve (0–300 μM of $FeCl_3$) was used to determine samples' concentrations.

3.7 In vivo studies

3.7.1 Effects of bovine lactoferrin on pregnant women affected by Chlamydia trachomatis infection

Study design: we conducted an open-label cohort study in accordance with the ethical principles of the Declaration of Helsinki. Approval was granted by the Ethics Committee of Clinica Fabia Mater, Via Olevano Romano, 25 Rome, Italy (FM MOD 26022010). All of the pregnant women gave written informed consent.

One hundred ninety-eight pregnant women from 20 to 40 years without ascertained pathologies, with normal uterine cavity, and intact membranes were enrolled regardless of trimester. Women were excluded if they had a pathological pregnancy or if during this study they were affected by bacterial vaginal infections unrelated to *C. trachomatis*.

The exclusion of pregnant women during the clinical trial was also considered on the basis of voluntary declaration, lack of treatment effectiveness, side effects, protocol infringement, and missed programmed visits. The enrolled pregnant women were on a monthly scheduled visit.

Laboratory tests: at each scheduled visit, in addition to standard assays (hematocrit, glycemia, uricemia, bilirubin, glutamicoxaloacetic transaminase, glutamic pyruvic transaminase, cholesterol, triglyceride acid, and electrolytes), cervical specimens were collected with polyethylene terephthalate (Dacron) swabs to detect the presence of *C. trachomatis*. In addition, cervical fluids were analyzed to detect IL-6 concentrations.

Chlamydia trachomatis detection: cervical specimens were analyzed by direct immunofluorescence assay (DFA) using Syva Microtrack kit (Syva Microtrack; Trinity Biotech) according to the manufacturer's instructions. Briefly, the smears were fixed with methanol and stained with fluorescein isothiocyanate conjugated (FITC) monoclonal antibody against *C. trachomatis* major

outer membrane protein (MOMP) for 30 min at 37 °C in a humid chamber. The slides were examined for the presence of IFUs using fluorescence microscope (100× magnification).

Treatment against *C. trachomatis* infection in pregnant women: among one hundred ninety-eight pregnant women, seven women, asymptomatically affected by *C. trachomatis*, were immediately treated with bLf intravaginal administration. The intravaginal tablet, containing 100 mg of lyophilized bLf 20% iron-saturated, was administered every 8 h for 30 days. The tablets were administered through a vaginal applicator to obtain a fast and adequate dissolution. If the treatment with bLf intravaginal administration for 30 days was ineffective, the pregnant women were submitted to antibiotic therapy [Workowski and Bolan 2015].

3.7.2 Effects of bovine lactoferrin on patients affected by SARS-CoV-2 infection

Study population: A clinical trial has been conducted to investigate effect and tolerability of an oral and intranasal liposomal bLf formulation as supplementary nutraceutical agent in the treatment of asymptomatic and mild-to-moderate COVID-19 patients. From April 2020 to June 2020 a total of 92 patients with confirmed COVID19 infection at rRT-PCR nasopharyngeal swab were recruited to participate in the study protocol. Patients were divided in three Groups: thirty-two COVID-19 patients were treated with oral and intranasal liposomal bLf; thirty-two other COVID-19 patients were treated with standard of care (SOC) regimen (hydroxychloroquine, azitromicin and lopinavir/darunavir); twenty-eight COVID-19 patients in home situations didn't receive any anti-COVID-19 treatment.

All the recruited patients were asymptomatic or showed mild-to-moderate symptoms. The classification of mild-to-moderate disease is based on less severe clinical symptoms with no evidence of pneumonia and not requiring Intensive Care Unit (ICU).

A control group of thirty-two healthy volunteers, with negative rRT-PCR at the naso-oropharingeal swab, was included in the study for ancillary analysis.

Enrollment criteria: Eligible patients were over 20 years old, with a confirmed COVID-19 rRT-PCR at the naso-oropharingeal swab and blood oxygen saturation (SpO_2) > 93% or Horowitz index (PaO_2 / FiO_2) > 300mmHg. Patients had not previously been treated against SARS-CoV-2. Exclusion criteria included pregnancy and breastfeeding, nitric oxide and nitrates assumptions, known allergy to milk proteins, a medical history of bronchial hyperactivity or pre-existing respiratory diseases. ICU COVID-19 in-patients were excluded.

In the clinical trial, performed in the middle phase of the pandemic, placebo and liposome arms have not been included due to the specific request of our Hospital Ethics Committee.

All patients gave written informed consent after receiving an extensive disclosure of the study purposes and risks. To be included, patients needed to be able to comprehend the content of

informed consent and accept to sign it. The trial was approved by the Tor Vergata University Hospital Ethics Committee (Code 42/20). It was registered at www.clinicalTrials.gov (NCT04475120) and reported according to CONSORT guidelines (Figure 10).

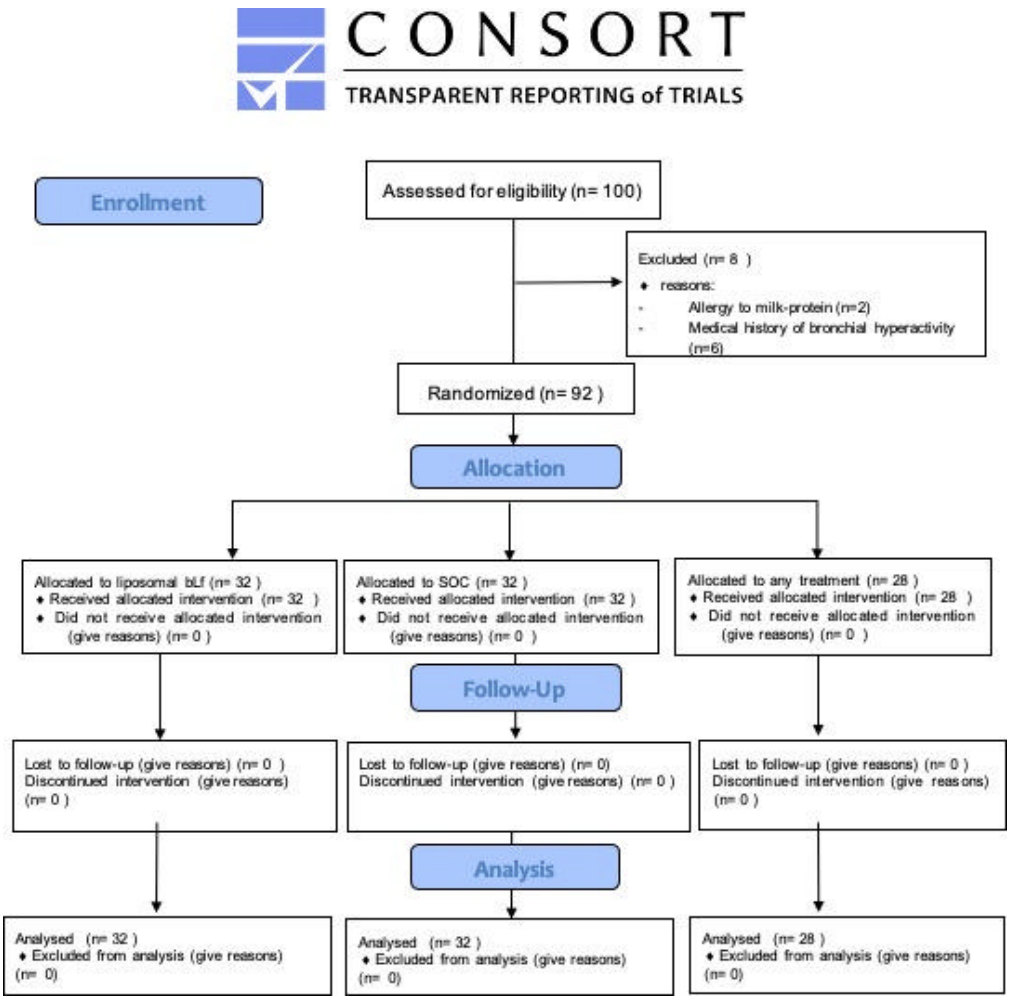

Figure 10. Flow diagram of enrolled patients according to CONSORT guidelines

Patient Groups: Thirty-two patients belonging to the first Group were treated with oral and intranasal liposomial bLf. BLf capsules for oral use contained 100 mg of bLf encapsulated in liposome while bLf nasal spray had about 8 mg/ml of bLf encapsulated in liposome. BLf, contained in both products, was checked by SDS-PAGE and silver nitrate staining and its purity was about 95%. The bLf iron saturation was about 5% as detected by optical spectroscopy at 468 nm based on an extinction coefficient of 0.54 (100% iron saturation, 1% solution). The scheduled dose treatment of liposomal bLf for oral use was 1gr per day for 30 days (10 capsules per day) in addition to the same formulation intranasally administered 3 times daily (a total of about 16 mg/nostril)

Thirty-two patients belonging to the second Group, SOC regimen, were treated with the following drugs provided by national guidelines: lopinavir / ritonavir cps 200/50 mg, 2 x 2 / day (alternatively darunavir 800 mg 1 cp / day + ritonavir 100 mg 1 cp / day or darunavir / cobicistat 800/150 mg 1 cp / day), chloroquine 500 mg, 1 x 2 / day or hydroxychloroquine cp 200 mg, 1 x 2 / day.

SOC regimen lasted from 5 to 20 days, with timing to be established according to clinical evolution.

Twenty-eight patients belonging to the third Group in home situations did not receive any therapy.

The control Group comprising thirty-two healthy volunteers did not receive any treatment or placebo. Blood samples and clinical assessments were evaluated at T0, after 15 days (T1) and after 30 days (T2).

Primary endpoint measures: Primary endpoint was to assess the mean time length needed to reach a rRT-PCR negative conversion rate of SARS-COV-2 RNA in each group of COVID-19 patients enrolled in the study.

Secondary endpoint: Secondary endpoint was to estimate the proportion of patients who achieved disease remission defined as symptoms recovery and improvement of those blood parameters, eventually deranged in COVID-19 patients. In addition, safety and tolerability of liposomal bLf for oral and intranasal use were assessed.

Tertiary endpoint: Tertiary endpoint was an ancillary analysis to evaluate iron, Tf and Ftn variation, together with the following inflammatory cytokines and markers, IL-6, IL-10, TNF-α, adrenomedullin serum levels, in bLf supplemented COVID-19 patients at T0 and T2, but also in comparison with healthy volunteers Group.

3.8 Statistical analysis

All values of *C. trachomatis* infection and related inflammation are the mean ± standard deviation (SD) of 3 replicates from 3 independent in vitro experiments. For the clinical trial, the concentrations of IL-6 in cervical fluid of pregnant women were expressed as mean values ± SD. Comparison of means was performed by using a 2-tailed t-test for independent samples. In each case, a p value ≤ 0.05 was considered statistically significant.

Statistical analysis of *P. aeruginosa* infection and related inflammation and iron homeostasis dysregulation were performed by GraphPad Prism using a two-way analysis of variance (ANOVA) with Bonferroni's multiple comparison test for the body weight lost evaluation and Mann–Whitney U test for the other analysis. Outlier data, identified by Grubbs' test, were excluded by the analysis. In each case, a p value ≤ 0.05 was considered statistically significant.

For in vitro SARS-CoV-2 infection experiments, the number of plaque forming units (pfu)/ml of SARS-CoV-2 on Vero E6 cells and the number of SARS-CoV-2 RNA copies/ml on Caco-2 cells in each experimental approach was compared with the control ones (untreated SARS-CoV-2 and cells)

at the same time point in order to assess the statistically significant differences by using unpaired student's t tests. Results are expressed as the mean values ± SD of three independent experiments. In each case, a p value ≤ 0.05 was considered statistically significant.

For what concerns the clinical trial, descriptive and inferential statistical analyses were performed. The Kolmogorov–Smirnov test was used to check the normal distribution of blood parameters.

Blood parameters obtained at T0 in COVID-19 group and control group were compared using t-test. Data were then analyzed with a significant two-tailed p-value ≤ 0.05.

All parameters obtained at T0 and T2 in COVID-19 group were then compared using paired t-test. In addition, the mean change between T0 and T2 was also assessed using paired t-test. Normally distributed data were then analyzed with a significant p-value ≤ 0.05.

4. RESULTS

4.1. Effect of bovine lactoferrin on infection

4.1.1. Effects of bovine lactoferrin on Chlamydia trachomatis infection

We evaluated the effects of bLf, at non-cytotoxic concentration corresponding to 100 µg/mL on *C. trachomatis* infections.

As shown in Figure 11A, no significant reduction in the number of chlamydial IFUs was observed when chlamydial EBs were pre-incubated with bLf for 1 h or 3 h, indicating no direct effect of bLf on *C. trachomatis*. In contrast, bLf inhibited *C. trachomatis* entry into host cells, as evidenced by a significant reduction of chlamydial IFU observed when HeLa-229 monolayers were pre-incubated with bLf for 1 or 3 h (1 h pre-incubation: $p = 0.0008$; 3 h pre-incubation: $p = 0.00007$) (Figure 11B and 11C). The inhibitory effect of bLf on *C. trachomatis* entry was more pronounced when HeLa-229 cells were preincubated with bLf for 3 h compared with 1 h ($p = 0.0124$) (Figure 11C).

To further confirm the inhibitory effect of bLf on *C. trachomatis* entry into host cells, bLf was added at the moment of HeLa-229 monolayer infection with *C. trachomatis*. The presence of bLf during the infection phase significantly inhibited *C. trachomatis* entry into HeLa-229 cells at the same extent evidenced when bLf was pre-incubated with cell monolayers for 1 or 3 h (Figure 11B, 11C, and 11D). To determine whether bLf inhibited chlamydial replication, bLf was added after 3 h of *C. trachomatis* infection. The addition of bLf under these experimental conditions resulted in no significant reduction of the number of intracellular chlamydial IFUs ($p = 0.28$) (Figure 11E).

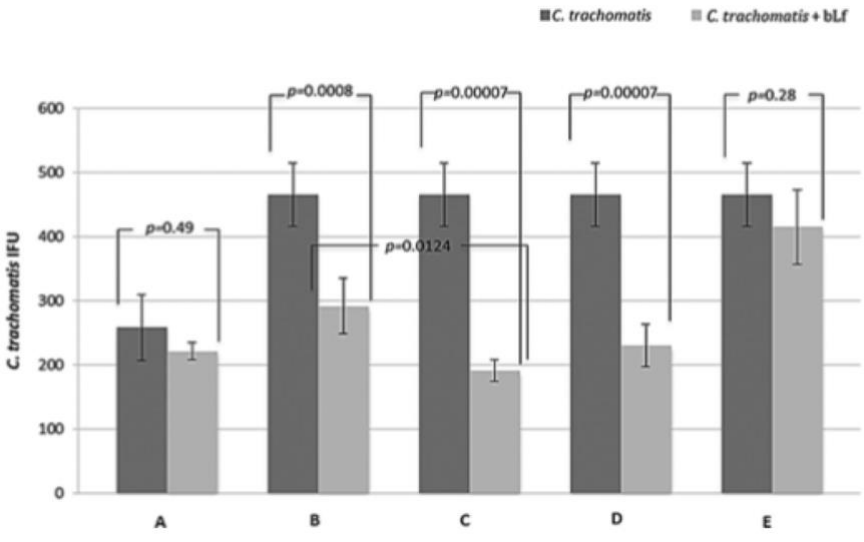

Figure 11. Inclusion forming units (IFU) of *Chlamydia trachomatis* observed by immunofluorescence assay in HeLa-229 cells infected at a MOI of 0.05 in the absence or presence of bLf added at different time. (A) 1 h preincubation of *C. trachomatis* EBs in the absence or presence of bLf; (B) 1 h preincubation of HeLa-229 cells in the absence or presence of bLf; (C) 3 h preincubation of HeLa-229 cells in the absence or presence of bLf; (D) HeLa-229 cells infected with *C. trachomatis* and treated with bLf; (E) Addition of bLf 3 hpi to HeLa-229 infected with *C. trachomatis*. Error bars: standard error of the mean.

4.1.2. Effects of bovine lactoferrin on Pseudomonas aeruginosa infection

To mimic a chronic lung infection similar to the one typically established in the lungs of CF patients, mice were inoculated by intratracheal (i.t.) injection with *P. aeruginosa* multidrug-resistant MDR-RP73 strain embedded in agar beads [Facchini et al. 2014]. Notably, the chronic infection model obtained by inoculating bacterial cells in an immobilizing agent, such as agar, favors long-term bacteria persistence in the lungs causing airway inflammation and damage. This model differs from acute pneumonia where administration of planktonic bacterial cells in mice is rapidly cleared by the host. In this work, the *P. aeruginosa* chronic infection was carried out for seven days. Although in the early phase of chronic infection, in our experience the bacterial load and percentage of infected mice from seven days to one month after infection are similar, indicating that this model develops a stable chronic infection [Facchini et al. 2014].

Local treatment with 200 µg of bLf or sterile saline by a MicroSprayer Aerosolizer device (Penn-Century Inc., Windmoor, PA, USA) started five minutes after infection and was repeated daily for a total of seven administrations.

To evaluate the antibacterial effect of aerosolized bLf, *P. aeruginosa* counts were performed in both BALFs and lung homogenates (Figure 12). A reduction of *P. aeruginosa* Colony Forming Units (CFUs) in bLf-treated vs. untreated WT mice was observed both in BALFs and lung homogenates but differences did not reach statistical significance. On the other hand, a significant reduction of *P. aeruginosa* counts was recorded in both BALFs and lung homogenates of bLf-treated CF mice compared with untreated controls ($p < 0.05$ for BALF and $p < 0.01$ for lung) (Figure 12A, B).

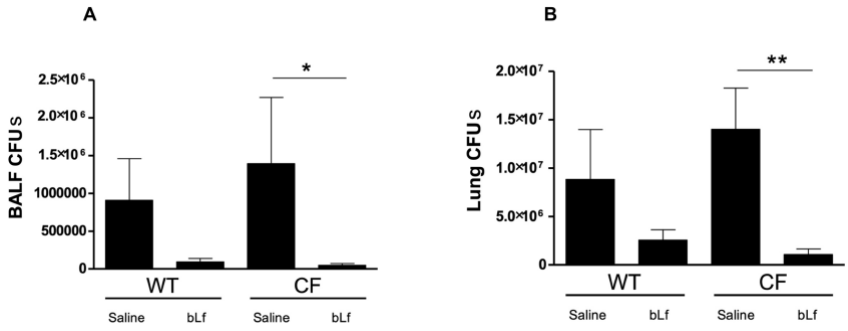

Figure 12. *P. aeruginosa* counts in bronchoalveolar lavage fluid (BALF) (A) and lung homogenates (B) of WT and CF mice after 7 treatments with aerosol administration of 50 µL sterile saline or 200 µg/50 µL bLf. Error bars: standard error of the mean. Statistical significance is indicated as follows: *: $p < 0.05$; **: $p < 0.01$ (Mann Whitney U test).

4.1.3. Effects of bovine lactoferrin on SARS-CoV-2 infection

The efficacy of different concentrations of bLf in inhibiting SARS-CoV-2 infection was tested on Vero E6 and Caco-2 cells according to different experimental procedures: i) control: untreated

SARS-CoV-2 and cells; ii) bLf pre-incubated with virus inoculum for 1 h at 37°C before cell infection; iii) bLf pre-incubated with cells for 1 h at 37°C before virus infection; iv) bLf added together with virus inoculum at the moment of infection step; v) virus and cells separately pre-incubated with bLf for 1 h at 37°C before infection.

The results obtained with Vero E6 cells are shown in Figure 13A (MOI 0.1) and 13B (MOI 0.01).

Regarding Vero E6 cells, an inhibition of SARS-CoV-2 replication of about 1 log at MOI 0.1 and about 2 logs at MOI 0.01 on cell monolayers was observed when 100 µg/ml of bLf were pre-incubated for 1 h with virus before infection compared to untreated SARS-CoV-2 infection ($p < 0.001$ and $p < 0.0001$, respectively) (Figure 13A and 13B). On the contrary, the data illustrated in Figure 13A and 13B, independently from the MOI used, indicate that bLf, at this concentration, does not block SARS-CoV-2 infection when it is pre-incubated with Vero E6 cells or when bLf is contemporary added to viral particles and cells at the moment of infection (Figure 13A, 13B). BLf is also ineffective when it is pre-incubated for 1 h at 37°C separately with virus and cells before infection (Figure 13A, 13B).

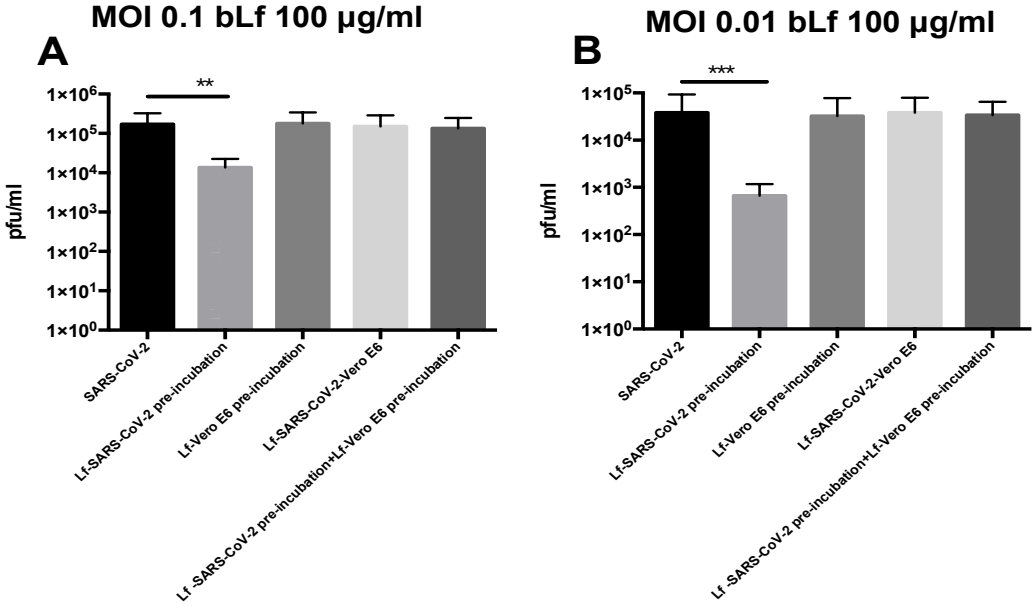

Figure 13. Plaque forming units (pfu)/ml of SARS-CoV-2 observed in Vero E6 cells infected at multiplicity of infection (MOI) of 0.1 (A) and 0.01 (B) in the presence or absence of 100 µg/ml of bovine lactoferrin (bLf) according to the following experimental procedures: i) control: untreated SARS-CoV-2 and Vero E6 cells; ii) bLf pre-incubated with SARS-CoV-2 inoculum for 1h at 37°C before cell infection iii) cells pre-incubated with bLf for 1 h at 37°C before SARS-CoV-2 infection; iv) bLf added together with SARS-CoV-2 inoculum during the adsorption step; v) virus and cells separately pre-incubated with bLf for 1 h at 37°C before infection. Data represent the mean values of three independent experiments. Error bars: standard error of the mean. Statistical significance is indicated as follows: **: $p < 0.001$, ***: $p < 0.0001$ (Unpaired student's *t* test).

The efficacy of 100 and 500 µg/ml of bLf against SARS-CoV-2, assayed in Caco-2 cells, is showed in Figure 14A and 14B (MOI 0.1) and in Figure 14C and 14D (MOI 0.01), respectively.

Regarding Caco-2 cells, at MOI 0.1, no significant differences were observed in all experimental conditions compared to the control ones when using bLf at 100 µg/ml (Figure 14A). At MOI 0.01, an inhibition of viral load in supernatants was observed at 24 hpi only when 100 µg/ml of bLf was pre-incubated with the viral inoculum and when the cells were pre-incubated with 100 µg/ml of bLf compared to the control one ($p < 0.05$) (Figure 14B). At 48 hpi, an inhibition of viral load was observed only when the cells were pre-incubated with bLf ($p < 0.05$) (Figure 14B).

When bLf was used at a concentration of 500 µg/ml, a decrease of viral load up to 48 hpi was observed when the viral inoculum was pre-incubated with bLf compared to the control group, independently from the MOI used ($p < 0.05$) (Figure 14C, 14D). When the cells were pre-incubated with bLf, a decrease of viral load up to 24 hpi was observed compared to the control at MOI 0.1 ($p < 0.001$ after 6 hpi and $p < 0.05$ after 24 hpi) (Figure 14C), while at MOI 0.01 the decrease of viral load remained statistically significant up to 48 hpi compared to the control group ($p < 0.05$) (Figure 14D). When bLf was added together with SARS-CoV-2 inoculum during the adsorption step a decrease of viral load up to 24 hpi was observed compared to untreated SARS-CoV-2 infection, independently from the MOI used ($p < 0.001$ after 6 hpi and $p < 0.05$ after 24hpi for MOI 0.1; $p < 0.05$ after 6 and 24 hpi for MOI 0.01) (Figure 14C, 14D). When the cells were pre-incubated with bLf and infected with SARS-CoV-2 previously pre-incubated with bLf, a decrease of viral load up to 24 hpi was observed for MOI 0.1 compared to untreated SARS-CoV-2 infection ($p < 0.001$ after 6 hpi and $p < 0.05$ after 24hpi for MOI 0.1) (Figure 14C), while at MOI 0.01 the decrease of viral load remains statistically significant up to 48 hpi compared to untreated SARS-CoV-2 infection ($p < 0.05$) (Figure 14D).

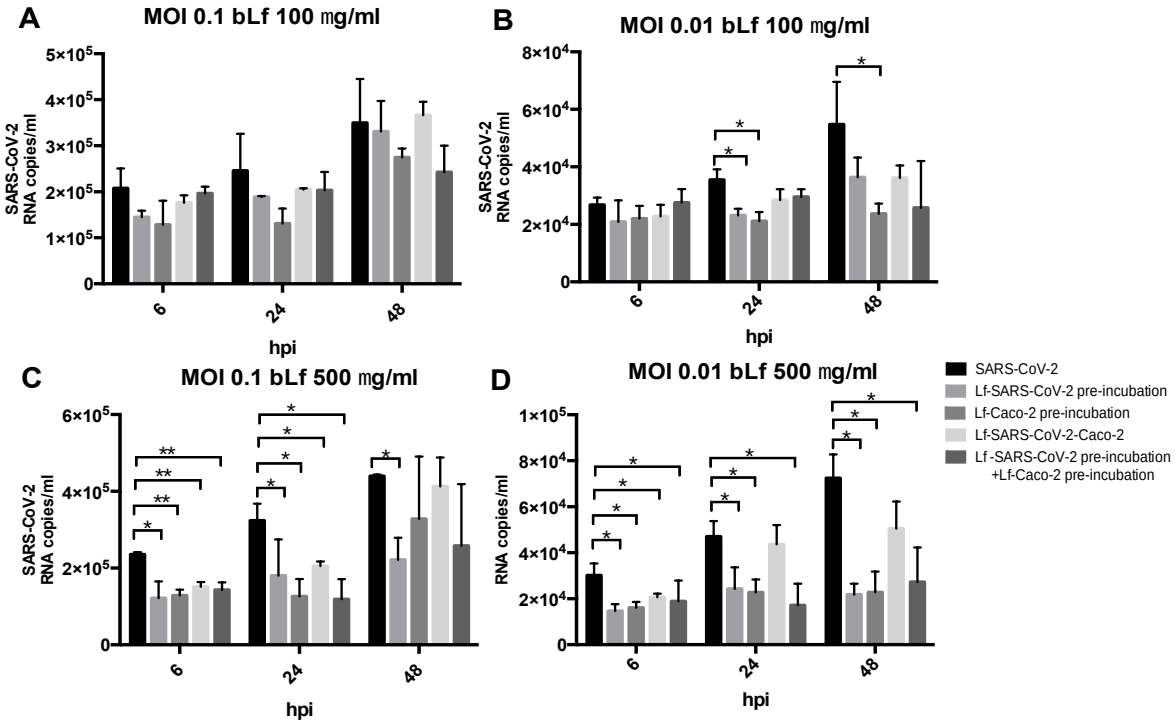

Figure 14. RNA copies/ml of SARS-CoV-2 observed in supernatants of Caco-2 cells infected at multiplicity of infection (MOI) of 0.1 (A,C) and 0.01 (B,D) in the presence or absence of 100 µg/ml (A,B) and 500 µg/ml (C,D) of bovine lactoferrin (bLf) according to the following experimental procedures: i) control: untreated SARS-CoV-2 and Caco-2 cells; ii) bLf pre-incubated with SARS-CoV-2 inoculum for 1h at 37°C before cell infection; iii) cells pre-incubated with bLf for 1 h at 37°C before SARS-CoV-2 infection; iv) bLf added together with SARS-CoV-2 inoculum during the adsorption step; v) virus and cells separately pre-incubated with bLf for 1 h at 37°C before infection. Viral supernatant samples were harvested at 6, 24 and 48 hours post infection (hpi). Viral loads were ascertained with quantitative rRT-PCR. Data represent the mean values of three independent experiments. Error bars: standard error of the mean. Statistical significance is indicated as follows: *: $p < 0.05$, **: $p < 0.001$ (Unpaired student's *t* test).

4.2 Computational results

The molecular docking simulation suggests a potential interaction of the bLf structure with the spike glycoprotein CDT1 domain in the up conformation (Figure 15A). The first three solutions obtained by Frodock clustering procedure account for more than 60% of the total generated complexes, which are almost completely superimposable to that shown in Figure 15A.

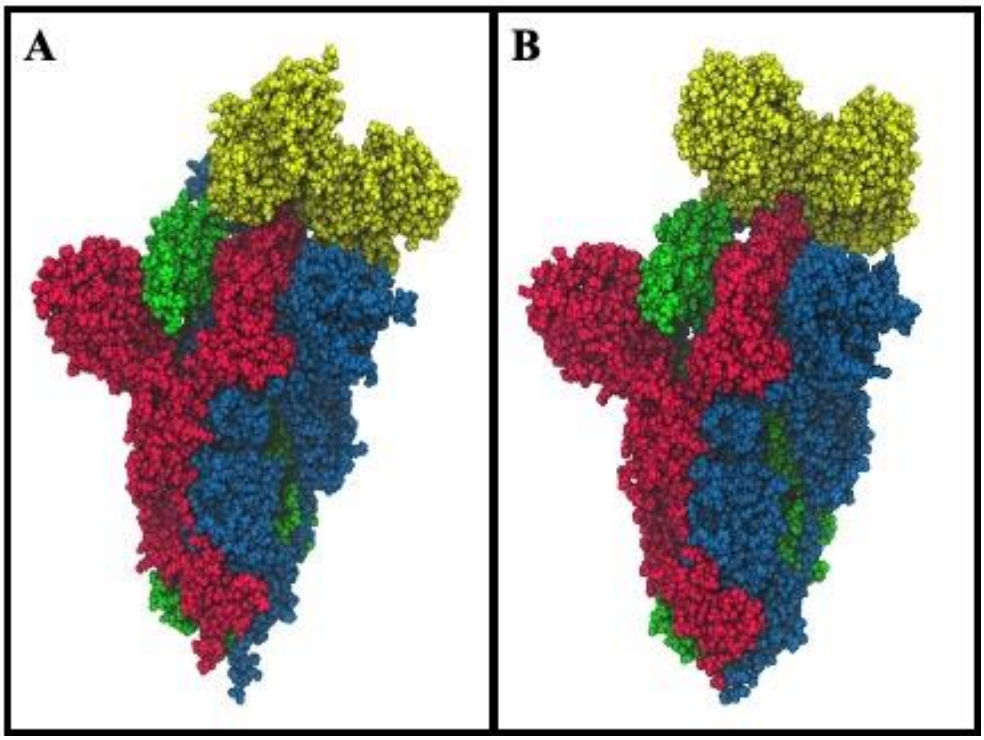

Figure 15. Spacefill representations of the best molecular complex obtained with Frodock between the bovine (A) and human (B) lactoferrin with the Spike glycoprotein. The red, blue and green colors represent the Spike glycoprotein chains, while the yellow depicts the lactoferrin molecules.

Starting from the first Frodock solution, we performed a 30 ns long classical MD simulation in order to verify the stability of the complex and check for the presence of persistent interactions between the two proteins. As shown in Figure 16A, the distance between the centers of the mass of Spike and bLf, calculated as a function of time, oscillates around the value of 4.5 nm, indicating a constant close contact between the two molecules.

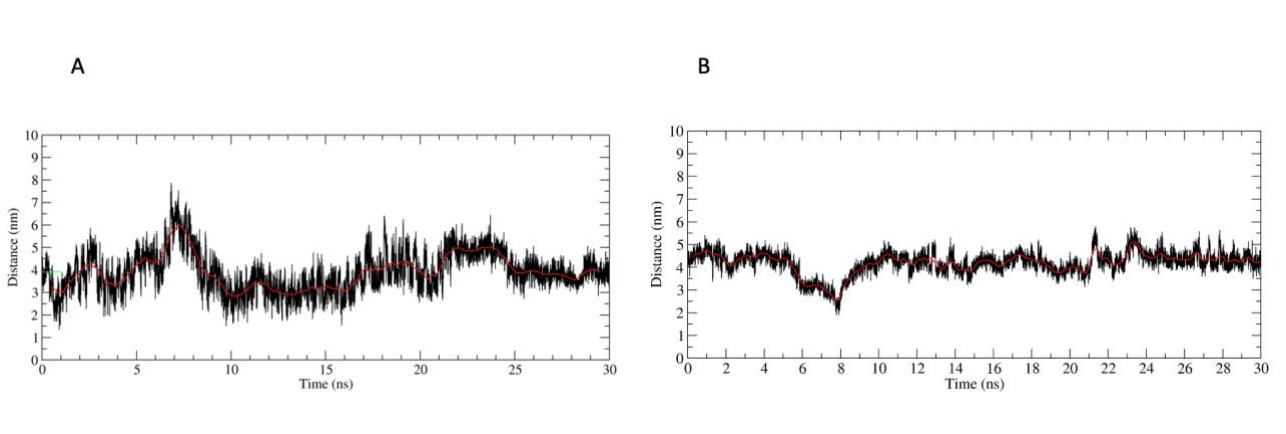

Figure 16. A) Time-dependent analysis of the distance evaluated between the centers of mass of the CTD1 domain in the up conformation and of the bovine lactoferrin. The red line represents the distance values averaged over 250 trajectory frames. B) Time-dependent analysis of the distance evaluated between the centers of mass of the CTD1 domain in the up conformation and of the human lactoferrin. The red line represents the distance values averaged over 250 trajectory frames.

MM/GBSA analysis confirmed the high affinity of the bLf for the Spike CDT1 domain, showing interaction energy of -28.02 kcal/mol (Table 2). In particular, MM/GBSA results highlighted that the Van der Waals term mainly contribute to the binding energy (Table 2).

Table 2. A) Results of the MM/GBSA analyses performed over the last 15 ns of the Spike-bovine lactoferrin complex simulation. B) Results of the MM/GBSA analyses performed over the last 15 ns of the Spike-human lactoferrin complex simulation.

A) Spike-Bovine lactoferrin complex simulation				
VdW (kcal/mol)	**Electrostatic (kcal/mol)**	**Nonpolar solvation (kcal/ mol)**	**Polar solvation (kcal/ mol)**	**Interaction energy (kcal/ mol)**
-138.27	125.11	-42.29	-18.35	-28.02
B) Spike-Human lactoferrin complex simulation				
VdW (kcal/ mol)	**Electrostatic (kcal/mol)**	**Nonpolar solvation (kcal/ mol)**	**Polar solvation (kcal/ mol)**	**Interaction energy (kcal/ mol)**
-158.27	-115.80	-21.18	209.78	-48.25

A detailed analysis of the interaction network reveals the presence of 28 different interactions, which persist for more than 25% of the simulation time, in agreement with the high interaction energy calculated. In detail, we found 3 salt bridges, 5 hydrogen bonds and 20 residue pairs involved in hydrophobic contacts (Table 3).

Table 3. (LEFT SIDE) Molecular interactions established between the RBD domain of the Spike protein and the bovine lactoferrin. Only interactions identified for more than 50% of simulation time are shown. Residues highlighted in grey are shared in the interfaces of Spike-ACE2 and Spike-bovine lactoferrin. (RIGHT SIDE) Molecular interactions established between the RBD domain of the Spike protein and the human lactoferrin. Only interactions identified for more than 50% of simulation time have been showed. Residues highlighted in grey are shared in the interfaces of Spike-ACE2 and Spike-Human lactoferrin.

Interaction (Spike – Bovine lactoferrin)	**Interaction type**	**Interaction (Spike-Human Lactoferrin)**	**Interaction type**
Glu159-Arg408	salt bridge	Lys378-Glu356	salt bridge
Glu162-Lys417	salt bridge	Asp405-Arg362	salt bridge

Glu355-Arg408	salt bridge	Asp405-Arg628	salt bridge
		Glu406-Arg362	salt bridge
Gly404-Glu355	non-polar contact	Glu406-Arg628	salt bridge
Asp405-Glu355	non-polar contact	Arg408-Glu355	salt bridge
Arg408-Ala354	non-polar contact	Arg408-Glu356	salt bridge
Arg408-Glu355	non-polar contact	Lys444-Glu128	salt bridge
Arg408-Lys358	non-polar contact	Lys462-Asp449	salt bridge
Arg408-Thr353	non-polar contact	Glu465-Hie635	salt bridge
Asn437-Gln386	non-polar contact	Glu465-Lys639	salt bridge
Asn439-Gln386	non-polar contact	Arg466-Asp646	salt bridge
Gly502-Glu356	non-polar contact		
Gly502-Thr353	non-polar contact	Arg403-Arg362	non-polar contact
Val503-Ala359	non-polar contact	Asp405-Arg362	non-polar contact
Val503-Arg363	non-polar contact	Arg408-Arg362	non-polar contact
Val503-Glu352	non-polar contact	Asn437-Asn157	non-polar contact
Val503-Glu355	non-polar contact	Asn439-Asn127	non-polar contact
Val503-Glu356	non-polar contact	Asn439-Pro154	non-polar contact
Val503-Thr353	non-polar contact	Ser443-Asn127	non-polar contact
Gly504-Glu355	non-polar contact	Ser443-Asn254	non-polar contact
Gly504-Glu356	non-polar contact	Ser443-Phe155	non-polar contact
Tyr505-Gln386	non-polar contact	Asn440-Gln130	non-polar contact
Gln506-Gln386	non-polar contact	Lys444-Asn127	non-polar contact
		Lys444-Glu128	non-polar contact
Asp405-Ser160	hydrogen bond	Pro499-Asn254	non-polar contact
Arg434-Glu355	hydrogen bond	Pro499-Asp253	non-polar contact
Thr526-Ser160	hydrogen bond	Pro499-Leu126	non-polar contact
Asn527-Ser160	hydrogen bond	Pro499-Phe155	non-polar contact
Val529-Ser160	hydrogen bond	Pro499-Pro252	non-polar contact
		Thr500-Asp253	non-polar contact
		Thr500-Pro252	non-polar contact
		Val503-Arg362	non-polar contact
		Gly504-Arg362	non-polar contact
		Tyr505-Pro154	non-polar contact
		Tyr508-Thr159	non-polar contact
		Asp405-Arg362	hydrogen bond
		Arg408-Glu356	hydrogen bond
		Asn437-Asn157	hydrogen bond
		Asn437-Pro154	hydrogen bond
		Asn439-Pro154	hydrogen bond
		Asn440-Gln130	hydrogen bond
		Ser443-Asn127	hydrogen bond
		Lys444-Asn127	hydrogen bond
		Lys444-Glu128	hydrogen bond
		Thr500-Pro252	hydrogen bond

To check if some of the Spike residues targeted by the bLf protein are involved in the binding with ACE2, we have compared the average structure extracted from the simulation with the ACE2/CDT1 domain complex structure (PDB ID: 6LZG [Wang et al. 2020] (Figure 17).

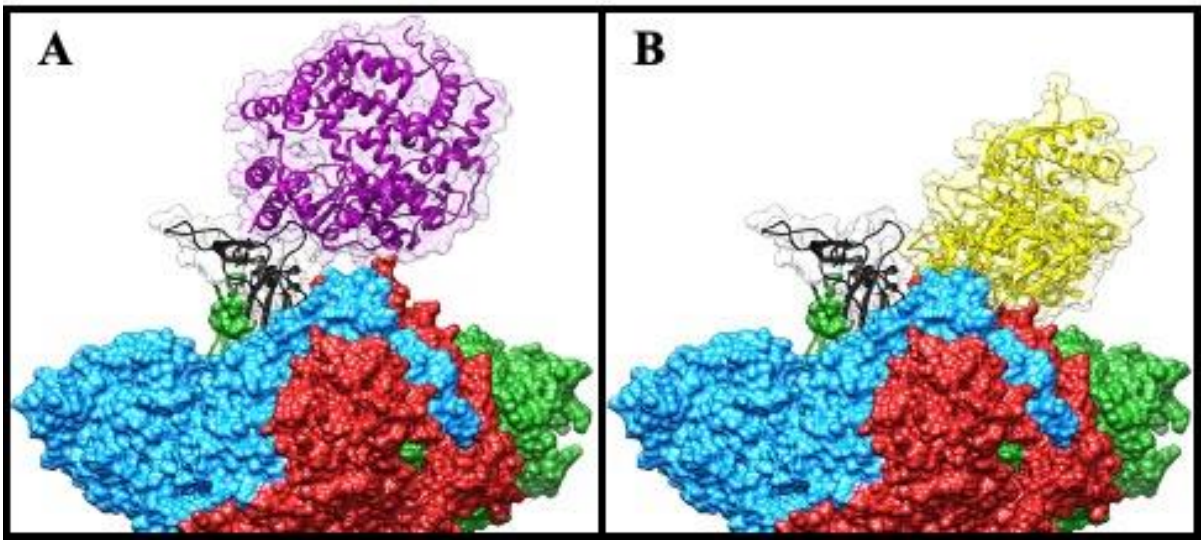

Figure 17. Comparison of the Frodock best complex and of the ACE2-Spike glycoprotein (PDB ID: 6LZG). The red, blue and green solid surfaces represent the three different chains composing the Spike glycoprotein. The black ribbons highlight the CTD1 domain in the up conformation. The magenta and yellow ribbons represent the ACE2 (A) and the bovine lactoferrin (B), respectively, surrounded by a transparent molecular surface representation, in order to point out the positions occupied in the space by the different structures.

Surprisingly, only two Spike residues (Gly502 and Tyr505) are shared between the complexes interfaces (Table 3, left side), as evaluated from the inspection of the superimposed structures and from the paper analysis [Wang et al. 2020]. Despite this, bLf holds the same position assumed by the ACE2 enzyme, i.e. above the up CDT1 domain.

We performed the same analysis over the evaluated hLf-Spike complex, obtaining a binding pose superimposable to that observed for the bovine protein (Figure 15B). Besides the fact that using the human protein we can still observe a persistent and close contact between the two molecules (Figure 16B), the analysis of the interaction network reveals the presence of a larger number of interactions (45), in agreement with an higher interaction energy revealed by the MM/GBSA approach (-48.25 kcal/mol, Table 2). In detail, we found 12 salt bridges, 10 hydrogen bonds and 23 residue pairs involved in hydrophobic contacts (Table 3 right side), in agreement with the presence of a negative electrostatic contribution term (Table 2). Comparing the average structure extracted from the simulation with the ACE2/CDT1 domain complex structure (PDB ID: 6LZG [Wang et al. 2020] (Figure 18), we observed that also for the hLf only two residues (Thr500 and Tyr505) are shared between the complexes interfaces (Table 3 right side).

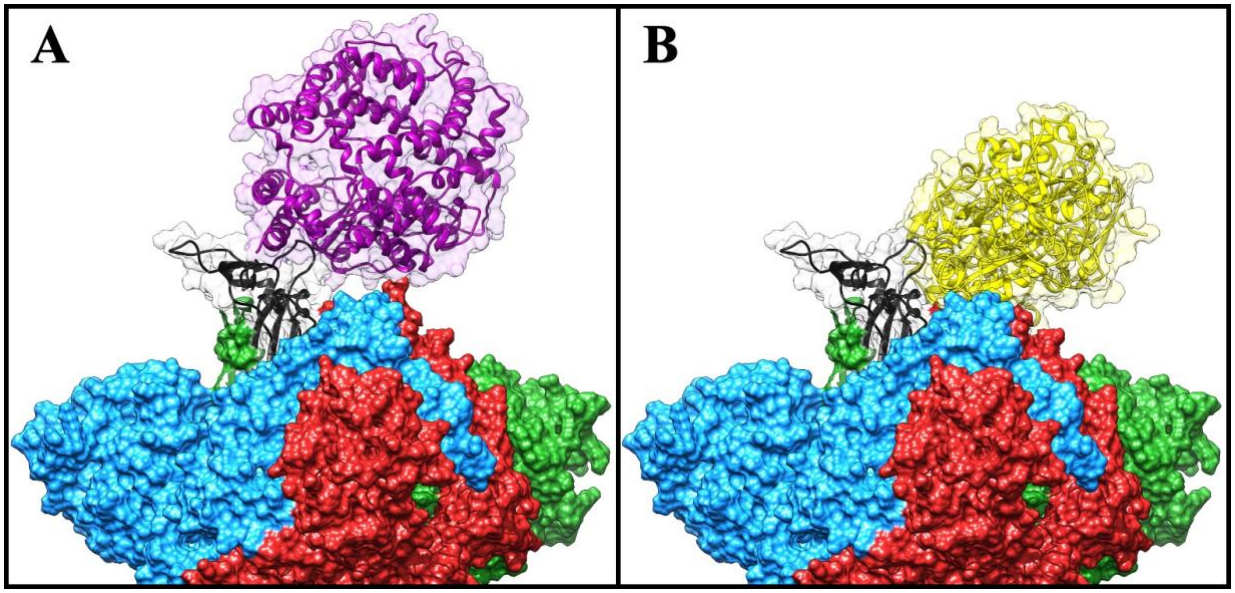

Figure 18. Structural superposition of the Frodock best complex and of the ACE2-Spike glycoprotein (PDB ID: 6LZG). The red, blue and green solid surfaces represent the three different chains composing the Spike glycoprotein. The black ribbons highlight the CTD1 domain in the up conformation. The magenta and yellow ribbons represent the ACE2 (A) and the human lactoferrin (B), respectively, surrounded by a transparent molecular surface representation, in order to point out the positions occupied in the space by the different structures.

These results allow us to hypothesize that, in addition to the HSPGs binding [Lang et al. 2011], both bLf and hLf should be able to hinder the spike glycoprotein attachment to the ACE2 receptor, consequently blocking the virus from entering into the cells.

4.3 Effect of bovine lactoferrin on pathogens-induced inflammation

4.3.1 Effects of bovine lactoferrin on Chlamydia trachomatis-induced inflammation

To investigate the effect of bLf on the inflammatory response, HeLa-229 cells were infected with *C. trachomatis* at a MOI of 5, and after 3 hpi, bLf was added to the medium. Of note, the addition of bLf at 3 hpi did not influence the intracellular number of *C. trachomatis* infecting the cell monolayers at the MOI of 0.05 (Fig. 10E) or at the MOI of 5 (data not shown), thus allowing the detection of the actual synthesis of IL-6 and IL-8 by the same number of intracellular *C. trachomatis*. The production of IL-6 and IL-8 was evaluated in the supernatants (Figure 19A and 19B, respectively). The treatment with bLf did not raise the cytokine levels in noninfected cells compared with the cell monolayers alone. On the contrary, the infection with *C. trachomatis* induced a significant increase of both IL-6 and IL-8 levels. The addition of bLf to infected cells 3 hpi caused a significant decrease of both IL-6 and IL-8 levels compared with infected cells not treated with bLf ($p < 0.05$). In particular, bLf significantly decreased IL-6 and IL-8 concentrations, even if cytokine levels remained higher than those synthesized by noninfected cell monolayers (Figure 19A and 19B).

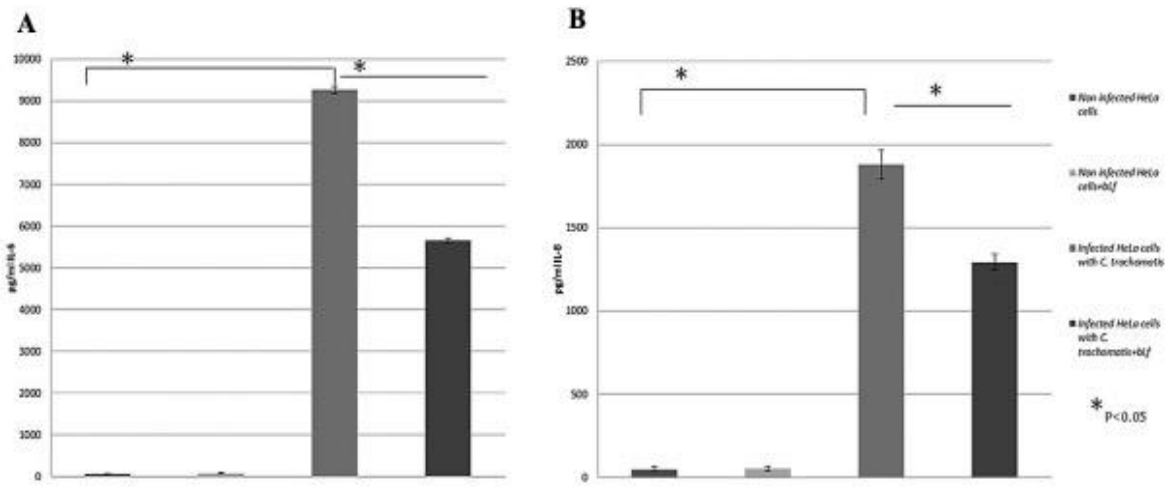

Figure 19. IL-6 (A) and IL-8 (B) levels in the supernatants of HeLa-229 cell cultures after 48 h of incubation. The infection was performed at a MOI of 5, and bLf was added 3 h post-infection. The IL-6 and IL-8 concentrations are mean values ± SD. A value for $p < 0.05$ was considered statistically significant. Error bars: standard error of the mean. Statistical significance is indicated as follows: *: $p < 0.05$.

4.3.2 Effects of bovine lactoferrin on Pseudomonas aeruginosa-induced inflammation

The effect of bLf on host immune cells recruitment in the BALF and cytokine/chemokine production in lung tissues of WT and CF mice following *P. aeruginosa* infection has been evaluated. As shown in Figure 20, significant ($p < 0.05$) reductions of neutrophils, macrophages and total cells were recorded for CF mice, while only a significant reduction in neutrophils was observed for WT mice treated with bLf compared with saline-treated controls.

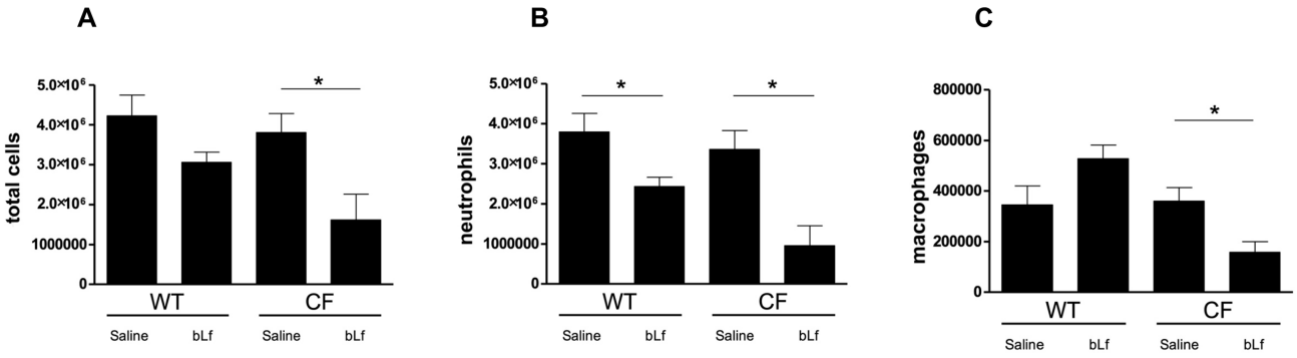

Figure 20. Total cell (A), neutrophils (B) and macrophages (C) counts in BALFs of WT and CF mice after 7 treatments with aerosol administration of 50 µL sterile saline or 200 µg/50 µL bLf, evaluated 6 days after challenge. Error bars: standard error of the mean. Statistical significance is indicated as follows: *: $p < 0.05$ (Mann-Whitney U test).

Cytokine/chemokine profiles showed that IL-2, IL-4, IL-9 and granulocyte-macrophage colony-stimulating factor (GM-CSF) were not expressed at all or were expressed at very low levels. Out of 18 cytokine/chemokines detected, the most striking result was obtained with Monocyte Chemoattractant Protein (MCP)-1 and Macrophage Inflammatory Protein (MIP)-1α. As shown in

Figure 21, levels of these chemokines were higher in transgenic CF mice compared to WT mice and bLf-treatment significantly reduced their concentrations to levels of untreated WT mice.

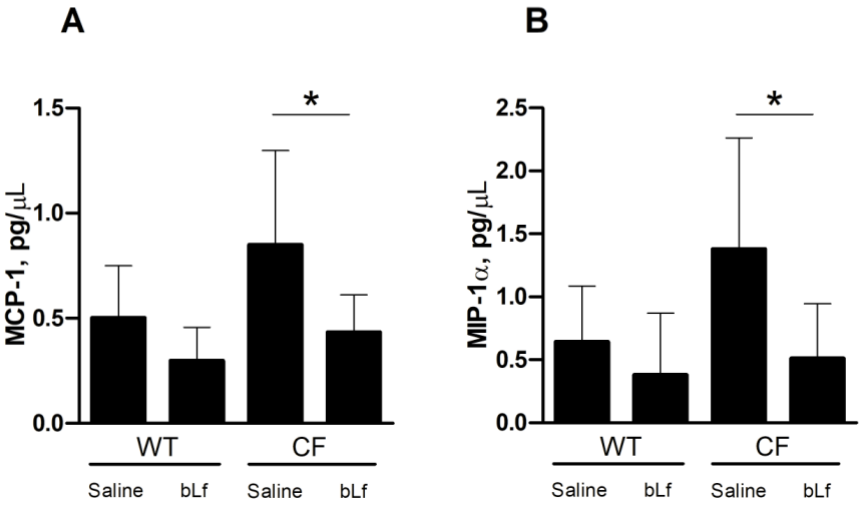

Figure 21. Changes in Monocyte Chemoattractant Protein (MCP)-1 and Macrophage Inflammatory Protein (MIP)-1α levels in lung homogenates of WT and CF mice after 7 treatments with aerosol administration of 50 µL sterile saline or 200 µg/50 µL bLf. Error bars: standard error of the mean. Statistical significance is indicated as follows: *: $p < 0.05$ (Mann-Whitney U test).

Other cytokine/chemokine showed higher levels in CF compared to WT mice and a trend in reduction, yet not significant, for bLf-treatment. Table 4 summarizes analytical data for all cytokines/chemokines tested.

Table 4. Cytokines/chemokines levels in infected wild-type (WT) and cystic fibrosis (CF) mice treated or not treated with bovine lactoferrin (bLf). IL: Interleukin; G-CSF: Granulocyte Colony-Stimulating Factor; GM-CSF: granulocyte-macrophage colony–stimulating factor; IFN: Interferon; KC: Keratinocyte Chemoattractant; TNF: Tumor Necrosis Factor. ND: Not Detected.

Cytokine/chemokine (pg/mL)	WT	WT bLf	CF	CF bLf
IL-1α	95 ± 22	78±45	167 ± 93	110 ± 82
IL-1β	130 ± 32	119 ± 40	175 ± 65	124 ± 66
IL-2	ND	ND	ND	ND
IL-3	3 ± 1	3 ± 2	3 ± 1	3 ± 2
IL-4	ND	ND	ND	ND
IL-5	3 ± 1	6 ± 2	5 ± 2	5 ± 1
IL-6	9 ± 5	6 ± 4	11 ± 4	9 ± 4
IL-9	ND	ND	ND	ND
IL-10	12 ± 3	10 ± 4	17 ± 4	12 ± 4
IL-12(p40)	10 ± 6	16 ± 9	7 ± 1	9 ± 4
IL-12(p70)	69 ± 14	64 ± 18	105 ± 35	71 ± 43

Cytokine/chemokine (pg/mL)	WT	WT bLf	CF	CF bLf
IL-13	77 ± 15	83 ± 17	92 ± 13	78 ± 10
IL-17	11 ± 3	14 ± 8	5 ± 2	11 ± 6
Eotaxin	540 ± 167	417 ± 93	612 ± 149	390 ± 120
G-CSF	301 ± 216	134 ± 162	479 ± 252	283 ± 225
GM-CSF	ND	ND	ND	ND
IFN-γ	11 ± 1	12 ± 5	11 ± 2	11 ± 5
KC	90 ± 50	67 ± 29	131 ± 63	79 ± 41
RANTES	42 ± 44	63 ± 26	20 ± 21	40 ± 14
TNF-α	35 ± 14	33 ± 9	52 ± 22	38 ± 23

4.3 Effect of bovine lactoferrin on pathogens-induced iron homeostasis disorders

4.3.1 Effects of bovine lactoferrin on Chlamydia trachomatis-induced iron homeostasis disorders

To evaluate the effect of bLf on cellular iron homeostasis, TfR1, Ftn and Fpn were analyzed in HeLa cells infected with *C. trachomatis* (MOI 5). In these experiments, bLf was added 3 h after the infection.

Concerning TfR1, the addition of bLf to non-infected cells did not change its expression respect to control. On the contrary, the infection with *C. trachomatis* induced a significant increase of the protein (about 50% increase) respect the non-infected cells. The addition of bLf to infected cells determined the significant decrease of TfR1 respect to infected cells (about 50% decrease) as well as to non-infected cells even if at not significant level (Figure 22).

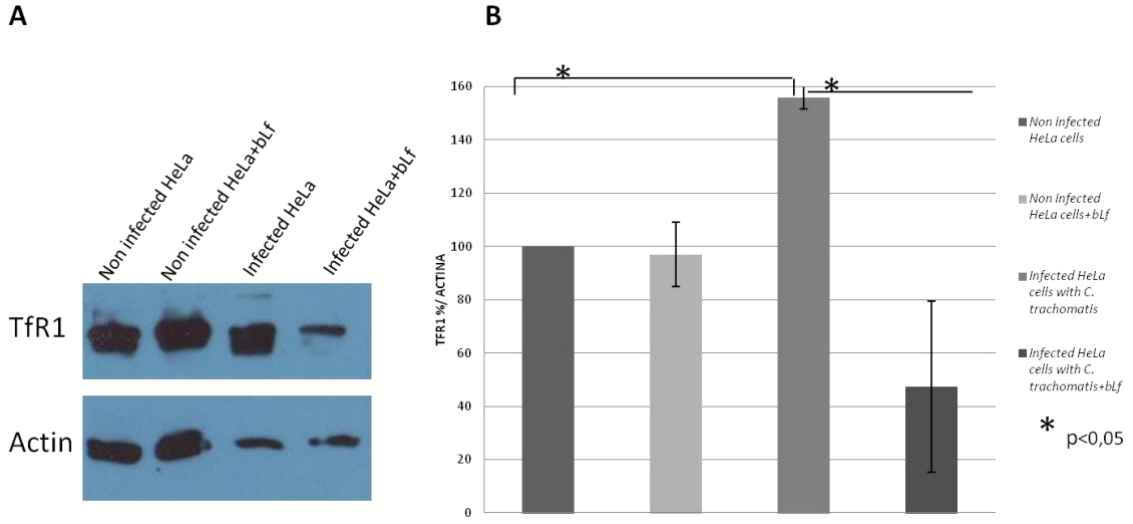

Figure 22. Western blot and densitometric evaluations of TfR1 expression in HeLa cells at 24 h. Bovine lactoferrin (bLf) (100 μg/ml) was added after 3 hours of infection. Left panel representative western blot of TfR1 and β-actin; right panel mean values of densitometric

evaluation of TfR1 expression normalized on actin. Error bars: standard error of the mean. Statistical significance is indicated as follows: *: $p < 0.05$.

Concerning Ftn, it was not affected by bLf in non-infected cells and similar values were found in presence or absence of bLf. On the contrary, the infection with *C. trachomatis* induced a significant decrease of the Ftn (about 60-70% decrease) respect to the non-infected cells in absence of bLf. The addition of bLf to infected cells did not determine any significant change in Ftn expression (Figure 23).

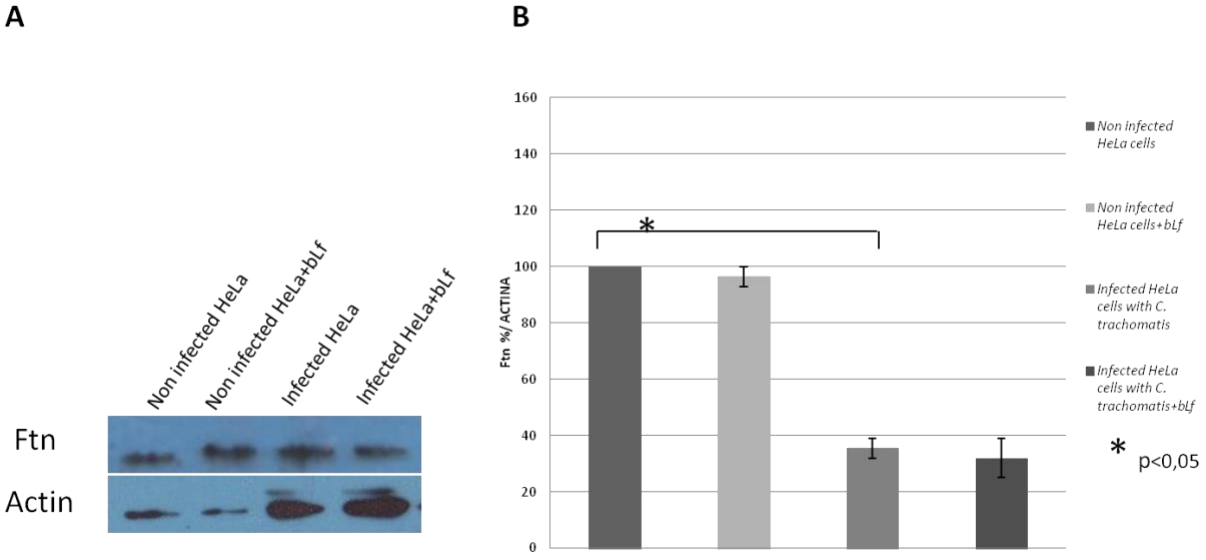

Figure 23. Western blot and densitometric evaluations of Ftn expression in HeLa cells at 24 h. Bovine lactoferrin (bLf) (100 µg/ml) was added after 3 hours of infection. Left panel representative western blot of Ftn and β-actin; right panel mean values of densitometric evaluation. Error bars: standard error of the mean. Statistical significance is indicated as follows: *: $p < 0.05$.

The expression of Fpn in non-infected cells was not affected by bLf and values similar to controls were found**.** The infected cells showed a notable (not significant) decrease in the immunoreactive band of the protein as compared to the non-infected cells. The addition of bLf after 3 h of infection significantly increased the Fpn protein (about 30 % increase) as compared to infected cells (Figure 24).

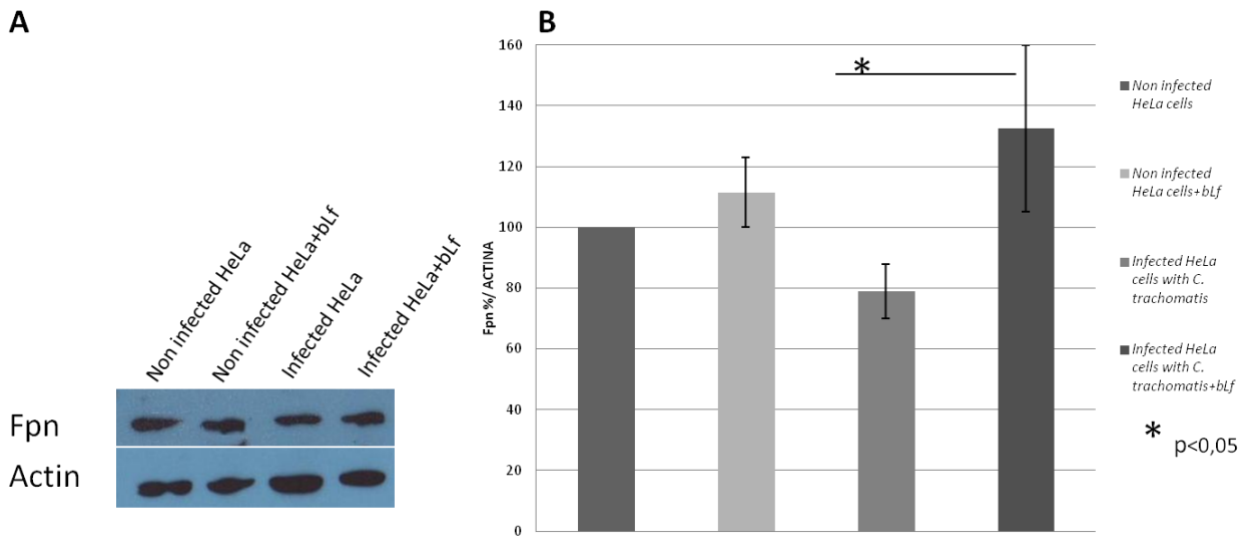

Figure 24. Western blot and densitometric evaluations of Fpn expression in HeLa cells at 24 h. Bovine lactoferrin (bLf) (100 µg/ml) was added after 3 hours of infection. Left panel representative western blot of Fpn and β-actin; right panel mean values of densitometric evaluation of Fpn expression normalized on actin. Error bars: standard error of the mean. Statistical significance is indicated as follows: *: $p < 0.05$.

In addition, here for the first time we describe HeLa cells expressing Fpn protein. To further confirm this finding, we performed an RT-PCR for Fpn on both HeLa and CaCo-2 cells, this latter cell line was chosen as positive control. We carried out the analysis using two different pairs of primers for Fpn, D39-D181 and D181-D365, both giving a PCR product of about 450 bp; as control for RNA quality β-actin was analyzed as well. As shown in Figure 25, both pairs of primers for Fpn produced a PCR positive band, in both Caco-2 and HeLa cells. Expression levels of Fpn were lower in HeLa cells compared to CaCo-2 cells (Figure 25).

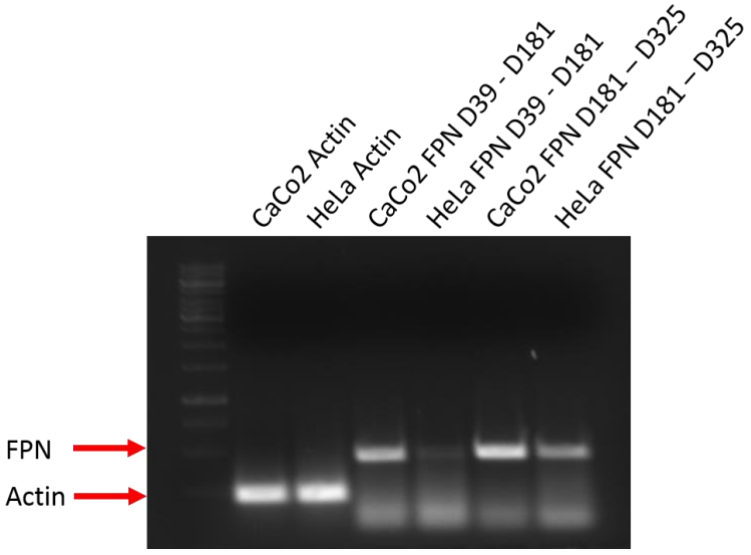

Figure 25. RT-PCR for Fpn expression in both CaCo-2 and HeLa cells.

4.3.2 Effects of bovine lactoferrin on Pseudomonas aeruginosa-induced iron homeostasis disorders

To investigate the role of bLf on iron homeostasis of mice infected by *P. aeruginosa*, lung homogenates of WT and CF mice, treated with saline or bLf, were analyzed for the expression of the main iron-related proteins involved in cell and systemic iron homeostasis, as Fpn, Ftn and TfR1, and total iron content in the BALF was also assessed. As shown in Figure 26A and 26B, a reduced expression of Fpn and Ftn both in WT and CF infected mice was observed upon treatment with bLf. For both proteins, reduction was statistically significant both for WT and CF animals ($p < 0.05$). On the other hand, TfR1 was unaffected by bLf administration (Figure 26C). As far as total iron content in BALF is concerned, a significant decrease in bLf treated mice, both WT and CF, could be observed, with a mean drop of 65% and 55% in the case of WT and CF animals, respectively (Figure 26D).

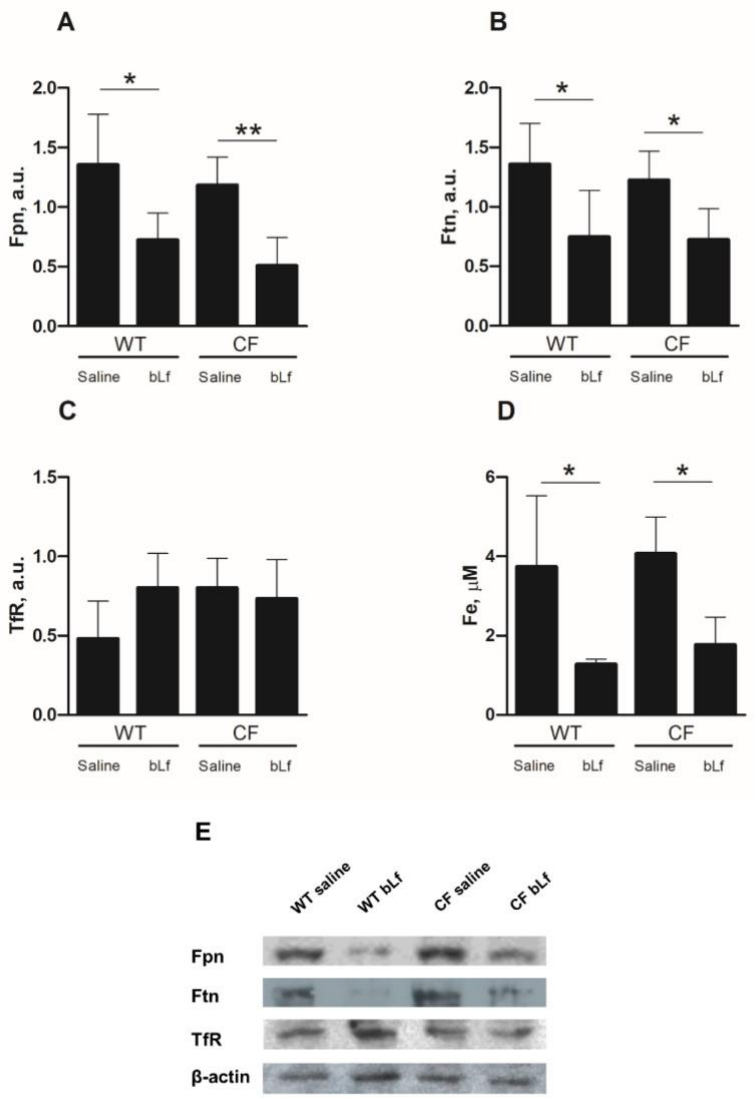

Figure 26. Changes in Ferroportin (A), Ferritin (B), Transferrin Receptor (C) levels in lung homogenates analyzed by Western blot and total iron content (D) in BALFs of WT and CF mice after 7 treatments with aerosol administration of 50 µL sterile saline or 200 µg/50 µL bLf. (E)

Representative Western blot. Error bars: standard error of the mean. Statistical significance is indicated as follows: *: $p < 0.05$; **: $p < 0.01$ (Mann-Whitney U test). a.u: arbitrary unit.

4.4 Clinical trial results

4.4.1 Effects of bovine lactoferrin on pregnant women affected by Chlamydia trachomatis infection

Among one hundred ninety-eight pregnant women, we excluded sixteen women affected by bacterial vaginosis unrelated to *C. trachomatis*, and 6 women for protocol violation. One hundred seventy-six pregnant women completed the study and, among them, seven asymptomatic pregnant women, positive to *C. trachomatis* DFA with high concentration of IL-6 in cervical fluids, were treated with the intravaginal administration of bLf (100 mg) every 8 h for 30 days.

After 1 month, six out of seven cervical specimens were negative to *C. trachomatis* DFA, and the cervical fluids showed a decrease in IL-6 concentration (from mean values of 250±19 to 50±11 pg/mL) (Table 5). One out of seven pregnant women was positive to *C. trachomatis* DFA and cervical IL-6 levels did not decrease, ranging between about 270 and 300 pg/mL (Table 5). This patient was treated with antibiotics. No maternal and neonatal side effects by bLf intravaginal administration were observed.

Table 5. General characteristics of pregnant women positive for *Chlamydia trachomatis* before and after intravaginal administration of bovine lactoferrin (100 mg every 8 h/day); n, number of pregnant women; DFA, direct immunofluorescence assay.

	Before treatment	**After treatment**
n=6		
C. trachomatis DFA	Positive	Negative
Mean values for cervical IL-6 (pg/ml)	250±19	50±11
Spontaneous delivery (week)	39-40	-
Mean values of birth weight (g)	3,727±175	-
Apgar scores	9/10	-
n=1		
C. trachomatis DFA	Positive	Positive
Mean values for cervical IL-6 (pg/ml)	263	285
Caesarean section (week)	39	-
Mean values of birth weight (g)	3,378	-
Apgar scores	9	-

4.4.2 Effects of bovine lactoferrin on patients affected by SARS-CoV-2 infection

Demographic data: a total of ninety-two patients with confirmed COVID-19 infection at rRT-PCR were recruited to participate in the study protocol (Figure 27).

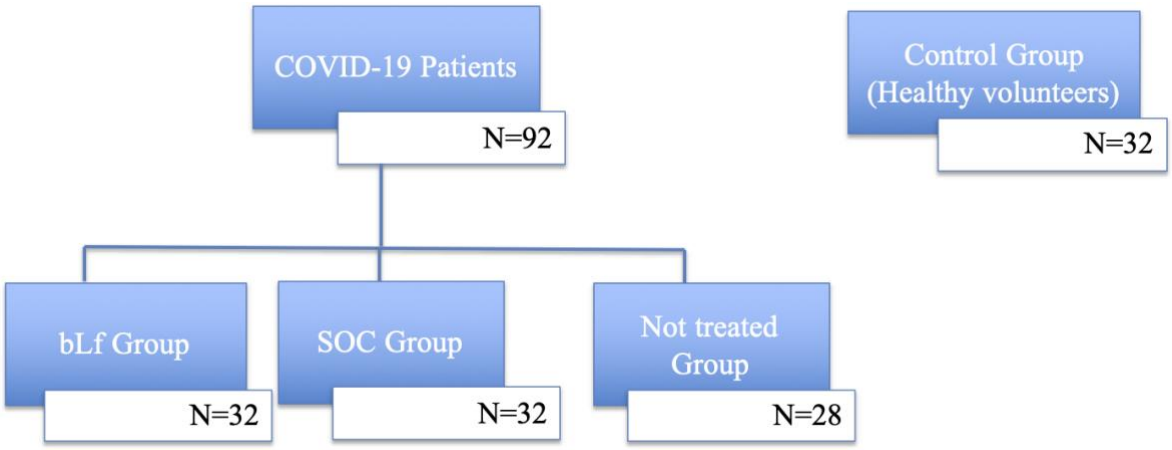

Figure 27. Flowchart of enrolled patients.

Among the thirty-two bLf-supplemented patients, ten patients were asymptomatic and twenty-two of them had mild-to-moderate symptoms. Demographic data of the Groups are summarized in Table 6.

Table 6. Demographic data of enrolled patients

Demographic Data		bLf-Treated COVID-19 Group		SOC-Treated COVID-19 Group		Not Treated COVID-19 Group		Control Group Healthy Volunteers	
		Mean±SD	N (%)	Mean±SD	N (%)	Mean±SD	N (%)	Mean±SD	N (%)
Age		54.56±16.86		49.90±13.20		41.32±11.77		52.80±15.54	
Sex	Male		14 (44%)		17 (53%)		10 (36%)		12 (41%)
	Female		18 (56%)		15 (47%)		18 (64%)		19 (59%)
Asymptomatic patients			10 (31%)		3 (10%)		12 (43%)		
Mild-to-moderate patients			22 (68.7%)		29 (90%)		16 (57%)		

The mean age was 54.6±16.9 years old (Table 6). Fourteen patients were males and eighteen females (Table 6). The most prevalent comorbidity was hypertension (28%) followed by cardiovascular diseases (15.6%) and dementia (12.5%).

In the group of thirty-two SOC-treated COVID-19, three patients were asymptomatic and twenty-nine patients had mild to moderate symptoms. The mean age was 49.9±13.2, seventeen patients were males and fifteen females (Table 6). The most prevalent comorbidity was hypertension (15,6%), followed by asthma (12,5%) and hypotiroidism (6,5%).

Among the twenty-eight COVID-19 patients, in home situations, not taking any drug against COVID-19, twelve were asymptomatic and sixteen patients had mild-to-moderate symptoms (Table 6). Mean age was 41.3±11.8 years old (Table 6). Ten patients were male and eighteen females

(Table 6). Furthermore, four out of these patients worsened their clinical profile with consequent hospitalization.

Among the thirty-two healthy volunteers (mean age 52.8±15.5 years old) with negative rRT-PCR for SARS-CoV-2 RNA, thirteen subjects were male and nineteen females (Table 6).

Primary Endpoint: bLf-supplemented COVID-19 patients revealed a mean time length of rRT-PCR SARS-COV-2 RNA negative conversion of the naso-oropharingeal swab in 14.25±6.0 days, shorter than that observed in SOC-treated or in not-treated COVID-19 Group.

SOC-treated COVID-19 patients showed a mean rRT-PCR SARS-COV-2 RNA negative conversion in 27.13±14.4 days, whereas non-treated COVID-19 patients revealed a mean time length of negative conversion in 32.61±12.2 days (Figure 28).

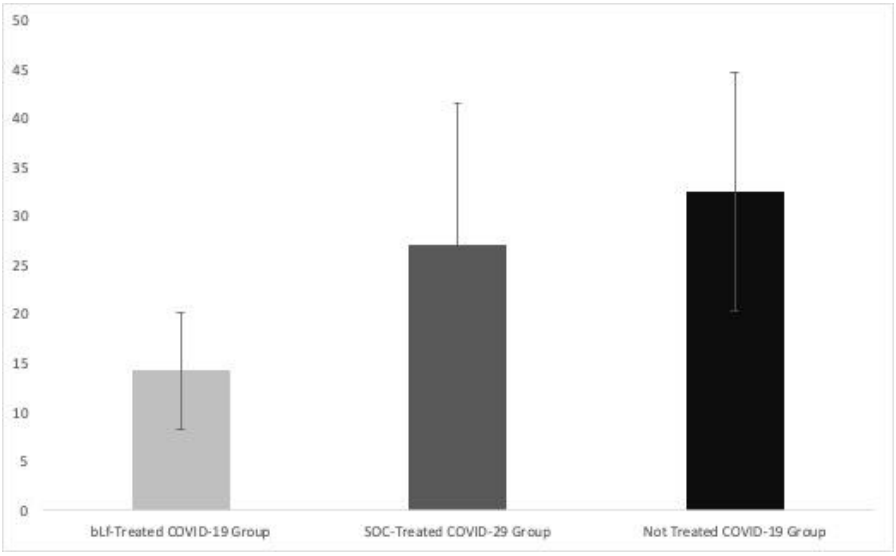

Figure 28. Mean time ± standard deviation of SARS-CoV-2 RNA negativization in bLf-treated Group, SOC-treated Group and not treated Group

Secondary Endpoints: in bLf-treated COVID-19 patients, we evaluated clinical symptoms before (T0) and after therapy (T2) (Figure 29). At T0 among thirty-two patients ten were asymptomatic and twenty-two mild-to-moderate. The most frequent symptoms were fatigue (50%), followed by arthralgia (37.5%) and cough (28%). At T1, seven patients previously symptomatic became asymptomatic, with a total seventeen asymptomatic and fifteen symptomatic patients. At T2 other six patients, previously symptomatic at T1, became asymptomatic with a total of twenty-three asymptomatic patients and nine symptomatic patients. Among these symptomatic patients the most frequent remaining symptom was fatigue followed by rare manifestations related to diarrhea, myalgia and skin manifestations (Figure 29).

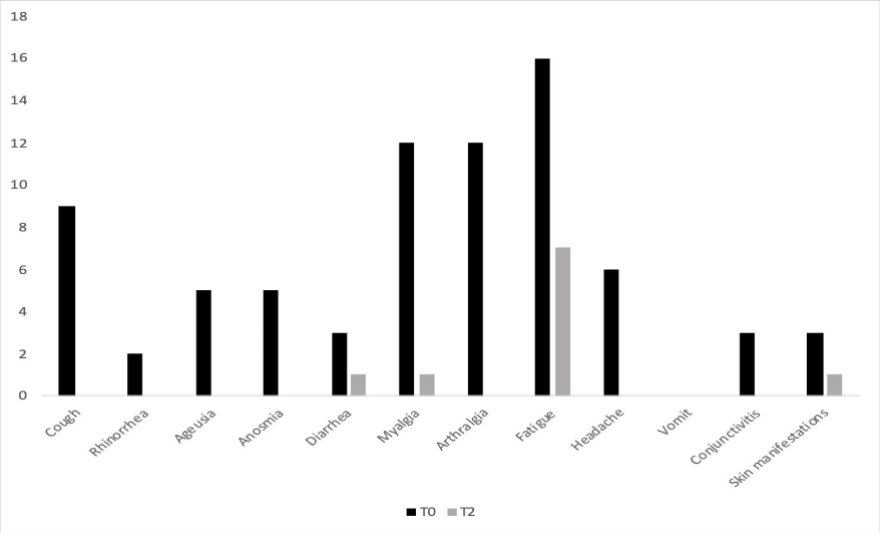

Figure 29. Clinical symptoms at T0 and T2 of bLf-treated Group.

Then, we evaluated difference between blood parameters before and after bLf supplementation. We noticed in bLf-Group an improvement in the platelet count (T0: 239.63±83.05; T2: 243.70±65.5; ΔT2-T0 10.05±10.26) and a decrease of alanine transaminase (ALT) (T0: 29.36±22.7; T2: 23.52±12.34; ΔT2-T0: -7.32±4.36) and aspartate aminotransferase (AST) (T0: 24.36±9.80; T2: 22.64±8.33; ΔT2-T0 -2.68±2.52). Moreover, D-dimer showed a significant decrease between T2 and T0 (ΔT2-T0: -392.56±142.71, p-value 0.01) in bLf-Group. (Table 7).

Table 7. A) Statistical analysis evaluation between COVID-19 bLf group and control group**; B)** Statistical analysis evaluation between T2 and T0 in COVID-19 bLf group**; C)** Statistical analysis evaluation between T2 and T0 in COVID-19 SOC group.

A) Statistical analysis evaluation between COVID-19 bLf group and control group

	COVID-19 bLf patient platelet count (10^3/µl)	**Healthy control platelet count (10^3/µl)**	**COVID-19 bLf patient neutrophils count (10^3/µl)**	**Healthy control neutrophils count (10^3/ µl)**
Mean	239,63	255,97	4,46	5,84
Variance	6897,09	4652,45	5,66	113,06
standard deviation	179324,34	134921,05	113,2	3278,74
t _Student		-3,07		-2,05
two-tailed p-value		< 0,0001		0,04
	COVID-19 bLf patient monocytes count (10^3/ µl)	**Healthy control monocytes count (10^3/ µl)**	**COVID-19 bLf Patient D-Dimer (ng/ml)**	**Healthy control D-dimer (ng/ml)**
Mean	0,5	0,69	1546,82	484
Variance	0,04	1,22	13034194,25	420241,48
standard deviation	0,8	35,38	273718079,3	11346519,96
t _Student		-2,73		5,37

two-tailed p-value		0,006		< 0,0001
	COVID-19 bLf patient AST (U/L)	**Healthy control AST (U/L)**	**COVID-19 bLf patient Ferritin (ng/ml)**	**Healthy control Ferritin (ng/ml)**
Mean	24,36	26,17	201,43	119,24
Variance	95,99	76,35	57729,26	23855,76
standard deviation	2303,76	2214,15	1039126,68	429403,68
t _Student		-2,67		3,87
two-tailed p-value		0.008		< 0,0001
	COVID-19 bLf patient lymphocytes count (10^3/µl)	**Healthy control lymphocytes count (10^3/µl)**	**COVID-19 bLf patient ALT (U/L)**	**Healthy control ALT (U/L)**
Mean	1,75	3,06	29,36	26,8
Variance	0,3	27,38	515,49	229,13
standard deviation	6	794,02	12371,76	6644,77
t _Student		-4		1,84
two-tailed p-value		< 0,0001		0,059
	COVID-19 bLf patient Adrenomedullin (pg/ml)	**Healthy control Adrenomedullin (pg/ml)**	**COVID-19 bLf patient IL-6 (pg/ml)**	**Healty control IL-6 (pg/ml)**
Mean	0,57	0,42	38,1	7,48
Variance	0,19	0,01	13232,16	0,03
standard deviation	1,71	0,15	198482,4	0,45
t _Student		3,32		3,01
two-tailed p-value		< 0,0001		< 0,0001

B) Statistical analysis evaluation between T2 and T0 in COVID-19 bLf group

Statistical analysis	**D-Dimer (ng/ml) $\Delta(T_2 - T_0)$**	**Ferritin (ng/ml) $\Delta(T_2 - T_0)$**	**IL-6 (pg/ml) $\Delta(T_2 - T_0)$**
Mean	-392,56	-90,63	-2,52
Variance	366600,7	42319,88	36,31
Standard Deviation	142,71	48,49	1,46
t-Student	-2,75	-1,87	-1,73
p-value	0,01	0,04	0,05

Regarding safety assessment in the bLf-Group, two patients (6.2%) showed gastrointestinal complaints related to liposomal bLf at T2. The patients didn't suspend liposomal bLf administration and the adverse event resolved itself spontaneously.

In SOC-treated COVID-19 patients, we evaluated clinical symptoms before (T0) and after therapy (T2) (Figure 30).

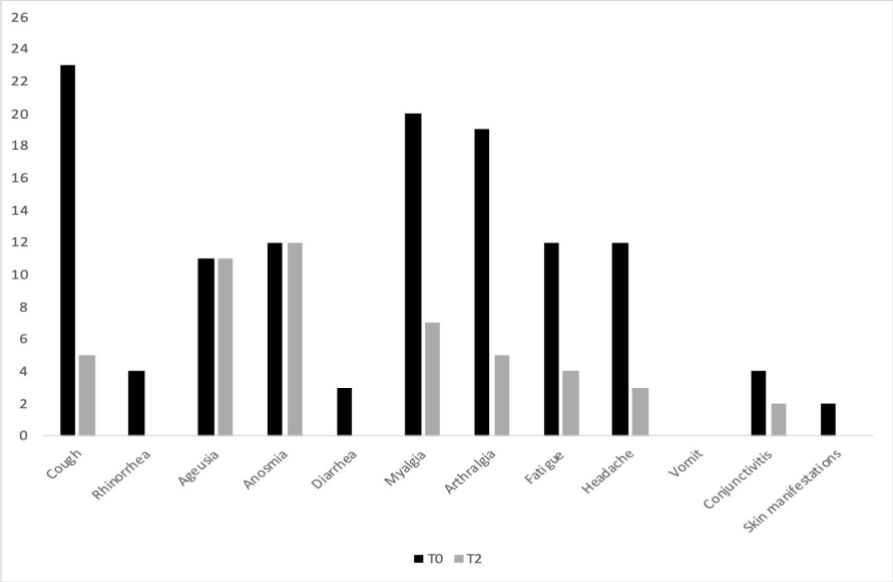

Figure 30. Clinical symptoms at T0 and T2 of SOC-treated Group.

At T0, the most frequent symptoms were cough (72%), followed by myalgia (62%) and arthralgia (59%). Particularly, all the patients that presented ageusia (11) and anosmia (12) at T0 did not achieve remission at T2.

Then, in SOC treated COVID-19 patients, we compared blood parameters before and after therapy. Among blood parameters, statistically significant variations of RBCs (ΔT1-T0: -0.43± 0.17, p-value = 0.05), Hb (ΔT1 -T0: -2.22± 0.95, p-value = 0.05), platelets count (ΔT1-T0: 89.56±18.9, p-value = 0.001) were noted. (Table 7).

Tertiary endpoints: the iron profile analysis before (T0) and after supplementation (T2) in the bLf group revealed statistically significant values in Ftn reduction (ΔT2-T0: -90.63 ±48.49, p-value = 0.04), while not statistically significance was found for serum iron and Tf. Regarding inflammatory blood parameters, IL-6 value showed a significant decrease between T2 and T0 (ΔT2-T0: -2.52 ±1.46, p-value = 0.05). Adrenomedullin remained at the same level all over the analyzed period (ΔT2-T0: -0.01±0.03). IL-10 levels increased between T0 (8.67±3.26) and T2 (11.42±6.05), without showing statistical significance (ΔT2-T0: 2.55±2.09). TNF-α decreased between T2 (25.97±21.74) and T0 (37.34 ±19.95) without showing statistical significance (ΔT2-T0: -12.92±8.81).

The comparison between bLf-supplemented COVID-19 patients and healthy volunteers group showed a significant difference in adrenomedullin (p-value < 0.0001) and IL-6 (p-value < 0.0001) (Table 7).

5. DISCUSSION

Human pathogens have evolved a plethora of mechanisms to obtain host iron. In response to infection, the innate immune system further strengthens iron-withholding defenses, ensuring that the host-pathogen interface remains an ever-evolving battleground for this essential metal. Moreover, in the presence of the infection, inflammation can take place. Therefore, infection, inflammation and iron disorders reinforce each other, establishing an unsafe vicious circle difficult to counteract and solve in vivo. For this reason, it's imperative to design a therapy able to simultaneously counteract infection and related inflammatory and iron homeostasis disorders. As matter of fact, aggressive antibiotic and anti-inflammatory treatments may ameliorate the infection symptoms in the short-term, but they do not consistently reduce inflammation and microbial load, which may be related to dysregulated iron concentrations.

In recent years, the interest in the use of natural substances endowed with anti-microbial and anti-inflammatory activity is increasing. Among natural compounds, bLf, without side effects, has been shown to play a key role in counteracting iron and inflammatory homeostasis disorders associated to different pathological conditions [Lepanto et al. 2019 and reference therein].

In this study, I highlight the role of milk derivative bLf in counteracting infection, inflammation and related iron homeostasis disorders in different infection models.

The first model regards the in vitro and in vivo role of bLf against *C. trachomatis* infection and related iron and inflammatory homeostasis disorders. The incubation of cell monolayers with bLf before the infection or at the moment of the infection significantly inhibited the adhesion and entry of *C. trachomatis* into epithelial cells [Sessa et al. 2017]. Therefore, the inhibition of *C. trachomatis* infectivity by bLf was dependent on its interaction with the cell surface. Moreover, bLf could bind to cell surface glycosaminoglycans as well as to heparan sulfate proteoglycans [Wu et al. 1995; Lang et al. 2011], which are potential receptors for *C. trachomatis* adhesion [Stallmann and Hegemann 2015]. Conversely, the preincubation of bLf with *C. trachomatis* did not influence its infectivity, supporting the idea that the specific interaction between bLf and epithelial host cells seems to be the sole pivotal mechanism responsible for the inhibition of *C. trachomatis* invasion.

Similar to the results obtained in epithelial cell monolayers infected with other facultative intracellular pathogens [Berlutti et al. 2006; Valenti et al. 2011; Frioni et al. 2014], the addition of bLf to infected Hela cells significantly decreased the IL-8 and IL-6 levels synthetized by *C. trachomatis* infected cells [Sessa et al. 2017]. To avoid the possibility that the decrease of IL-8 and IL-6 was related to the different number of *C. trachomatis* IFUs, these experiments were carried out by adding bLf after 3 hpi. These results demonstrated once again the ability of bLf to down-regulate pro-inflammatory cytokine synthesis [Sessa et al. 2017]. Although it has been known for years that

exogenous bLf localized to cell nucleus where it is able to interact with genes coding for pro-inflammatory cytokines [Ashida et al. 2004; Suzuki et al. 2008; Valenti et al. 2011], the mechanisms by which bLf could perform its anti-inflammatory activity are still under debate. In addition, *C. trachomatis* infection influences the synthesis of the major proteins involved in iron homeostasis, such as Fpn, Ftn and TfR1. In this study, a down-regulation of Fpn and an up-regulation of TfR1 were observed after *C. trachomatis* infection on HeLa cells. This result indicates an iron accumulation into host cells that facilitates *C. trachomatis* developmental cycle. Of note, here for the first time we describe HeLa cells expressing Fpn protein. As positive control, Caco-2 cells were used. Expression levels of Fpn were lower in HeLa cells compared to Caco-2 cells. Regarding intracellular Ftn expression, a down-regulation of this protein expression was observed in HeLa infected cells indicating a putative competition of iron acquisition between intracellular Ftn and *C. trachomatis*. The addition of bLf at cell monolayers 3 hpi induces an upregulation of Fpn and a downregulation of TfR1 synthesis, thus indicating an intracellular iron detoxification. Regarding Ftn, the addition of bLf to infected cells did not determine any significant change in the protein expression. These in vitro results, showing for the first time the protective effects of bLf against *C. trachomatis* infection, led us to investigate its efficacy also in asymptomatic pregnant women positive to *C. trachomatis* and with high levels of IL-6 in cervical fluids. Seven out of one hundred seventy-six pregnant women enrolled in this pilot study, showing cervical specimens positive to *C. trachomatis*, were treated with the intravaginal administration of bLf (100 mg) every 8 h for 30 days [Sessa et al. 2017]. After 1 month, six pregnant women tested negative for *C. trachomatis* and showed decreased IL-6 levels in their cervical fluids (from mean values of 250 ± 19 to 50 ± 11 pg/mL) [Sessa et al. 2017]. Similar to what we observed in the in vitro model, intravaginal administration of bLf seems to act by protecting host cells against the adhesion and entry of chlamydial EBs, which are released extracellularly after redifferentiation of RBs to EBs. The simultaneous decrease of IL-6 levels could be a marker for the lack of reinfection by *C. trachomatis* EBs in the presence of bLf [Sessa et al. 2017].

The second model regards the in vivo role of aerosolized bLf in counteracting infection and inflammation as well as iron dysbalance in a CF mouse model characterized by chronic *Pseudomonas aeruginosa* lung infection. Despite the improvement of infection therapy based on aerosolized antibiotics [Waters and Smyth 2015], chronic *P. aeruginosa* infections remain very difficult to treat [Gibson et al 2003; Vidya et al. 2016]. Aggressive antibiotic and anti-inflammatory treatments may ameliorate CF patient symptoms in the short-term, but they do not consistently reduce inflammation and bacterial load, which may be related to persistently elevated iron concentrations in the airway [Reid et al. 2007]. So far, it has not been established whether iron

dyshomeostasis in lung is a cause or a consequence of *P. aeruginosa* infection in CF, while it is known that decreasing available iron generally ameliorates lung injury associated to inflammation states [Ghio et al. 1994; Louie et al. 1993]. Therefore, since inflammation is a hallmark also in CF, iron is likely to be a major actor in the maintenance of this disease.

In CF airways, iron dysbalance is mainly correlated to an increased expression of two pivotal proteins of iron homeostasis, namely Ftn and Fpn [Ghio et al. 2013]. With the present study, I shed some light on the role of bLf treatment on relieving iron dysbalance in a CF mouse model of *P. aeruginosa* chronic lung infection. The results are consistent with previous findings demonstrating that aerosolized bLf was efficient in diminishing both neutrophil recruitment and pro-inflammatory cytokine levels in pre-clinical mouse models of *P. aeruginosa* acute and chronic lung infection [Valenti et al. 2017]. Here, I show that bLf treatment is significantly efficient in reducing bacterial load in both BALFs and lung homogenates in CF mice, compared with saline-treated ones. As far as the WT controls are concerned, the results confirm previous data that no significant difference in CFUs counts between bLf and saline-treated mice has been observed [Valenti et al. 2017]. The central role of bLf as an anti-inflammatory agent is confirmed by the significant decrease of both total immune cells, such as neutrophils and macrophages, and some pro-inflammatory cytokines in CF compared to WT mice. In particular, MCP-1 and MIP-1α levels were significantly reduced in bLf-treated CF mice with respect to controls [Cutone et al. 2019]. It is interesting to note that these cytokines are involved in the migration of monocytes/macrophages [Standiford et al. 1995; Deshmane et al. 2009] and that the migration of blood into the airway supports neutrophil-mediated tissue injury in CF [Rao et al. 2009]. Thus, the observed decrease of both MCP-1 and MIP-1α levels suggests a reduced pro-inflammatory monocytes infiltration of CF mouse airway upon bLf treatment.

In association with the anti-bacterial and anti-inflammatory activity of bLf, the ability of bLf to counteract lung iron disorders in both WT and CF mice infected by *P. aeruginosa* has been demonstrated, by reducing iron overload, along with a drop of detoxifying proteins in lung homogenates and of iron concentration in BALF. In particular, bLf-treated mice, both WT and CF, showed a marked reduction in both Fpn and Ftn expression when compared to saline-treated ones [Cutone et al. 2019]. Fpn and Ftn are considered hallmarks of iron overload in lung epithelium, that reacts to excess iron by upregulating proteins able to trap (Ftn) or export (Fpn) the metal into the lumen. It is interesting to note that Fpn is usually downregulated in conditions of iron overload [Ghio 2009] since its primary localization is on the basal membrane of enterocytes and on macrophages, both cells being in charge of refurnishing circulating blood with iron through Fpn when needed. In our experimental set, the high expression levels observed for both proteins in both

WT and CF infected animals are consistent with a dysregulation of lung iron homeostasis that is presumably induced in WT mice, and exacerbated in CF ones, by *P. aeruginosa* infection. The effect of bLf is striking in both cases, with a marked reduction of the proteins' levels. Since iron levels in BALFs are also decreased in bLf-treated mice, these results allow to hypothesize that treatment with bLf, along with its anti-bacterial activity, may also prevent iron entry into the epithelial layer, thus inducing a decrease in intracellular iron which in turn downregulates Ftn and Fpn and makes iron concentrations in the airway lumen secretion drop [Cutone et al. 2019]. Certainly, more experiments are required to demonstrate and confirm this putative mechanistic model. Concerning TfR1 expression, no significant difference between saline- and bLf-treated mice was observed [Cutone et al. 2019]. Notably, Heilig et al. [2006] reported that TfR1 levels in whole lung remained unchanged in condition of iron overload, while an increase in Ftn levels was observed. However, since TfR1 has been described to be localized on both basolateral and apical side of airways epithelium [Ghio 2009], a dysregulation of its local expression cannot be ruled out.

Recently, the bLf ability in modulating iron homeostasis disorders has been reported in in vitro models of infected human CF and intestinal epithelium as well as in LPS-challenged human monocytes/macrophages [Frioni et al. 2014; Cutone et al. 2014; Cutone et al 2017]. This modulation has been demonstrated to be correlated to the concomitant down-regulation of IL-6, the main pro-inflammatory cytokine involved in iron homeostasis [Nemeth et al. 2004; Lee et al. 2005; Wrighting and Andrews 2006]. However, at odds from this Fpn positive modulation exerted by bLf in epithelial and macrophagic models, here I show that bLf decreases pulmonary Fpn expression in both WT and CF mice, with no modulation of either IL-6 or other pro- or anti-inflammatory cytokines directly involved in iron homeostasis. This intriguing result highlights, once again, how bLf exerts its multifunctional activities depending on the cell system it acts upon [Frioni et al. 2014; Valenti et al. 2017; Rosa et al. 2017; Lepanto et al. 2019]. In this respect, I have to recall that pulmonary Fpn, as well as Ftn, seems to be related to an iron detoxifying function [Ghio 2009], rather than to systemic iron transport and recycling, activities which are instead associated to the main cells involved in iron homeostasis, namely enterocytes, macrophages, and hepatocytes.

The finding of diminished iron concentrations in BALFs of bLf-treated mice, both WT and CF, is of outmost importance because of the biological relevance of excessive iron in enhancing bacterial growth and pathogenesis as well as chronic inflammatory states. Overall, these results indicate that bLf, along with its anti-bacterial and anti-inflammatory functions, can act as a clearing agent, able to restore the physiological iron detoxification pathway, thus leading to a progressive decrease of iron concentrations in both airways and lung epithelium. In this respect, the decrease of both Fpn and Ftn, after seven days of bLf treatments, can be considered as a signal of an efficient iron

clearance in lung epithelium, with the cells no longer needing to detox intracellular excess iron by Ftn storage and Fpn-mediated export [Cutone et al. 2019].

The third and last model regards the role of bLf on SARS-CoV-2 infection. As still recently reported [Kim et al. 2020], there is a significant lack of treatments on COVID-19 patients proven to be efficacious in early phase or mild infection, since immediate benefits of such strategies could lead to the improvement of patient outcomes and prevention of hospital recovery. Longer-term benefits may include prevention of the chronic consequences of infection as well as prevention of transmission by shortening the time length of infectiousness.

Hence, in this study, I focused our attention on the well-known anti-viral and immunomodulating properties of bLf as potential supplementary nutraceutical agent in the management of mild-to-moderate and asymptomatic COVID-19 patients.

The in vitro antiviral activity of bLf against enveloped and naked DNA and RNA viruses has been widely demonstrated [van der Strate et al. 2001; Lang et al. 2011; Berlutti et al. 2011; Wakabayashi et al. 2014; Ng et al. 2015], while some papers have been published on its *in vivo* efficacy against viral infection [Lu et al. 1997; Tanaka et al. 1999; Okada et al. 2002; Hirashima et al. 2004; Ishibashi et al. 2005; Shin et al. 2005; Ueno et al. 2006; Egashira et al. 2007; Chen et al. 2008; Yen et al. 2011; Vitetta et al. 2013].

The ability of bLf to inhibit viral infection is generally attributed to its binding to cell surface molecules and/or viral particles. BLf is able to competitively bind to heparan sulfate proteoglycans, present on the host cell surface and identified as initial interaction sites for enveloped viruses [Spear 2004; Sapp and Bienkowska-Haba 2009], thus hindering the viral adhesion and internalization [Lang et al. 2011; Marchetti et al. 2004; Chien et al. 2008]. Moreover, bLf can also bind directly to surface proteins of virus particles as HIV V3 loop of the gp120 [Swart et al. 1996] and HCV E2 envelope proteins [Nozaki et al. 2003].

The results, presented here, obtained by monitoring the effect of bLf against on SARS-CoV-2 on different experimental procedures indicate that the antiviral activity of bLf, pre-incubated with host cells, seems to vary according to MOI, different cell lines and bLf concentration. As a matter of fact, the pre-incubation of Vero E6 monolayers with 100 µg/ml of bLf, before SARS-CoV-2 infection at MOI 0.1 and 0.01, were ineffective in inhibiting virus internalization, differently to that observed when 100 µg/ml of bLf were pre-incubated with Caco-2 cells and the infection was performed at MOI 0.01 [Campione et al. 2020]. This antiviral activity was observed until 48 hpi [Campione et al. 2020].

The pre-incubation of 100 µg/ml of bLf with SARS-CoV-2 showed a significant antiviral activity higher at 0.01 MOI compared to 0.1 MOI after infection of Vero E6 cells, while a significant

antiviral activity assayed on Caco-2 cell lines was observed only with MOI 0.01 at 24 hpi [Campione et al. 2020]. In the other two experimental conditions, bLf did not show any significant antiviral activity on both Vero E6 and Caco-2 cells [Campione et al. 2020].

The pre-incubation of 500 µg/ml of bLf with Caco-2 cells showed a decrease of viral load until 24 hpi at MOI 0.1 and up to 48 hpi at MOI 0.01. Furthermore, the pre-incubation of 500 µg/ml of bLf with SARS-CoV-2 showed a significant decrease of SARS-CoV-2 RNA copies at both MOI 0.1 and 0.01. This antiviral activity persisted from 6 to 48 hpi [Campione et al. 2020]. In the other two experimental conditions, bLf exerted a significant antiviral activity only at 6 and 24 hpi when the MOI corresponded to 0.1. At MOI 0.01, a decrease of viral load up to 24 hpi was observed when bLf was added together with SARS-CoV-2 inoculum during the adsorption step, while a decrease of viral load until 48 hpi was observed when both the cell monolayer and SARS-CoV-2 were previously pre-incubated with bLf [Campione et al. 2020].

Our experimental results indicate that bLf exerts its antiviral activity either by direct attachment to the viral particles or by obscuring their cellular receptors. Moreover, the results obtained through the molecular docking and molecular dynamics simulation approaches strongly support the hypothesis of a direct recognition between the bLf and the Spike S glycoprotein. The affinity between their molecular surfaces, the large number of atomistic interactions detected and their persistence during the simulation suggest that this recognition is very likely to occur and that bLf may hinder the Spike S attachment to the human ACE2 receptor, consequently blocking the virus from entering into the cells [Campione et al. 2020].

Taken together these results reveal that, even if the definitive mechanism of action still has to be completely investigated, the antiviral properties of bLf are also extendable to SARS-CoV-2 virus.

In order to explore the helpful antiviral and immunomodulating effect of bLf and its possible role in the management of asymptomatic and mild-to-moderate COVID-19 patients, a clinical trial to investigate the effect and safety of this nutraceutical agent was designed.

Several studies based on COVID-19 clinical epidemiology indicate and propose the use of bLf in protecting against the virus also in vivo. Indeed, it has been reported that the incidence of COVID-19 in children aged 0-10 was only 0.9% in the Chinese cases, and infants developed a less severe disease form [Hong et al. 2020]. Consecutively, some authors postulated that breastfeeding or extensive use of bLf containing infant formula in this population may have protected from contagion or worst disease evolution [Chang et al. 2020; Root-Bernstein 2020].

The focus of this research is carried out on asymptomatic and mild-to-moderate COVID-19 patients, considering them a transmission reservoir with possible evolution to the most severe disease form [Jiang et al. 2020]. Li, W. et al. [2020], analyzing the viral shedding dynamics in

asymptomatic and mildly symptomatic patients infected with SARS-CoV-2, observed a long-term viral shedding, also in the convalescent phase of the disease, where specific antibody production to SARS-CoV-2 may not guarantee viral clearance after hospital discharge. In their study, the median duration of viral shedding appeared to be shorter in pre-symptomatic patients (11.5 days) than in asymptomatic (28 days) and mild symptomatic cases (31 days) [Li, W. et al. 2020]. Accordingly, a significantly reduced mean time length of rRT-PCR SARS-COV-2 RNA negative conversion in bLf-supplemented group comparing SOC-treated and non-treated patients was observed, thus suggesting a favoring gradual viral clearance and clinical symptoms recovery with a potential decrease in the risk of transmission and contagion [Campione et al. 2020].

Although there are currently rare satisfactory markers for predicting the worsening of the disease, some cytokines, including IL-6, IL-10 and TNF-α, and D-Dimer levels have been described as biomarkers related to the severe SARS-CoV-2 infection [Aziz et al. 2020; Li, L.Q. et al 2020; Tang et al. 2020; Xu et al. 2020]. In this study, a statistically significant difference between bLf-supplemented COVID-19 patients and the control group of COVID-19 negative subjects was observed in several blood parameters, including IL-6, D-Dimer, Ftn and liver function parameters [Campione et al. 2020]. Particularly, IL-6, D-Dimer and Ftn showed a significant decrease after bLf supplementation, possibly focusing them, if confirmed in a larger series of cases, as suitable COVID-19 treatment target markers [Campione et al. 2020].

Mainly, IL-6 elevation is considered to be associated with higher disease severity; IL-6 inhibitors, such as tocilizumab, have been used to treat severe COVID-19 patients [Cortegiani et al. 2020; Maeda et al. 2020]. The ability of bLf to down-regulate pro-inflammatory cytokines, such as IL-6, has already been demonstrated both in in vitro [Cutone et al. 2017] and in vivo [Valenti et al. 2017; Cutone et al. 2019] models, as well as in clinical trials [Lepanto et al. 2018]. To our knowledge, even though in a small sample size, it should be the first evidence showing an IL-6 down-regulation in COVID-19 patients after bLf supplementation during SARS-CoV-2 infection, without side effects [Campione et al. 2020].

It was also observed a statistically significant decline in D-Dimer levels, crucial to define disease prognosis, possibly leading to a reduction in SARS-CoV-2 complications related to coagulation derangement. Recently, it has been shown that bLf can regulate the activation of plasminogen and control coagulation cascade with a remarkable antithrombotic activity [Zwirzitz et al. 2018]. This property could be relevant considering that COVID-19 is a prothrombotic disease and that the severity of the coagulation parameters impairment is related to a poor prognosis. In light of this view, SARS-CoV-2 is able to active prominent prothrombotic state rarely observed in viral diseases. Patients affected by severe COVID-19 pneumonia are at higher risk of imbalance of

coagulation parameters and thus treated with low molecular weight heparin or unfractionated heparin at doses registered for prevention of venous thromboembolism [Marietta et al. 2020].

This clinical experience could lead us to speculate a potential protective and safe role of an early supplementation of bLf in COVID-19 patients in controlling the risk of a thromboembolic evolution of the disease [Campione et al. 2020]. BLf can exert negative regulatory effects on cell migration via inhibition of plasminogen activation and through the regulation of fibrinolysis [Zwirzitz et al. 2018]. In addition, it was observed an increased platelet count after bLf treatment [Campione et al. 2020]. Indeed, COVID-19 induces thrombocytopenia as SARS-CoV-2 seems to entrap megakaryocytes and block the release of platelets. A bLf rebalanced platelet count induces COVID-19 viral clearance [Thachil 2020].

Ftn, besides reflecting the status of iron stores in healthy individuals, represents also an acute-phase-protein up-regulated and elevated in both infectious and non-infectious inflammation. In COVID-19, it has been reported to be relevant for assessing disease severity and patients' outcome [Bolondi et al. 2020; Kappert et al. 2020]. In particular, serum Ftn concentration shows significant higher values in COVID-19 patients with worse outcome compared to good outcome [Satis et al. 2021]. Iron chelators, such as bLf, have been repeatedly proposed as a potential therapeutic target during infections [Dalamaga et al. 2020] and even in COVID-19. The reduction of Ftn levels observed after bLf administration demonstrates its anti-inflammatory activity together with iron chelating ability [Campione et al. 2020], which is pivotal for bacterial and viral replication, and at the basis of its antibacterial and antiviral activity [Valenti and Antonini 2005; Berlutti et al. 2011; Wakabayashi et al. 2014].

Liver function is known to be deranged in COVID-19 and a meta-analysis showed that 16% and 20% of patients with COVID-19 had ALT and AST levels higher than the normal range [Deng et al. 2020]. Liver biochemistry abnormality in COVID-19 patients could be ascribed to several factors, such as direct hepatocyte injury by the virus, drug-induced liver injury, hypoxic-ischemic microcirculation disorder, and underlying liver diseases [Xu et al. 2020]. In this study, it was observed that bLf reduced transaminases levels [Campione et al. 2020], decreasing the risk of liver-injury among COVID-19 patients, which is a frequent complication in SARS-CoV-2 severe forms [Wang et al. 2020].

Regarding clinical symptoms recovery in the bLf arm it was observed a gradual reduction of all symptoms, with the exception of fatigue, which persisted in 21.9% of patients [Campione et al. 2020]. This result could be due to by patients age and concomitant comorbidities, which could create a bias to identify COVID-19 symptoms. On the other hand, in SOC-treated patients, a partial

symptoms recovery and particularly the persistence of anosmia and ageusia in all the affected patients, even at the end of treatment were observed [Campione et al. 2020].

Concerning bLf safety, it was seen gastrointestinal complaints in 2 patients that did not lead to treatment discontinuation [Campione et al. 2020]. Regarding the SOC regimen group limited adverse events related to the assumption of HCQ were observed [Campione et al. 2020] even though its use is controversial as in literature are reported cases of liver injuries linked to the drug [Kelly et al. 2020].

Of note, in this study was used formulations containing bLf embedded in liposomes for nasal/oral administration. Indeed, the bLf at 5% of iron saturation form is best suited to obtain the maximum chelating effect. Nucleic digestion, in the nasal cavities, and proteases and lipases hydrolysis, at gastric and intestinal level, inactivate the protein at its first entry, cancelling or extremely reducing the activity. BLf is unstable in water and is particularly sensitive to bacterial and human proteases. This results in protein denaturation, poor absorption and inactivation. The inclusion of bLf in preserving structures, such as liposomes, reduces gastric and intestinal denaturation while maintaining its integrity and therefore its biological functionality [Kato et al. 1993; Liu et al. 2017; Meshulam and Lesmes 2014].

One of the limitations of this study was the small sample size of the clinical trial. Further studies, both in vitro and in vivo are needed to better deepen bLf placement against COVID-19, both as a preventive, adjunctive or in monotherapy. Further studies on larger samples are needed to better evaluate the role bLf in treating SARS-CoV-2 [Campione et al. 2020].

BLf could be considered as an effective supplement in mild to moderate and asymptomatic COVID-19 patients, which are not clearly included in therapeutically guidelines, allowing improvement of patient outcomes and prevention of hospital recovery, but also prevention of the chronic consequences of infection as well as prevention of transmission by shortening the time length of infectiousness.

6. CONCLUSIONS

As emerging from this study, bLf is a natural iron-binding cationic glycoprotein able to hinder bacterial and viral infection as well as inflammatory and iron homeostasis disorders. These multifunctional bLf activities are exerted through (i) its ability to bind two ferric ions per molecule with high affinity; (ii) its cationic feature and (iii) its ability to enter inside the nucleus of the host cells. The integrity, purity and iron and metal saturation rate of commercial bLf preparations influence all these functions.

Thanks to iron binding ability, bLf inhibits microbial growth. Iron is an essential element for several microorganisms and when it is in excess, induces an increasing of host susceptibility to infections. In this respect, the ability of bLf to bind this metal leads to the decrease of free iron thus inhibiting bacterial and viral multiplication.

From the cationic feature, bLf hinders the bacterial and viral adhesion to and the entry into cells. In fact, bLf can interact with negatively charged compounds of host cell surfaces, thus inhibiting bacterial and viral interaction with host cell receptors.

From the ability to enter inside the nucleus, bLf exerts a potent anti-inflammatory activity modulating pro-inflammatory gene expression in the host cells. In addition, it is well known the correlation between inflammatory condition and iron homeostasis disorders. The capacity of bLf to act as an anti-inflammatory glycoprotein is based on the reduction of pro-inflammatory cytokines and, consequently, to restore the iron homeostasis disorders.

It is important to be aware that, when investigating bLf activities, several parameters influence the results, including its physico-chemical properties [Rosa et al. 2018]. In fact, the use of different commercial or self-produced bLf preparations, showing unlike rates of purity, integrity, iron binding ability and iron or metal saturation rate, can affect the multifunctional activities of this glycoprotein [Rosa et al. 2018].

Concerning the anti-bacterial and anti-viral activities exerted by bLf, the iron saturation rate, the integrity and the absence of ineffective digestive fragments influence these functions.

Regarding the anti-inflammatory activity, even if Suzuki et al. [2008] have demonstrated the importance of the sole N-lobe, with respect to C-lobe, for bLf binding, internalization, and targeting to the nucleus, the integrity of bLf preparation is essential to exert its anti-inflammatory activity. Another pivotal parameter to be checked in bLf preparations is the different degree of LPS contamination. Indeed, bLf-bound LPS has been found to interfere with inflammatory pathways in in vitro experiments [Curran et al. 2006].

From all the above, a meticulous quality analysis of commercial or self-produced bLf preparations is of the utmost importance when studying its activities against bacterial and viral infection as well as related inflammatory and iron homeostasis disorders.

In conclusion, even if several other in vitro experiments are required to understand the molecular mechanisms by which bLf exerts the multifunctional activities, we can conclude that bLf is the sole glycoprotein able to contemporarily act against bacterial and viral infection as well as inflammation and iron homeostasis disorders.

7. REFERENCES

Abraham, M.J.; Murtola, T.; Schulz, R.; Páll, S.; Smith, J.C.; Hess, B.; Lindahl, E. GROMACS: High performance molecular simulations through multi-level parallelism from laptops to supercomputers. *SoftwareX* **2015**, 1–2, 19–25.

Adams-Chapman, I.; Stoll, B.J. Systemic inflammatory response syndrome. *Semin. Pediatr. Infect. Dis.* **2001**, 12, 5–16.

Agarwal, A.; Chen, A.; Ravindran, N.; To, C.; Thuluvath, P.J. Gastrointestinal and Liver Manifestations of COVID-19. *J. Clin. Exp. Hepatol.* **2020**, 10, 263–265.

Ajello, M.; Greco, R.; Giansanti, F.; Massucci, M.T.; Antonini, G.; Valenti, P. Anti-invasive activity of bovine lactoferrin towards group A streptococci. *Biochem. Cell Biol.* **2002**, 80, 119–124.

Akiyama, Y.; Oshima, K.; Kuhara, T.; Shin, K.; Abe, F.; Iwatsuki, K.; Nadano, D.; Matsuda, T. A lactoferrin-receptor, intelectin 1, affects uptake, sub-cellular localization and release of immunochemically detectable lactoferrin by intestinal epithelial Caco-2 cells. *J. Biochem.* **2013**, *154*, 437–448.

Al-Younes, H. M.; Rudel, T.; Brinkmann, V.; Szczepek, A. J.; Meyer, T. F. Low iron availability modulates the course of Chlamydia pneumoniae infection. *Cell. Microbiol.* **2001**, 3, 427–437.

Alanagreh L, Alzoughool F, Atoum M. The Human Coronavirus Disease COVID-19: Its Origin, Characteristics, and Insights into Potential Drugs and Its Mechanisms. Pathogens. 2020, 29;9(5):331.

Alexander, D.B.; Iigo, M.; Yamauchi, K.; Suzui, M.; Tsuda, H. Lactoferrin: An alternative view of its role in human biological fluids. *Biochem. Cell Biol.* **2012**, *90*, 279–306.

Ammendolia, M.G.; Bertuccini, L.; Iosi, F.; Minelli, F.; Berlutti, F.; Valenti, P.; Superti, F. Bovine lactoferrin interacts with cable pili of *Burkholderia cenocepacia*. *Biometals* **2010**, *23*, 531–542.

Anderson, B.F.; Baker, H.M.; Norris, G.E.; Rumball, S.V.; Baker, E.N. Apolactoferrin structure demonstrates ligand-induced conformational change in transferrins. *Nature.* **1990**, *344*, 784–787.

Anderson, M.R.; Klink, K.; Cohrssen, A. Evaluation of vaginal complaints. JAMA 2004, 291, 1368–1379.

Andrews, N.C. Disorders of iron metabolism. *N. Engl. J. Med.* **2000**, *341*, 1986–1995.

Antonini, G.; Catania, M.R.; Greco, R.; Longhi, C.; Pisciotta, M.G.; Seganti, L.; Valenti, P. Antiinvasive activity of bovine lactoferrin towards *Listeria monocytogenes*. *J. Food Protect.* **1997**, *1*, 60–72.

Appelmelk, B.J.; An, Y.Q.; Geerts, M.; Thijs, B.G.; de Boer, H.A.; MacLaren, D.M.; de Graaff, J.; Nuijens, J.H. Lactoferrin is a lipid A-binding protein. *Infect. Immun.* **1994**, *62*, 2628–2632.

Araújo, A.N.; Giugliano, L.G. Human milk fractions inhibit the adherence of diffusely adherent *Escherichia coli* (DAEC) and enteroaggregative *E. coli* (EAEC) to HeLa cells. *FEMS Microbiol. Lett.* **2000**, *184*, 91–94.

Arias, M.; Hilchie, A.L.; Haney, E.F.; Bolscher, J.G.; Hyndman, M.E.; Hancock, R.E.; Vogel, H.J. Anticancer activities of bovine and human lactoferricin-derived peptides. *Biochem. Cell Biol.* **2017**, *95*, 91–98.

Armitage, A.E.; Stacey, A.R.; Giannoulatou, E.; Marshall, E.; Sturges, P.; Chatha, K.; Smith, N.M.; Huang, X.; Xu, X.; Pasricha, S.R. Distinct patterns of hepcidin and iron regulation during HIV-1, HBV, and HCV infections. *PNAS* **2014**, 111, 12187–12192.

Armstead, A.L.; Li, B. Nanomedicine as an emerging approach against intracellular pathogens. *Int. J. Nanomed.***2011**, *6*, 3281–3293.

Ashida, K.; Sasaki, H.; Suzuki, Y.A.; Lönnerdal, B. Cellular internalization of lactoferrin in intestinal epithelial cells. *Biometals* **2004**, *17*, 311–315.

Aziz, M.; Fatima, R.; Assaly, R. Elevated interleukin-6 and severe COVID-19: A meta-analysis. *J. Med. Virol.* **2020**.

Baker, E.N. Structure and reactivity of transferrins. *Adv. Inorg. Chem.* **1994**, *41*, 389–463.

Baker, E.N.; Anderson, B.F.; Baker, H.M.; Day, C.L.; Haridas, M.; Norris, G.E.; Rumball, S.V.; Smith, C.A.; Thomas, D.H. Three-dimensional structure of lactoferrin in various functional states. *Adv. Exp. Med. Biol.* **1994**, *357*, 1–12.

Baker, E.N.; Baker, H.M. A structural framework for understanding the multifunctional character of lactoferrin. *Biochimie* **2009**, *91*, 3–10.

Baker, E.N.; Baker, H.M.; Kidd, R.D. Lactoferrin and transferrin: Functional variations on a common structural framework. *Biochem. Cell Biol.* **2002**, *80*, 27–34.

Baker, E.N.; Lindley, P.F. New perspectives on the structure and function of transferrins. *J. Inorg. Biochem.* **1992**, *47*, 147–160.

Baker, E.P.; Rumball, S.V.; Anderson, B.F. Transferrins: Insights into structure and function from studies on lactoferrin. *Trends Biochem Sci.* **1987**, *12*, 350–353.

Baker, H.M.; Baker, E.N. A structural perspective on lactoferrin function. *Biochem. Cell. Biol.* **2012**, *90*, 320–328.

Barrile, R., Kasendra, M., Rossi-Paccani, S., Merola, M., Pizza, M., Baldari, C., et al. Neisseria meningitidis subverts the polarized organization and intracellular trafficking of host cells to cross the epithelial barrier. *Cell. Microbiol.* **2015**, 17, 1365–1375.

Bastidas, R.J.; Elwell, C.A.; Engel, J.N.; Valdivia, R.H. Chlamydial intra- cellular survival strategies. *Cold Spring Harb. Perspect. Med.* **2013**, 3, a010256.

Beddek, A.J.; Schryvers, A.B. The lactoferrin receptor complex in Gram negative bacteria. *Biometals* **2010**, *23*, 377–386.

Behnia, F.; Sheller, S.; Menon, R. Mechanistic Differences Leading to Infectious and Sterile Inflammation. *Am. J. Reprod. Immunol.* **2016**, *75*, 505–518.

Beigi, R.H.; Yudin, M.H.; Cosentino, L.; Meyn, L.A.; Hillier, S.L. Cytokines, pregnancy, and bacterial vaginosis: Comparison of levels of cervical cytokines in pregnant and non-pregnant women with bacterial vaginosis. *J. Infect. Dis.* **2007**, 196, 1355–1360.

Bellamy, W.; Takase, M.; Wakabayashi, H.; Kavase, K.; Tomita, M. Antibacterial spectrum of lactoferricin B, a potent bactericide peptide derived from the N-terminal region of bovine lactoferrin. *J. Appl. Bacteriol.* **1992**, *73*, 472–479.

Bellmann-Weiler R, Lanser L, Barket R, et al. Prevalence and predictive value of anemia and dysregulated iron homeostasis in patients with COVID-19 infection. *J Clin Med.* **2020**; 9: 2429- 2439.

Berghella, V.; Rafael, T.J.; Szychowski, J.M.; Rust, O.A.; Owen, J. Cerclage for short cervix on ultrasonography in women with singleton gestations and previous pre-term birth: A meta-analysis. *Obstet. Gynecol.* **2011**, *117*, 663–671.

Berlutti, F.; Catizone, A.; Ricci, G.; Frioni, A.; Natalizi, T.; Valenti, P.; Polimeni, A. *Streptococcus mutans* and *Streptococcus sobrinus* are able to adhere and invade human gingival fibroblast cell line. *Int. J. Immunopathol. Pharmacol.* **2010**, *23*, 1253–1260.

Berlutti, F.; Morea, C.; Battistoni, A.; Sarli, S.; Cipriani, P.; Superti, F.; Ammendolia, M.G.; Valenti, P. Iron availability influences aggregation, biofilm, adhesion and invasion of *Pseudomonas aeruginosa* and *Burkholderia cenocepacia*. *Int. J. Immunopathol. Pharmacol.* **2005**, *18*, 661–670.

Berlutti, F.; Pantanella, F.; Natalizi, T.; Frioni, A.; Paesano, R.; Polimeni, A.; Valenti, P. Antiviral properties of lactoferrin–a natural immunity molecule. *Molecules* **2011**, *16*, 6992–7018.

Berlutti, F.; Schippa, S.; Morea, C.; Sarli, S.; Perfetto, B.; Donnarumma, G.; Valenti, P. Lactoferrin downregulates pro-inflammatory cytokines up-expressed in intestinal epithelial cells infected with invasive or noninvasive *Escherichia coli* strains. *Biochem. Cell Biol.* **2006**, *84*, 351–357.

Berlutti, F.; Superti, F.; Nicoletti, M.; Morea, C.; Frioni, A.; Ammendolia, M.G.; Battistoni, A.; Valenti, P. Bovine lactoferrin inhibits the efficiency of invasion of respiratory A549 cells of different iron-regulated morphological forms of *Pseudomonas aeruginosa* and *Burkholderia cenocepacia*. *Int. J. Immunopathol. Pharmacol.* **2008**, *21*, 51–59.

Bianconi, I.; Jeukens, J.; Freschi, L.; Alcalá-Franco, B.; Facchini, M.; Boyle, B.; Molinaro, A.; Kukavica-Ibrulj, I.; Tümmler, B.; Levesque, R.C.; et al. Comparative genomics and biological characterization of sequential Pseudomonas aeruginosa isolates from persistent airways infection. *BMC Genomics* **2015**, 16, 1105.

Bogavac, M.; Brkic, S.; Simin, N.; Celic, D. Mid-pregnancy interleukin levels in serum and amniotic fluid as predictors of preterm delivery. *J. Matern. Fetal Neonatal Med.* **2012**.

Bolondi, G.; Russo, E.; Gamberini, E.; Circelli, A.; Meca, M.C.C.; Brogi, E.; Viola, L.; Bissoni, L.; Poletti, V.; Agnoletti, V. Iron metabolism and lymphocyte characterisation during Covid-19 infection in ICU patients: an observational cohort study. *World J Emerg Surg* **2020**, *15*.

Bonaccorsi di Patti, M.C.; Cutone, A.; Polticelli, F.; Rosa, L.; Lepanto, M.S.; Valenti, P.; Musci, G. The ferroportin-ceruloplasmin system and the mammalian iron homeostasis machine: Regulatory pathways and the role of lactoferrin. *BioMetals* **2018**, *31*, 399–414.

Bragonzi, A.; Horati, H.; Kerrigan, L.; Lorè, N.I.; Scholte, B.J.; Weldon, S. Inflammation and host-pathogen interaction: Cause and consequence in cystic fibrosis lung disease. J. Cyst. Fibros. 2017, 17, S40–S45.

Brandenburg, K.; Jurgens, G.; Muller, M.; Fukuoka, S.; Koch, M.H.J. Biophysical characterization of lipopolysaccharide and lipid A inactivation by lactoferrin. *Biol. Chem.* **2001**, *382*, 1215–1225.

Brissot, P.; Pietrangelo, A.; Adams, P.; de Graaff, B.; McLaren, C.E.; Loréal, O. Haemochromatosis. *Nat Rev Dis Primers* **2018** 4, 18016.

Brissot, P.; Troadec, M.B.; Loréal, O.; Brissot, E. Pathophysiology and classification of iron overload diseases; update 2018. *Transfus. Clin. Biol.* **2019**, *26*, 80–88.

Brotman, R.M.; Klebanoff, M.A.; Nansel, T.R.; Yu, K.F.; Andrews, W.W.; Zhang, J.; Schwebke, J.R. Bacterial vaginosis assessed by gram stain and diminished colonization resistance to incident gonococcal, chlamydial, and trichomonal genital infection. *J. Infect. Dis.* **2010**, 202, 1907–1915.

Bruns, C.M.; Nowalk, A.J.; Arvai, A.S.; McTigue, M.A.; Vaughan, K.G.; Mietzner, T.A.; McRee, D.E. Structure of Haemophilus influenzae Fe (+3)-binding protein reveals convergent evolution within a superfamily. *Nat. Struct. Biol.* **1997**, *4*, 919–924.

Burckhardt, C.J.; Greber, U.F. Virus Movements on the Plasma Membrane Support Infection and Transmission between Cells. *PLoS Pathog.* **2009**, *5*, e1000621.

Burgueño, J.F.; Reich, A.; Hazime, H.; A Quintero, M.; Fernandez, I.; Fritsch, J.; Santander, A.M.; Brito, N.; Damas, O.M.; Deshpande, A.; et al. Expression of SARS-CoV-2 Entry Molecules ACE2 and TMPRSS2 in the Gut of Patients With IBD. *Inflamm. Bowel Dis.* **2020**, 26, 797–808.

Camaschella, C.; Nai, A.; Silvestri, L. Iron metabolism and iron disorders revisited in the hepcidin era. *Haematologica.* **2020**; 105: 260- 272.

Campione, E.; Lanna, C.; Cosio, T.; Rosa, L.; Conte, M.P.; Iacovelli, F.; Romeo, A.; Falconi, M.; et al. Lactoferrin as potential supplementary nutraceutical agent in COVID-19 patients: *in vitro* and *in vivo* preliminary evidences. *bioRxiv*, **2020**.

Carnevale, S.; Beretta, P.; Morbini, P. Direct endothelial damage and vasculitis due to SARS-CoV-2 in small bowel submucosa of COVID-19 patient with diarrhea. *J. Med Virol.* 2020.

Carrano, C. J.; Raymond, K. N. Ferric Iron Sequestering agents. 2. kinetics and mechanism of iron removal from transferrin by enterobactin and synthetic tricatechols. *J. Am. Chem. Soc.* 1979, 101, 5401–5404.

Case, D.; Betz, R.; Cerutti, D.; Cheatham, T.; Darden, T.; Duke, R.; Giese, T.; Gohlke, H.; Goetz, A.; Homeyer, N. Amber 2016; *Univ. California: San Fr*, **2016**.

Casu, C.; Nemeth, E.; Rivella, S. Hepcidin agonists as therapeutic tools. *Blood* **2018**, *131*, 1790–1794.

Chang, R.; Ng, T.B.; Sun, W.-Z. Lactoferrin as potential preventative and treatment for COVID-19. *Int. J. Antimicrob. Agents* **2020**, 106118.

Chen, H.-L.; Wang, L.-C.; Chang, C.-H.; Yen, C.-C.; Cheng, W.T.K.; Wu, S.-C.; Hung, C.-M.; Kuo, M.-F.; Chen, C.-M. Recombinant porcine lactoferrin expressed in the milk of transgenic mice protects neonatal mice from a lethal challenge with enterovirus type 71. *Vaccine* **2008**, *26*, 891–898.

Chen, L.; Zhong, L. Genomics functional analysis and drug screening of SARS-CoV-2. Genes Dis. 2020.

Chen, Y.; Guo, Y.; Pan, Y.; Zhao, Z.J. Structure analysis of the receptor binding of 2019-nCoV. *Biochem. Biophys. Res. Commun*. **2020**, 525, 135–140.

Chien, Y.-J.; Chen, W.-J.; Hsu, W.-L.; Chiou, S.-S. Bovine lactoferrin inhibits Japanese encephalitis virus by binding to heparan sulfate and receptor for low density lipoprotein. *Virology* **2008**, *379*, 143–151.

Chien, Y.J.; Chen, W.J.; Hsu, W.L.; Chiou, S.S. Bovine lactoferrin inhibits japanese encephalitis virus by binding to heparan sulfate and receptor for low density lipoprotein. *Virology* **2008**, *379*, 143–151.

Chu, H.; Chan, J.F.-W.; Yuen, T.T.-T.; Shuai, H.; Yuan, S.; Wang, Y.; Hu, B.; Yip, C.C.-Y.; Tsang, J.O.-L.; Huang, X.; et al. Comparative tropism, replication kinetics, and cell damage profiling of SARS-CoV-2 and SARS-CoV with implications for clinical manifestations, transmissibility, and laboratory studies of COVID-19: an observational study. *The Lancet Microbe* **2020**, 1, e14–e23.

Cigana, C.; Lorè, N.I.; Riva, C.; De Fino, I.; Spagnuolo, L.; Sipione, B.; Rossi, G.; Nonis, A.; Cabrini, G.; Bragonzi, A. Tracking the immunopathological response to *Pseudomonas aeruginosa* during respiratory infections. *Sci Rep.* **2016**, 6, 21465.

Ciofu O, Hansen CR, Høiby N. Respiratory bacterial infections in cystic fibrosis. *Curr Opin Pulm Med.* **2013**, 19:251–258.

Cockx, M.; Gouwy, M.; Van Damme, J.; Struyf, S. Chemoattractants and cytokines in primary ciliary dyskinesia and cystic fibrosis: Key players in chronic respiratory diseases. *Cell Mol. Immunol.* **2018**, 15, 312–323.

Coffey, R.; Ganz, T. Iron homeostasis: An anthropocentric perspective. *J. Biol. Chem.* **2017**, *292*, 12727–12734.

Conti, P.; Ronconi, G.; Caraffa, A.; Gallenga, C.; Ross, R.; Frydas, I.; Kritas, S. Induction of pro-inflammatory cytokines (IL-1 and IL-6) and lung inflammation by Coronavirus-19 (COVI-19 or SARS-CoV-2): Anti-inflammatory strategies. *J. Biol. Regul. Homeost. Agents* **2020**, 34, 1.

Corman, V.M.; Landt, O.; Kaiser, M.; Molenkamp, R.; Meijer, A.; Chu, D.K.; Bleicker, T.; Brünink, S.; Schneider, J.; Schmidt, M.L.; et al. Detection of 2019 novel coronavirus (2019-nCoV) by real-time RT-PCR. *Euro Surveill.* **2020**, 25.

Corna, G.; Campana, L.; Pignatti, E.; Castiglioni, A.; Tagliafico, E.; Bosurgi, L.; Campanella, A.; Brunelli, S.; Manfredi, A.A.; Apostoli, P.; et al. Polarization dictates iron handling by inflammatory and alternatively activated macrophages. *Haematologica* **2010**, *95*, 1814–1822.

Cortegiani, A.; Ippolito, M.; Greco, M.; Granone, V.; Protti, A.; Gregoretti, C.; Giarratano, A.; Einav, S.; Cecconi, M. Rationale and evidence on the use of tocilizumab in COVID-19: a systematic review. *Pulmonology* **2020**.

Cui, J.; Li, F.; Shi, Z. Origin and evolution of pathogenic coronaviruses. *Nat. Rev. Genet.* **2018**, 17, 181–192.

Curran, C.S.; Demick, K.P.; Mansfield, J.M. Lactoferrin activates macrophages via TLR4-dependent and -independent signaling pathways. *Cell. Immunol.* **2006**, *242*, 23–30.

Cutone, A.; Colella, B.; Pagliaro, A.; Rosa, L.; Lepanto, M.S.; Bonaccorsi di Patti, M.C.; Valenti, P.; Di Bartolomeo, S.; Musci, G. Native and iron-saturated bovine lactoferrin differently hinder migration in a model of human glioblastoma by reverting epithelial-to-mesenchymal transition-like process and inhibiting interleukin-6/STAT3 axis. *Cell Signal.* **2020**, *65*, 109461.

Cutone, A.; Frioni, A.; Berlutti, F.; Valenti, P.; Musci, G.; Bonaccorsi di Patti, M.C. Lactoferrin prevents LPS-induced decrease of the iron exporter ferroportin in human monocytes/macrophages. *BioMetals* **2014**, *27*, 807–813.

Cutone, A.; Rosa, L.; Ianiro, G.; Lepanto, M.S.; Bonaccorsi di Patti, M.C.; Valenti, P.; Musci, G. Lactoferrin's Anti-Cancer Properties: Safety, Selectivity, and Wide Range of Action. *Biomolecules.* **2020**;10(3):456.

Cutone, A.; Rosa, L.; Lepanto, M.S.; Scotti, M.J.; Berlutti, F.; Bonaccorsi di Patti, M.C.; Musci, G.; Valenti, P. Lactoferrin efficiently counteracts the inflammation-induced changes of the iron homeostasis system in macrophages. *Front. Immunol.* **2017**, *15*.

Czosnykowska-Łukacka, M.; Orczyk-Pawiłowicz, M.; Broers, B.; Królak-Olejnik, B. Lactoferrin in Human Milk of Prolonged Lactation. *Nutrients.* **2019**, *11*, 2350.

Dakin, C.J.; Numa, A.H.; Wang, H.; Morton, J.R.; Vertzyas, C.C.; Henry, R.L. Inflammation, infection, and pulmonary function in infants and young children with cystic fibrosis. *Am. J. Respir. Crit. Care Med.* **2002**, 165, 904–910.

Dalamaga, M.; Karampela, I.; Mantzoros, C.S. Commentary: Could iron chelators prove to be useful as an adjunct to COVID-19 Treatment Regimens? *Metab. Clin. Exp.* **2020**, *108*, 154260.

Dall'Agnola, A.; Tome, D.; Kaufman, D.A.; Tavella, E.; Pieretto, M.; Messina, A.; De Luca, D.; Bellaïche, M.; Mosca, A.; Piloquet, H.; et al. Role of Lactoferrin in Neonates and Infants: An Update. *Am. J. Perinatol.* **2018**, 35, 561–565.

Dalmastri, C.; Valenti, P.; Visca, P.; Vittorioso, P.; Orsi, N. Enhanced antimicrobial activity of lactoferrin by binding to the bacterial surface. *Microbiologica* **1988**, *11*, 225–230.

De Domenico, I.; Ward, D.M.; Kaplan, J. Regulation of iron acquisition and storage: Consequences for iron-linked disorders. *Nat. Rev. Mol. Cell Biol.* **2008**, *9*, 72–81.

Demmelmair, H.; Prell, C.; Timby, N.; Lönnerdal, B. Benefits of Lactoferrin, Osteopontin and Milk Fat Globule Membranes for Infants. *Nutrients* **2017**, *9*, 817.

Deng, X.; Liu, B.; Li, J.; Zhang, J.; Zhao, Y.; Xu, K. Blood biochemical characteristics of patients with coronavirus disease 2019 (COVID-19): a systemic review and meta-analysis. *Clin. Chem. Lab. Med.* **2020**, *58*, 1172–1181.

Deshmane, S.L.; Kremlev, S.; Amini, S.; Sawaya, B.E. Monocyte chemoattractant protein-1 (MCP-1): An overview. *J. Interferon Cytokine Res.* **2009**, 29, 313–326.

Dhar, D.; Mohanty, A. Gut microbiota and Covid-19- possible link and implications. *Virus Res.* **2020**, 285, 198018.

Di Biase, A.M.; Tinari, A.; Pietrantoni, A.; Antonini, G.; Valenti, P.; Conte, M.P.; Superti, F. Effect of bovine lactoferricin on enteropathogenic Yersinia adhesion and invasion in HEp-2 cells. *J. Med. Microbiol.* **2004**, *53*, 407–412.

Di Pietro, M., Filardo, S., De Santis, F., Sessa, R. New insights into Chlamydiae persistence: an energy metabolism strategy? *Int. J. Immunopathol. Pharmacol.* **2013**, 26(2): 525–528.

Dial, E.J.; Lichtenberger, L.M. Effect of lactoferrin on *Helicobacter felis* induced gastritis. *Biochem. Cell Biol.* **2002**, *80*, 113–117.

Diarra, M.S.; Petitclerc, D.; Deschenes, E.; Lessard, N.; Grondin, G.; Talbot, B.G.; Lacasse, P. Lactoferrin against *Staphylococcus aureus* mastitis. Lactoferrin alone or in combination with penicillin G on bovine polymorphonuclear function and mammary epithelial cells colonisation by *Staphylococcus aureus*. *Vet. Immunol. Immunopathol.* **2003**, *95*, 33–42.

Dickson, R.P. The microbiome and critical illness. *Lancet Respir. Med.* **2016**, 4, 59–72.

Donovan, A.; Lima, C.A.; Pinkus, J.L.; Pinkus, G.S.; Zon, L.I.; Robine, S.; Andrews, N.C. The iron exporter ferroportin/Slc40a1 is essential for iron homeostasis. *Cell Metab.* **2005**, *1*, 191–200.

Donovan, S.M. The Role of Lactoferrin in Gastrointestinal and Immune Development and Function: A Preclinical Perspective. *J. Pediatr.* **2016**, *173*, S16–S28.

Döring, G; Parameswaran, I.G.; Murphy, T.F. Differential adaptation of microbial pathogens to airways of patients with cystic fibrosis and chronic obstructive pulmonary disease. FEMS Microbiol Rev **2011**, 35:124 –146.

Drago-Serrano, M.E.; Campos-Rodriguez, R.; Carrero, J.C.; de la Garza, M. Lactoferrin and Peptide-derivatives: Antimicrobial Agents with Potential Use in Nonspecific Immunity Modulation. *Curr Pharm. Des.* **2018**, *24*, 1067–1078.

Drakesmith, H.; Prentice, A. Viral infection and iron metabolism. *Nat. Rev. Microbiol.* **2008**, 6, 541–552.

Dumas, A.; Bernard, L.; Poquet, Y.; Lugo-Villarino, G.; Neyrolles, O. The role of the lung microbiota and the gut-lung axis in respiratory infectious diseases. *Cell. Microbiol.* **2018**, 20, e12966.

Egashira, M.; Takayanagi, T.; Moriuchi, M.; Moriuchi, H. Does daily intake of bovine lactoferrin-containing products ameliorate rotaviral gastroenteritis? *Acta Paediatr.* **2007**, *96*, 1242–1244.

El Yazidi-Belkoura, I.; Legrand, D.; Nuijens, J.; Slomianny, M.C.; van Berkel, P.; Spik, G. The binding of lactoferrin to glycosaminoglycans on enterocyte-like HT29–18-C1 cells is mediated through basic residues located in the N-terminus. *Biochim. Biophys. Acta* **2001**, *1568*, 197–204.

Emerson, J.; Rosenfeld, M.; McNamara, S.; Ramsey, B.; Gibson, R.L. Pseudomonas aeruginosa and other predictors of mortality and morbidity in young children with cystic fibrosis. *Pediatr. Pulmonol.* **2002**, 34, 91–100.

Epand, R.M.; Vogel, H.J. Diversity of antimicrobial peptides and their mechanisms of action. *Biochim. Biophys. Acta.* **1999**, *1462*, 11–28.

Facchini, M.; De Fino, I.; Riva, C.; Bragonzi, A. Long term chronic Pseudomonas aeruginosa airway infection in mice. *J. Vis. Exp.* **2014**, 85.

Farage, M.A.; Miller, K.W.; Ledger, W.J. Determining the cause of vulvovaginal symptoms. *Obstet. Gynecol. Surv.* **2008**, 63, 445–464.

Fernandes, K.E.; Carter, D.A. The Antifungal Activity of Lactoferrin and Its Derived Peptides: Mechanisms of Action and Synergy with Drugs against Fungal Pathogens. *Front. Microbiol.* **2017**, *18*, 8:2.

Fillebeen, C.; Pantopoulos, K. Hepatitis C virus infection causes iron deficiency in Huh7.5.1 cells. *Plos One* **2013**, 8, e83307.

Fisher, A.L.; Nemeth, E. Iron homeostasis during pregnancy. *Am. J. Clin. Nutr.* **2017**, *106*, 1567S–1574S.

Folkesson A, Jelsbak L, Yang L, Johansen HK, Ciofu O, Høiby N, Molin S. Adaptation of *Pseudomonas aeruginosa* to the cystic fibrosis air- way: an evolutionary perspective. *Nat Rev Microbiol* **2012**, 10:841–851

Frazer, D.M.; Anderson, G.J. The orchestration of body iron intake: How and where do enterocytes receive their cues? *Blood Cells Mol. Dis.* **2003**, 30, 288–297.

Freidank, H. M., Billing, H., and Wiedmann-Al-Ahmad, M. Influence of iron restriction on Chlamydia pneumoniae and C. trachomatis. *J. Med. Microbiol.* **2001**, 50, 223–227.

Frioni, A.; Conte, M.P.; Cutone, A.; Longhi, C.; Musci, G.; di Patti, M.C.; Natalizi, T.; Marazzato, M.; Lepanto, M.S.; Puddu, P.; et al. Lactoferrin differently modulates the inflammatory response in epithelial models mimicking human inflammatory and infectious diseases. *Biometals* **2014**, 27, 843–856.

Fujitani S, Sun HY, Yu VL, Weingarten JA. Pneumonia due to *Pseudomonas aeruginosa*. Part I. Epidemiology, clinical diagnosis, and source. *Chest* **2011**, 139:909 –919.

Ganz, T. Iron and infection. *Int. J. Hematol.* **2018**, *107*, 7–15.

Ganz, T. Systemic iron homeostasis. *Physiol. Rev.* **2013**, 93, 1721–1741.

Garzon, J.I.; Lopéz-Blanco, J.R.; Pons, C.; Kovacs, J.; Abagyan, R.; Fernandez-Recio, J.; Chacon, P. FRODOCK: a new approach for fast rotational protein-protein docking. *Bioinformatics* **2009**, 25, 2544–2551.

Ghio, A.J. Disruption of iron homeostasis and lung disease. *Biochim. Biophys. Acta* **2009**, 1790, 731–739.

Ghio, A.J.; Fracica, P.J.; Young, S.L.; Piantadosi, C.A. Synthetic surfactant scavenges oxidants and protects against hyperoxic lung injury. *J. Appl. Physiol. (1985)*, **1994**, 77, 1217–1223.
Ghio, A.J.; Roggli, V.L.; Soukup, J.M.; Richards, J.H.; Randell, S.H.; Muhlebach, M.S. Iron accumulates in the lavage and explanted lungs of cystic fibrosis patients. *J. Cyst. Fibros.* **2013**, 12, 390–398.
Giannetti, A.M.; Snow, P.M.; Zak, O.; Bjorkman, P.J. Mechanism for multiple ligand recognition by the human transferrin receptor. *PLOS Biol.* **2003**, 1, e51.
Giansanti, F.; Leboffe, L.; Pitari, G.; Ippoliti, R.; Antonini, G. Physiological roles of ovotransferrin. *Biochim. Biophys. Acta* **2012**, *1820*, 218–225.
Gibson, R.L.; Burns, J.L.; Ramsey, B.W. Pathophysiology and management of pulmonary infections in cystic fibrosis. Am. J. Respir. *Crit. Care Med.* **2003**, 168, 918–951.
Gifford, A.H.; Moulton, L.A.; Dorman, D.B.; Olbina, G.; Westerman, M.; Parker, H.W.; Stanton, B.A.; O'Toole, G.A. Iron homeostasis during cystic fibrosis pulmonary exacerbation. *Clin. Transl. Sci.* **2012**, 5, 368–373.
Gifford, J.L.; Hunter, H.N.; Vogel, H.J. Lactoferricin: A lactoferrin-derived peptide with antimicrobial, antiviral, antitumor and immunological properties. *Cell. Mol. Life Sci.* **2005**, *62*, 2588–2598.
Gomez, H.F.; Ochoa, T.J.; Carlin, L.G.; Cleary, T.G. Human lactoferrin impairs virulence of *Shigella flexneri*. *J. Infect. Dis.* **2003**, *187*, 87–95.
Gómez, M.I.; Prince, A. Opportunistic infections in lung disease: Pseudomonas infections in cystic fibrosis. *Curr. Opin. Pharmacol.* **2007**, 7, 244–251.
Gomme, P.T.; McCann, K.B.; Bertolini, J. Transferrin: Structure, function and potential therapeutic actions. *Drug Discov. Today.* **2005**, *10*, 267–273.
Groot, F.; Geijtenbeek, T.B.; Sanders,R.W.; Baldwin, C.E.; Sanchez Hernandez, M.; Floris, R.; vanKooyk, Y.; de Jong, E.C.; Berkhout, B. Lactoferrin prevents dendritic cell-mediated human immunodeficiency virus type 1 transmission by blocking the Dc-SIGN—gp120 interaction. *J. Virol.* **2005**, *79*, 3009–3015.
Guo, Y.-R.; Cao, Q.-D.; Hong, Z.; Tan, Y.-Y.; Chen, S.; Jin, H.; Tan, K.-S.; Wang, D.Y.; Yan, Y. The origin, transmission and clinical therapies on coronavirus disease 2019 (COVID-19) outbreak-an update on the status. *Mil. Med Res.* **2020**, 7, 1–10.
Haberger, V.; Elgner, F.; Roos, J.; Bender, D.; Hildt, E. Regulation of the Transferrin Receptor Recycling in Hepatitis C Virus-Replicating Cells. *Front. Cell. Dev. Biol.* **2020**, 8, 44.
Hainer, B.L.; Gibson, M.V. Vaginitis: Diagnosis and Treatment. *Am. Fam. Physician.* **2011**, 83, 807–815.
Han, C.; Duan, C.; Zhang, S.; Spiegel, B.; Shi, H.; Wang, W.; Zhang, L.; Lin, R.; Liu, J.; Ding, Z.; et al. Digestive Symptoms in COVID-19 Patients with Mild Disease Severity. Am. J. Gastroenterol. **2020**, 115, 916–923.
Harding, C.; Heuser, J.; Stahl, P. Receptor-mediated endocytosis of transferrin and recycling of the transferrin receptor in rat reticulocytes biochemical approaches to transferrin. *J. Cell Biol.* **1983**, 97, 329–339.
Haridas, M.; Anderson, B.F.; Baker, E.N. Structure of human diferric lactoferrin refined at 2.2 A resolution. *Acta Crystallogr. D. Biol. Crystallogr.* **1995**, *51*, 629–646.
Hedges, S.R.; Barrientes, F.; Desmond, R.A.; Schwebke, J.R. Local and systemic cytokine levels in relation to changes in vaginal flora. *J. Infect. Dis.* **2006**, 193, 556–562.
Heilig, E.A.; Thompson, K.J.; Molina, R.M.; Ivanov, A.R.; Brain, J.D.; Wessling-Resnick, M. Manganese and iron transport across pulmonary epithelium. *Am. J. Physiol. Lung Cell Mol. Physiol.* **2006**, *290*, L1247–L1259.
Hendrixson, D.R.; Qiu, J.; Shewry, S.C.; Fink, D.L.; Petty, S.; Baker, E.N.; Plaut, A.G.; St. Geme, J.W. Human milk lactoferrin is a serine protease that cleaves *Haemophilus* surface proteins at arginine-rich sites. *Mol. Microbiol.* **2003**, *47*, 607–617.
Hentze, M.W.; Muckenthaler, M.U.; Andrews, N.C. Balancing acts: Molecular control of mammalian iron metabolism. *Cell* **2004**, 117, 285–297.
Herz, J.; Strickland, D.K. LRP: A multifunctional scavenger and signaling receptor. *J. Clin. Invest.* **2001**, *108*, 779–784.
Hirashima, N.; Orito, E.; Ohba, K.; Kondo, H.; Sakamoto, T.; Matsunaga, S.; Kato, A.; Nukaya, H.; Sakakibara, K.; Ohno, T.; et al. A randomized controlled trial of consensus interferon with or without lactoferrin for chronic hepatitis C patients with genotype 1b and high viral load. *Hepatol. Res.* **2004**, *29*, 9–12.

Hoffmann, M.; Kleine-Weber, H.; Schroeder, S.; Krüger, N.; Herrler, T.; Erichsen, S.; Schiergens, T.S.; Herrler, G.; Wu, N.-H.; Nitsche, A.; et al. SARS-CoV-2 Cell Entry Depends on ACE2 and TMPRSS2 and Is Blocked by a Clinically Proven Protease Inhibitor. *Cell* **2020**, 181, 271–280.e8.

Hogan, R.J.; Mathews, S.A.; Mukhopadhyay, S.; Summersgill, J.T.; Timms, P. Chlamydial persistence: beyond the biphasic paradigm. *Infect. Immun.* **2004**, 72(4): 1843–1855.

Hogardt, M.; Heesemann, J. Microevolution of Pseudomonas aeruginosa to a chronic pathogen of the cystic fibrosis lung. *Curr. Top Microbiol. Immunol.* **2013**, 358, 91–118.

Hong, H.; Wang, Y.; Chung, H.-T.; Chen, C.-J. Clinical characteristics of novel coronavirus disease 2019 (COVID-19) in newborns, infants and children. *Pediatr Neonatol* **2020**, *61*, 131–132.

Huang, W.; Wilks, A. Extracellular Heme Uptake and the Challenge of Bacterial Cell Membranes. *Annu. Rev. Biochem.* **2017**, *86*, 799–823.

Hunter, H.N.; Fulton, D.B.; Ganz, T.; Vogel, H.J. The solution structure of human hepcidin, a peptide hormone with antimicrobial activity that is involved in iron uptake and hereditary hemochromatosis. *J. Biol. Chem.* **2002**, *277*, 37597–37603.

Hurst, S.M.; Wilkinson, T.S.; McLoughlin, R.M.; Jones, S.; Horiuchi, S.; Yamamoto, N.; Rose-John, S.; Fuller, G.M.; Topley, N.; Jones, S.A. Il-6 and its soluble receptor orchestrate a temporal switch in the pattern of leukocyte recruitment seen during acute inflammation. *Immunity* **2001**, *14*, 705–714.

Iigo, M.; Kuhara, T.; Ushida, Y.; Sekine, K.; Moore, M.A.; Tsuda, H. Inhibitory effects of bovine lactoferrin on colon carcinoma 26 lung metastasis in mice. *Clin. Exp. Metastasis* **1999**, *17*, 35–40.

Ishibashi, Y.; Takeda, K.; Tsukidate, N.; Miyazaki, H.; Ohira, K.; Dosaka-Akita, H.; Nishimura, M. Randomized placebo-controlled trial of interferon alpha-2b plus ribavirin with and without lactoferrin for chronic hepatitis C. *Hepatol. Res.* **2005**, *32*, 218–223.

Jeon, H.; Blacklow, S.C. Structure and physiologic function of the low-density lipoprotein receptor. *Annu. Rev. Biochem.* **2005**, *74*, 535–562.

Jeukens, J.; Boyle, B.; Bianconi, I.; Kukavica-Ibrulj, I.; Tümmler, B.; Bragonzi, A.; Levesque, R.C. Complete Genome Sequence of Persistent Cystic Fibrosis Isolate *Pseudomonas aeruginosa* Strain RP73. *Genome Announc.* **2013**, 1.

Jiang, R.; Lönnerdal, B. Apo- and holo-lactoferrin stimulate proliferation of mouse crypt cells but through different cellular signaling pathways. *Int. J. Biochem. Cell. Biol.* **2012**, *44*, 91–100.

Jiang, R.; Lopez, V.; Kelleher, S.L.; Lönnerdal, B. Apo- and holo-lactoferrin are both internalized by lactoferrin receptor via clathrin-mediated endocytosis but differentially affect ERK-signaling and cell proliferation in Caco-2 cells. *J. Cell Physiol.* **2011**, *226*, 3022–3031.

Jiang, X.-L.; Zhang, X.-L.; Zhao, X.-N.; Li, C.-B.; Lei, J.; Kou, Z.-Q.; Sun, W.-K.; Hang, Y.; Gao, F.; Ji, S.-X.; et al. Transmission Potential of Asymptomatic and Paucisymptomatic Severe Acute Respiratory Syndrome Coronavirus 2 Infections: A 3-Family Cluster Study in China. *J. Infect. Dis.* **2020**, *221*, 1948–1952.

Johanson, B. Isolation of an iron-containing red protein from human milk. *Acta. Chem. Scand.* **1960**, *14*, 510–512.

Kadiiska, M.B.; Burkitt, M.J.; Xiang, Q.H.; Mason, R.P. Iron supplementation generates hydroxyl radical *in vivo*. An ESR spintrapping investigation. *J. Clin. Investig.* **1995**, *96*, 1653–1657.

Kappert, K.; Jahić, A.; Tauber, R. Assessment of serum ferritin as a biomarker in COVID-19: bystander or participant? Insights by comparison with other infectious and non-infectious diseases. *Biomarkers* **2020**, *0*, 1–36.

Karthikeyan, S.; Paramasivam, M.; Yadav, S.; Srinivasan, A.; Singh, T.P. Structure of buffalo lactoferrin at 2.5 Å resolution using crystals grown at 303 K shows different orientations of the N and C lobes. *Acta Crystallogr. D. Biol. Crystallogr.* **1999**, *55*, 1805–1813.

Kato, Y.; Hosokawa, T.; Hayakawa, E.; Ito, K. Influence of liposomes on tryptic digestion of insulin. II. *Biol. Pharm. Bull.* **1993**, *16*, 740–744.

Kato, Y.; Takagi, C.; Tanaka, J.; Masaki, Y.; Furuya, H. Effect of daily subcutaneous administration of recombinant erythropoietin on chronic anemia in rheumatoid arthritis. *Intern. Med.* **1994**, *33*, 193–197.

Kawakami, H.; Lönnerdal, B. Isolation and function of a receptor for human lactoferrin in human fetal intestinal brush-border membranes. *Am. J. Physiol.* **1991**, *261*, G841–G846.

Kawasaki, Y.; Tazume, S.; Shimizu, K.; Matsuzawa, H.; Dosako, S.; Isoda, H.; Tsukiji, M.; Fujimura, R.; Muranaka, Y.; Isihida, H. Inhibitory effects of bovine lactoferrin on the adherence of enterotoxigenic *Escherichia coli* to host cells. *Biosci. Biotechnol. Biochem.* **2000**, *64*, 348–354.

Kelly, M.; O'Connor, R.; Townsend, L.; Coghlan, M.; Relihan, E.; Moriarty, M.; Carr, B.; Melanophy, G.; Doyle, C.; Bannan, C.; et al. Clinical outcomes and adverse events in patients hospitalised with COVID -19, treated with off- label hydroxychloroquine and azithromycin. *Br J Clin Pharmacol* **2020**.

Kim, P.S.; Read, S.W.; Fauci, A.S. Therapy for Early COVID-19: A Critical Need. *JAMA* **2020**.

Kollef MH, Chastre J, Fagon JY, François B, Niederman MS, Rello J, Torres A, Vincent JL, Wunderink RG, Go KW, Rehm C. Global prospective epidemiologic and surveillance study of ventilator-associated pneumonia due to *Pseudomonas aeruginosa*. *Crit Care Med* **2014**, 42:2178– 2187.

Kono, S.; Yoshida, K.; Tomosugi, N.; Terada, T.; Hamaya, Y.; Kanaoka, S.; Miyajima, H. Biological effects of mutant ceruloplasmin on hepcidin-mediated internalization of ferroportin. *Biochim. Biophys. Acta* **2010**, *1802*, 968–975.

Krause, A.; Neitz, S.; Mägert, H.J.; Schulz, A.; Forssmann, W.G.; Schulz-Knappe, P.; Adermann, K. LEAP-1, a novel highly disulfide-bonded human peptide, exhibits antimicrobial activity. *FEBS Lett.* **2000**, *1480*, 147–150.

Kruzel, M.L.; Zimecki, M.; Actor, J.K. Lactoferrin in a Context of Inflammation-Induced Pathology. *Front. Immunol.***2017**, *8*, 1438.

Kuhara, T.; Iigo, M.; Itoh, T.; Ushida, Y.; Sekine, K.; Terada, N.; Okamura, H.; Tsuda, H. Orally administered lactoferrin exerts an antimetastatic effect and enhances production of IL-18 in the intestinal epithelium. *Nutr. Cancer* **2000**, *38*, 192–199.

Lagunas-Rangel, F.A.; Chávez-Valencia, V. High IL-6/IFN-γ ratio could be associated with severe disease in COVID-19 patients. *J. Med. Virol.* **2020**.

Lai, R.; Tang, X.; Yang, M.; Duan, Z.; Liao, Z.; Liu, L.; Cheng, R.; Fang, M.; Wang, G.; Liu, H.; Xu, J.; Kamau, P.; Zhang, Z.; Yang, L.; Zhao, X.; Peng, X. Transferrin receptor is another receptor for SARS-CoV-2 entry. *BioRxiv* **2020**.

Lang, J.; Yang, N.; Deng, J.; Liu, K.; Yang, P.; Zhang, G.; Jiang, C. Inhibition of SARS Pseudovirus Cell Entry byLactoferrin Binding to Heparan Sulfate Proteoglycans. *PLoS ONE* **2011**, *6*, e23710.

Larsen, B.; Monif, G.R. Understanding the bacterial flora of the female genital tract. *Clin. Infect. Dis.* **2001**, 32, 69–77.

Lawrence, C.M.; Ray, S.; Babyonyshev, M.; Galluser, R.; Borhani, D.W.; Harrison, S.C. Crystal structure of the ectodomain of human transferrin receptor. *Science* **1999**, 286, 779–782.

Le Parc, A.; Dallas, D.C.; Duaut, S.; Leonil, J.; Martin, P.; Barile, D. Characterization of goat milk lactoferrin N-glycans and comparison with the N-glycomes of human and bovine milk. *Electrophoresis* **2014**, *35*, 1560–1570.

Lee, P.; Peng, H.; Gelbart, T.; Wang, L.; Beutler, E. Regulation of hepcidin transcription by interleukin-1 and interleukin-6. *PNAS* **2005**, *102*, 1906–1910.

Legrand, D. Overview of Lactoferrin as a Natural Immune Modulator. *J. Pediatr.* **2016**, *173*, S10–S15.

Lepanto, M.S.; Rosa, L.; Cutone, A.; Conte, M.P.; Paesano, R.; Valenti, P. Efficacy of Lactoferrin Oral Administration in the Treatment of Anemia and Anemia of Inflammation in Pregnant and Non-pregnant Women: An Interventional Study. *Front. Immunol.* **2018**, *9*, 2123.

Lepanto, M.S.; Rosa, L.; Cutone, A.; Scotti, M.J.; Conte, A.L.; Marazzato, M.; Zagaglia, C.; Longhi, C.; Berlutti, F.; Musci, G.; et al. Bovine Lactoferrin Pre-Treatment Induces Intracellular Killing of AIEC LF82 and Reduces Bacteria-Induced DNA Damage in Differentiated Human Enterocytes. *Int. J. Mol. Sci.* **2019**, *20*, 5666.

Lepanto, M.S.; Rosa, L.; Paesano, R.; Valenti, P.; Cutone, A. Lactoferrin in Aseptic and Septic Inflammation. *Molecules.* **2019**, *24*, 1323.

Li, F. Structure, Function, and Evolution of Coronavirus Spike Proteins. *Annu. Rev. Virol.* **2016**, 3, 237–261.

Li, H.; Liu, L.; Zhang, D.; Xu, J.; Dai, H.; Tang, N.; Su, X.; Cao, B. SARS-CoV-2 and viral sepsis: Observations and hypotheses. *Lancet* **2020**, 395, 1517–1520.

Li, H.; Zhou, Y.; Zhang, M.; Wang, H.; Zhao, Q.; Liu, J. Updated Approaches against SARS-CoV-2. *Antimicrob. Agents Chemother.* **2020**, 64, 64.

Li, L.-Q.; Huang, T.; Wang, Y.-Q.; Wang, Z.-P.; Liang, Y.; Huang, T.-B.; Zhang, H.-Y.; Sun, W.; Wang, Y. COVID-19 patients' clinical characteristics, discharge rate, and fatality rate of meta-analysis. *J. Med. Virol.* **2020**, *92*, 577–583.

Li, W.; Su, Y.-Y.; Zhi, S.-S.; Huang, J.; Zhuang, C.-L.; Bai, W.-Z.; Wan, Y.; Meng, X.-R.; Zhang, L.; Zhou, Y.-B.; et al. Viral shedding dynamics in asymptomatic and mildly symptomatic patients infected with SARS-CoV-2. *Clin. Microbiol. Infect.* **2020**.

Liang, W.; Feng, Z.; Rao, S.; Xiao, C.; Xue, X.; Lin, Z.; Zhang, Q.; Qi, W. Diarrhoea may be underestimated: A missing link in 2019 novel coronavirus. *Gut* **2020**, 69, 1141–1143.

Liao, Y.; Jiang, R.; Lönnerdal, B. Biochemical and molecular impacts of lactoferrin on small intestinal growth and development during early life. *Biochem. Cell. Biol.* **2012**, *90*, 476–484.

Lin, L.; Hu, K. LRP-1: Functions, Signalling and Implications in Kidney and Other Diseases. *Int. J. Mol. Sci.* **2014**, *15*, 22887–22901.

Lipuma, J.J. The changing microbial epidemiology in cystic fibrosis. *Clin. Microbiol. Rev.* **2010**, *23*, 299–323.

Liu, W.; Wei, F.; Ye, A.; Tian, M.; Han, J. Kinetic stability and membrane structure of liposomes during in vitro infant intestinal digestion: Effect of cholesterol and lactoferrin. *Food Chem* **2017**, *230*, 6–13.

Locci, M.; Nazzaro, G.; Merenda, A.; Pisaturo, M.L.; Laviscio, P.; Poppiti, R.; Miranda, M.; Stile, A.; De Placido, G. Atosiban vs ritodrine used prophylactically with cerclage in ICSI pregnancies to prevent pre-term birth in women identified as being at high risk on the basis of transvaginal ultrasound scan. *J. Obstet. Gynaecol.* **2006**, *26*, 396–401.

Longhi, C.; Conte, M.P.; Seganti, L.; Polidoro, M.; Alfsen, A.; Valenti, P. Influence of lactoferrin on the entry process of *Escherichia coli* HB101 (pRI203) in HeLa cells. *Med. Microbiol. Immunol.* **1993**, *182*, 25–35.

Losfeld, M.E.; Khoury, D.E.; Mariot, P.; Carpentier, M.; Krust, B.; Briand, J.P.; Mazurier, J.; Hovanessian, A.G.; Legrand, D. The cell surface expressed nucleolin is a glycoprotein that triggers calcium entry into mammalian cells. *Exp. Cell. Res.* **2009**, *315*, 357–369.

Louie, S.; Arata, M.A.; Offerdahl, S.D.; Halliwell, B. Effect of tracheal insufflation of deferoxamine on acute ozone toxicity in rats. *J. Lab. Clin. Med.* **1993**, 121, 502–509.

Lu, L.; Hangoc, G.; Oliff, A.; Chen, L.T.; Shen, R.N.; Broxmeyer, H.E. Protective influence of lactoferrin on mice infected with the polycythemia-inducing strain of Friend virus complex. *Cancer Res.* **1987**, *47*, 4184–4188.

Lu, R.; Zhao, X.; Li, J.; Niu, P.; Yang, B.; Wu, H.; Wang, W.; Song, H.; Huang, B.; Zhu, N.; et al. Genomic characterisation and epidemiology of 2019 novel coronavirus: Implications for virus origins and receptor binding. *Lancet* **2020**, 395, 565–574.

Luck, A.N.; Mason, A.B. Transferrin-mediated cellular iron delivery. *Curr Top. Membr.* **2012**, *69*, 3–35.

Ludwiczek, S.; Aigner, E.; Theurl, I.; Weiss, G. Cytokine-mediated regulation of iron transport in human monocytic cells. *Blood* **2003**, *101*, 4148–4154.

Ma, Y.; Abbate, V.; Hider, R.C. Iron-sensitive fluorescent probes: Monitoring intracellular iron pools. *Metallomics* **2015**, *7*, 212–222.

MacKenzie, E.L.; Iwasaki, K.; Tsuji, Y. Intracellular iron transport and storage: From molecular mechanisms to health implications. *Antioxid. Redox Signal.* **2008**, 10, 997–1030.

Maeda, T.; Obata, R.; Do, D.R.; Kuno, T. The Association of Interleukin-6 value, Interleukin inhibitors and Outcomes of Patients with COVID-19 in New York City. *Journal of Medical Virology*, **2020**.

Mancinelli, R.; Olivero, F.; Carpino, G.; Overi, D.; Rosa, L.; Lepanto, M.S.; Cutone, A.; Franchitto, A.; Alpini, G.; Onori, P.; et al. Role of lactoferrin and its receptors on biliary epithelium. *Biometals* **2018**, *31*, 369–379.

Marchetti, M.; Longhi, C.; Conte, M.P.; Pisani, S.; Valenti, P.; Seganti, L. Lactoferrin inhibits herpes simplex virus type 1 adsorption to Vero cells. *Antiviral Res.* **1996**, *29*, 221–231.

Marchetti, M.; Pisani, S.; Antonini,G.; Valenti, P.; Seganti, L.; Orsi, N. Metal complexes of bovine lactoferrin inhibit in vitro replication of herpes simplex virus type 1 and 2. *Biometals* **1998**, *11*, 89–94.

Marchetti, M.; Superti, F.; Ammendolia, M.G.; Rossi, P.; Valenti, P.; Seganti, L. Inhibition of poliovirus type 1 infection by iron-, manganese- and zinc-saturated lactoferrin. *Med. Microbiol. Immunol.* **1999**, *187*, 199–204.

Marchetti, M.; Trybala, E.; Superti, F.; Johansson, M.; Bergström, T. Inhibition of herpes simplex virus infection by lactoferrin is dependent on interference with the virus binding to glycosaminoglycans. *Virology* **2004**, *318*, 405–413.

Marietta, M.; Coluccio, V.; Luppi, M. COVID-19, coagulopathy and venous thromboembolism: more questions than answers. *Intern Emerg Med* **2020**.

Masson, P.L.; Heremans, J.F. Lactoferrin in milk from different species. *Comp. Biochem. Physiol. B.* **1971**, *39*, 119–129.

McDonald, B.; Pittman, K.; Menezes, G.B.; Hirota, S.A.; Slaba, I.; Waterhouse, C.C.; Beck, P.L.; Muruve, D.A.; Kubes, P. Intravascular danger signals guide neutrophils to sites of sterile inflammation. *Science* **2010**, *330*, 362–366.

McGibbon, R.T.; Beauchamp, K.A.; Harrigan, M.P.; Klein, C.; Swails, J.M.; Hernández, C.X.; Schwantes, C.R.; Wang, L.-P.; Lane, T.J.; Pande, V.S. MDTraj: A Modern Open Library for the Analysis of Molecular Dynamics Trajectories. *Biophys. J.* **2015**, 109, 1528–1532.

Meshulam, D.; Lesmes, U. Responsiveness of emulsions stabilized by lactoferrin nano-particles to simulated intestinal conditions. *Food Funct* **2014**, *5*, 65–73.

Metz-Boutigue, M.H.; Jolles, J.; Mazurier, J.; FranGoise Schoentgen, F.G.; Legrand, D.; Spik, G.; Montreuil, J.; Jolles, P. Human lactotransferrin: Amino acid sequence and structural comparisons with other transferrins. *FEBS* **1984**, *145*, 659–676.

Michels, K.; Nemeth, E.; Ganz, T.; Mehrad, B. Hepcidin and Host Defense against Infectious Diseases. *PLoS Pathogens* **2015** 11(8):e1004998.

Miller, J.L. Iron deficiency anemia: A common and curable disease. *Cold Spring Harb. Perspect. Med.* **2012**, *3*, a011866.

Mitchell, M.D.; Dudley, D.J.; Edwin, S.S.; Schiller, S.L. Interleukin-6 stimulates prostaglandin production by human amnion and decidual cells. *Eur. J. Pharmacol.* **1991**, 192, 189–191.

Moore, S.A.; Anderson, B.F.; Groom, C.R.; Haridas, M.; Baker, E.N. Three-dimensional Structure of Diferric Bovine Lactoferrin at 2.8A Resolution. *J. Mol. Biol.* **1997**, *274*, 222–236.

Nadeau-Vallée, M.; Obari, D.; Palacios, J.; Brien, M.È.; Duval, C.; Chemtob, S.; Girard, S. Sterile inflammation and pregnancy complications: A review. *Reproduction* **2016**, *152*.

Nai, A.; Lorè, N.I.; Pagani, A.; De Lorenzo, R.; Di Modica, S.; Saliu, F.; Cirillo, D.M.; Rovere-Querini, P.; Manfredi, A.A.; Silvestri, L. Hepcidin levels predict Covid-19 severity and mortality in a cohort of hospitalized Italian patients. *Am J Hematol.* **2020**.

Nemeth, E.; Ganz, T. Anemia of inflammation. *Hematol. Oncol. Clin. N. Am.* **2014**, *28*, 671–681.

Nemeth, E.; Ganz, T. Regulation of iron metabolism by hepcidin. *Annu. Rev. Nutr.* **2006**, *26*, 323–342.

Nemeth, E.; Rivera, S.; Gabayan, V.; Keller, C.; Taudorf, S.; Pedersen, B.K.; Ganz, T. IL-6 mediates hypoferremia of inflammation by inducing the synthesis of the iron regulatory hormone hepcidin. *J. Clin. Investig.* **2004**, *113*, 1271–1276.

Ng, T.B.; Cheung, R.C.F.; Wong, J.H.; Wang, Y.; Ip, D.T.M.; Wan, D.C.C.; Xia, J. Antiviral activities of whey proteins. *Appl. Microbiol. Biotechnol.* **2015**, *99*, 6997–7008.

Nichols, D.; Chmiel, J.; Berger, M. Chronic inflammation in the cystic fibrosis lung: Alterations in inter- and intracellular signaling. *Clin. Rev. Allergy Immunol.* **2008**, 34, 146–162.

Nozaki, A.; Ikeda, M.; Naganuma, A.; Nakamura, T.; Inudoh, M.; Tanaka, K.; Kato, N. Identification of a lactoferrin-derived peptide possessing binding activity to hepatitis C virus E2 envelope protein. *J. Biol. Chem.* **2003**, *278*, 10162–10173.

Oakley, B.B.; Fiedler, T.L.; Marrazzo, J.M.; Fredricks, D.N. Diversity of human vaginal bacterial communities and associations with clinically defined bacterial vaginosis. *Appl. Environ. Microbiol.* **2008**, 74, 4898–4909.

Ochoa, T.J.; Brown, E.L.; Guion, C.E.; Chen, J.Z.; McMahon, R.J.; Cleary, T.G. Effect of lactoferrin on enteroaggregative *E. coli* (EAEC) 1. *Biochem. Cell Biol.* **2006**, *84*, 369–376.

Ochoa, T.J.; Noguera-Obenza, M.; Ebel, F.; Guzman, C.A.; Gomez, H.F.; Cleary, T.G. Lactoferrin impairs type III secretory system function in enteropathogenic *Escherichia coli*. *Infect. Immun.* **2003**, *71*, 5149–5155.

Oho, T.; Mitoma, M.; Koga, T. Functional domain of bovine milk lactoferrin which inhibits the adherence of *Streptococcus mutans* cells to a salivary film. *Infect. Immun.* **2002**, *70*, 5279–5282.

Okada, S.; Tanaka, K.; Sato, T.; Ueno, H.; Saito, S.; Okusaka, T.; Sato, K.; Yamamoto, S.; Kakizoe, T. Dose-response trial of lactoferrin in patients with chronic hepatitis C. *Jpn. J. Cancer Res.* **2002**, *93*, 1063–1069.

Ong, J.; Young, B.E.; Ong, S. COVID-19 in gastroenterology: A clinical perspective. *Gut* **2020**, 69, 1144–1145.

Ortiz, R.; Toblli, J.E.; Romero, J.D.; Monterrosa, B.; Frer, C.; Macagno, E.; Breymann, C. Efficacy and safety of oral iron (III) polymaltose complex versus ferrous sulfate in pregnant women with iron-deficiency anemia: A multicenter, randomized, controlled study. *J. Matern. Fetal Neonatal Med.* **2011**, *24*, 1–6.

Paesano R, Pietropaoli M, Gessani S, Valenti P (2009) The influence of lactoferrin, orally administered, on systemic iron homeostasis in pregnant women suffering of iron deficiency and iron deficiency anaemia. *Biochimie* **2009,** 91:44–51.

Paesano, R.; Berlutti, F.; Pietropaoli, M.; Goolsbee, W.; Pacifici, E.; Valenti, P. Lactoferrin efficacy versus ferrous sulfate in curing iron disorders in pregnant and non-pregnant women. *Int. J. Immunopathol. Pharmacol.* **2010**, *23*, 577–587.

Paesano, R.; Berlutti, F.; Pietropaoli, M.; Pantanella, F.; Pacifici, E.; Goolsbee, W.; Valenti, P. Lactoferrin efficacy versus ferrous sulfate in curing iron deficiency and iron deficiency anemia in pregnant women. *Biometals* **2010,** 23:411–417.

Paesano, R.; Natalizi, T.; Berlutti, F.; Valenti, P. Body iron delocalization: The serious drawback in iron disorders in both developing and developed countries. *Pathog. Glob. Health* **2012**, *106*, 200–216.

Paesano, R.; Pacifici, E.; Benedetti, S.; Berlutti, F.; Frioni, A.; Polimeni, A.; Valenti, P. Safety and efficacy of lactoferrin versus ferrous sulphate in curing iron deficiency and iron deficiency anaemia in hereditary thrombophilia pregnant women: An interventional study. *Biometals* **2014**, *27*, 999–1006.

Paesano, R.; Torcia, F.; Berlutti, F.; Pacifici, E.; Ebano, V.; Moscarini, M.; Valenti, P. Oral administration of lactoferrin increases hemoglobin and total serum iron in pregnant women. *Biochem. Cell Biol.* **2006**, *84*, 377–380.

Palacios, S. The management of iron deficiency in menometrorrhagia. *Gynecol. Endocrinol.* **2011**, *27*, 1126–1130.

Park, C.H.; Valore, E.V.; Waring, A.J.; Ganz, T. Hepcidin, a urinary antimicrobial peptide synthesized in the liver. *J. Biol. Chem.* **2001**, *276*, 7806–7810.

Park, G.S.; Best, S.M.; Bloom, M.E. Two mink parvoviruses use different cellular receptors for entry into CRFK cells. *Virology* **2005**, 340, 1–9.

Parker, J.S.; Murphy, W.J.; Wang, D.; O'Brien, S.J.; Parrish, C.R. Canine and feline parvoviruses can use human or feline transferrin receptors to bind, enter, and infect cells. *J. Virol.* **2001**, 75, 3896–3902.

Parrow, N. L.; Abbott, J.; Lockwood, A. R.; Battisti, J. M.; Minnick, M. F. Function, regulation, and transcriptional organization of the hemin utilization locus of Bartonella quintana. *Infect. Immun.* **2009**, 77, 307–316.

Peeters, H.R.; Jongen-Lavrencic, M.; Vreugdenhil, G.; Swaak, A.J. Effect of recombinant human erythropoietin on anemia and disease activity in patients with rheumatoid arthritis and anemia of chronic disease: A randomized placebo controlled double blind 52 weeks clinical trial. *Ann. Rheum. Dis.* **1996**, *55*, 739–744.

Peipert, J.F.; Montagno, A.B.; Cooper, A.S.; Sung, C.J. Bacterial vaginosis as a risk factor for upper genital tract infection. *Am. J. Obstet. Gynecol.* **1997**, 177, 1184–1187.

Persichini, T.; De Francesco, G.; Capone, C.; Cutone, A.; di Patti, M.C.; Colasanti, M.; Musci, G. Reactive oxygen species are involved in ferroportin degradation induced by ceruloplasmin mutant Arg701Trp. *Neurochem. Int.* **2012**, *60*, 360–364.

Petrik, M.; Zhai, C.; Haas, H.; Decristoforo, C. Siderophores for molecular imaging applications. *Clin. Transl. Imaging* **2017**, *5*, 15–27.

Pettersen, E.F.; Goddard, T.D.; Huang, C.C.; Couch, G.S.; Greenblatt, D.M.; Meng, E.C.; Ferrin, T.E. UCSF Chimera--a visualization system for exploratory research and analysis. *J Comput Chem* **2004**, 25, 1605–1612.

Pettersson, T.; Rosenlöf, K.; Friman, C.; Mickos, A.; Teppo, A.M.; Fyhrquist, F. Successful treatment of the anemia of rheumatoid arthritis with subcutaneously administered recombinant human erythropoietin. Slower response in patients with more severe inflammation. *Scand. J. Rheumatol.* **1993**, *22*, 188–193.

Phillips, J.C.; Braun, R.; Wang, W.; Gumbart, J.; Tajkhorshid, E.; Villa, E.; Chipot, C.; Skeel, R.D.; Kalé, L.; Schulten, K. Scalable molecular dynamics with NAMD. *J Comput Chem* **2005**, 26, 1781–1802.

Pilarczyk-Zurek, M.; Strus, M.; Adamski, P.; Heczko, P.B. The dual role of *Escherichia coli* in the course of ulcerative colitis. *BMC Gastroenterol.* **2016**, *16*, 128.

Plaut, A.G.; Qiu, J.; St. Geme, J.W. Human lactoferrin proteolytic activity: Analysis of the cleaved region in the IgA protease of *Haemophilus influenzae*. *Vaccine* **2001**, *19*, 148–152.

Pogoutse, A.K.; Moraes, T.F. Iron acquisition through the bacterial transferrin receptor. *Crit. Rev. Biochem. Mol. Biol.* **2017**, *52*, 314–326.

Ponti, G.; Palombi, F.; Abate, D.; Ambrosino, F.; Aprea, G.; Bastianelli, T.; Beone, F.; Bertini, R.; Bracco, G.; Caporicci, M.; et al. The role of medium size facilities in the HPC ecosystem: the case of the new

CRESCO4 cluster integrated in the ENEAGRID infrastructure. *In Proceedings of the 2014 International Conference on High Performance Computing Simulation (HPCS)*; **2014**; pp. 1030–1033.
Potroz MG, Cho NJ. Natural products for the treatment of trachoma and *Chlamydia trachomatis*. *Molecule*s **2015** 20(3):4180-203.
Puddu, P.; Borghi, P.; Gessani, S.; Valenti, P.; Belardelli, F.; Seganti, L. Antiviral effect of bovine lactoferrin saturated with metal ions on early steps of human immunodeficiency virus type 1 infection. *Int. J. Biochem. Cell Biol.* **1998**, *30*, 1055–1063.
Puddu, P.; Latorre, D.; Carollo, M.; Catizone, A.; Ricci, G.; Valenti, P.; Gessani, S. Bovine lactoferrin counteracts Toll-like receptor mediated activation signals in antigen presenting cells. *PLoS ONE* **2011**, *6*, e22504.
Puddu, P.; Valenti, P.; Gessani, S. Immunomodulatory effects of lactoferrin on antigen presenting cells. *Biochimie* **2009**, *91*, 11–18.
Qi, F.; Qian, S.; Zhang, S.; Zhang, Z. Single cell RNA sequencing of 13 human tissues identify cell types and receptors of human coronaviruses. *Biochem. Biophys. Res. Commun.* **2020**, 526, 135–140.
Qiao, B.; Sugianto, P.; Fung, E.; Del-Castillo-Rueda, A.; Moran-Jimenez, M.J.; Ganz, T.; Nemeth, E. Hepcidin-induced endocytosis of ferroportin is dependent on ferroportin ubiquitination. *Cell Metab.* **2012**, *15*, 918–924.
Qiu, J.; Hendrixson, D.R.; Baker, E.N.; Murphy, T.F.; St Geme, J.W.; Plaut, A.G. Human milk lactoferrin inactivates two putative colonization factors expressed by *Haemophilus influenzae*. *PNAS* **1998**, *95*, 12641–12646.
Radoshitzky, S.R.; Abraham, J.; Spiropoulou, C.F.; Kuhn, J.H.; Nguyen, D. Transferrin receptor 1 is a cellular receptor for New World haemorrhagic fever arenaviruses. *Nature* **2007**, 446, 92–96.
Ramírez-Aportela, E.; López-Blanco, J.R.; Chacón, P. FRODOCK 2.0: fast protein-protein docking server. *Bioinformatics* **2016**, 32, 2386–2388.
Rampersauda, R.; Randis, T.M.; Ratner, A.J. Microbiota of the upper and lower genital tract. Semin. *Fetal Neonatal Med.* **2012**, 17, 51–57.
Ranganathan, S.C.; Parsons, F.; Gangell, C.; Brennan, B.; Stick, S.M.; Sly, P.D. Australian Respiratory Early Surveillance Team for Cystic Fibrosis. Evolution of pulmonary inflammation and nutritional status in infants and young children with cystic fibrosis. *Thorax* **2011**, 66, 408–413.
Rao, S.; Wright, A.K.A.; Montiero, W.; Ziegler-Heitbrock, L.; Grigg, J. Monocyte chemoattractant chemokines in cystic fibrosis. *J. Cyst. Fibros.* **2009**, *8*, 97–103.
Raulston, J. E. Response of Chlamydia trachomatis serovar E to iron restriction in vitro and evidence for iron-regulated chlamydial proteins. *Infect. Immun.* **1997**, 65, 4539–4547.
Recalcati, S.; Locati, M.; Marini, A.; Santambrogio, P.; Zaninotto, F.; De Pizzoli, M.; Zammataro, L.; Girelli, D.; Cairo, G. Differential regulation of iron homeostasis during human macrophage polarized activation. *Eur. J. Immunol.* **2010**, *40*, 824–835.
Redgrove, K.A.; McLaughlin, E.A. The role of the immune response in *Chlamydia trachomatis* infection of the male genital tract: a double-edged sword. *Front. Immunol.* **2014**, 5: 534.
Reid, D.W.; Carroll, V.; O'May, C.; Champion, A.; Kirov, S.M. Increased airway iron as a potential factor in the persistence of *Pseudomonas aeruginosa* infection in cystic fibrosis. *Eur. Respir. J.* **2007**, 30, 286–292.
Reid, D.W.; Lam, Q.T.; Schneider, H.; Walters, E.H. Airway iron and iron-regulatory cytokines in cystic fibrosis. *Eur. Respir. J.* **2004**, 24, 286–291.
Reid, D.W.; Withers, N.J.; Francis, L.; Wilson, J.W.; Kotsimbos, T.C. Iron deficiency in cystic fibrosis: Relationship to lung disease severity and chronic Pseudomonas aeruginosa infection. *Chest* **2002**, 121, 48–54.
Reifen, R.; Matas, Z.; Zeidel, L.; Berkovitch, Z.; Bujanover, Y. Iron supplementation may aggravate inflammatory status of colitis in a rat model. *Dig. Dis. Sci.* **2000**, *45*, 394–397.
Rizvi, S.; Schoen, R.E. Supplementation with oral vs. intravenous iron for anemia with IBD or gastrointestinal bleeding: Is oral iron getting a bad rap? *Am. J. Gastroenterol.* **2011**, *106*, 1872–1879.
Rogan, M.P.; Taggart, C.C.; Greene, C.M.; Murphy, P.G.; O'Neill, S.J.; McElvaney, N.G. Loss of microbicidal activity and increased formation of biofilm due to decreased lactoferrin activity in patients with cystic fibrosis. *J. Infect. Dis.* **2004**, *190*, 1245–1253.
Rohde, K. H.; Dyer, D. W. Analysis of haptoglobin and hemoglobin-haptoglobin interactions with the Neisseria meningitidis TonB- dependent receptor HpuAB by flow cytometry. *Infect. Immun.* **2004**, 72, 2494–2506.

Romeo, A.; Iacovelli, F.; Falconi, M. Targeting the SARS-CoV-2 spike glycoprotein prefusion conformation: virtual screening and molecular dynamics simulations applied to the identification of potential fusion inhibitors. *Virus Res* **2020**, *286*, 198068–198068.

Root-Bernstein, R. Age and Location in Severity of COVID-19 Pathology: Do Lactoferrin and Pneumococcal Vaccination Explain Low Infant Mortality and Regional Differences? *BioEssays* **2000**, 2000076.

Rosa, L.; Cutone, A.; Lepanto, M.S.; Paesano, R.; Valenti, P. Lactoferrin: A natural glycoprotein involved in iron and inflammatory homeostasis. *Int. J. Mol. Sci.* **2017**, *18*, 1985.

Rosa, L.; Cutone, A.; Lepanto, M.S.; Scotti, M.J.; Conte, M.P.; Paesano, R.; Valenti, P. Physico-chemical properties influence the functions and efficacy of commercial bovine lactoferrins. *Biometals* **2018**, *31*, 301–312.

Rose, J.E.; Meyer, D.H.; Fives-Taylor, P.M. Aae, an autotransporter involved in adhesion of *Actinobacillus actinomycetemcomitans* to epithelial cells. *Infect. Immun.* **2003**, *71*, 2384–2393.

Ross, S.L.; Tran, L.; Winters, A.; Lee, K.J.; Plewa, C.; Foltz, I.; King, C.; Miranda, L.P.; Allen, J.; Beckman, H.; et al. Molecular mechanism of hepcidin-mediated ferroportin internalization requires ferroportin lysines, not tyrosines or JAK-STAT. *Cell Metab.* **2012**, 15, 905–917.

Rossi, P.; Giansanti, F.; Boffi, A.; Ajello, M.; Valenti, P.; Chiancone, E.; Antonini, G. Ca^{2+} binding to bovine lactoferrin enhances protein stability and influences the release of bacterial lipopolysaccharide. *Biochem. Cell Biol.* **2002**, *80*, 41–48.

Russo, R.; Edu, A.; De Seta, F. Study on the effects of an oral lactobacilli and lactoferrin complex in women with intermediate vaginal microbiota. *Arch. Gynecol. Obstet.* **2018**, 298, 139–145.

Ryckaert, J.-P.; Ciccotti, G.; Berendsen, H.J.C. Numerical integration of the cartesian equations of motion of a system with constraints: molecular dynamics of n-alkanes. *Journal of Computational Physics* **1977**, 23, 327–341.

Saito, S.; Nakashima, A.; Shima, T.; Ito, M. Th1/Th2/Th17 and regulatory T-cell paradigm in pregnancy. *Am. J. Reprod. Immunol.* **2010**, *63*, 601–610.

Salsgiver, E.L.; Fink, A.K.; Knapp, E.A.; LiPuma, J.J.; Olivier, K.N.; Marshall, B.C.; Saiman, L. Changing epidemiology of the respiratory bacteriology of patients with cystic fibrosis. *Chest* **2016**, 149, 390–400.

Salomon-Ferrer, R.; Case, D.A.; Walker, R.C. An overview of the Amber biomolecular simulation package. *WIREs Computational Molecular Science* **2013**, 3, 198–210.

Sano, H.; Nagai, K.; Tsutsumi, H.; Kuroki, Y. Lactoferrin and surfactant protein A exhibit distinct binding specificity to F protein and differently modulate respiratory syncytial virus infection. *Eur. J. Immunol.* **2003**, *33*, 2894–2902.

Sapp, M.; Bienkowska-Haba, M. Viral entry mechanisms: human papillomavirus and a long journey from extracellular matrix to the nucleus. *FEBS J* **2009**, *276*, 7206–7216.

Sarute, N.; Ross, S.R. New World arenavirus biology. *Annu. Rev. Virol.* **2017**, 4, 141–158.

Satış, H.; Özger, H.S.; Aysert Yıldız, P.; Hızel, K.; Gulbahar, Ö.; Erbaş, G.; Aygencel, G.; Guzel Tunccan, O.; Öztürk, M.A.; Dizbay, M.; et al. Prognostic value of interleukin-18 and its association with other inflammatory markers and disease severity in COVID-19. *Cytokine* **2021**, *137*, 155302.

Sawada, M.; Otsuki, K.; Mitsukawa, K.; Yakuwa, K.; Nagatsuka, M.; Okai, T. Cervical inflammatory cytokines and other markers in the cervical mucus of pregnant women with lower genital tract infection. *Int. J. Gynaecol. Obstet.* **2006**, 92, 117–121.

Schmidt, S.M. The role of iron in viral infections. Front. Biosci. (Landmark Ed.) 2020, 25, 893–911.

Scholl, T.O. Iron status during pregnancy: Setting the stage for mother and infant. *Am. J. Clin. Nutr.* **2005**, 81,1218S–1222S.

Sessa, R.; Di Pietro, M.; Filardo, S.; Bressan, A.; Mastromarino, P.; Biasucci, A.V.; Rosa, L.; Cutone, A.; Berlutti, F.; Paesano, R.; et al. Lactobacilli-lactoferrin interplay in *Chlamydia trachomatis* infection. *Pathog Dis.* **2017**, 75.

Shah A, Frost JN, Aaron L, et al. Systemic hypoferremia and severity of hypoxemic respiratory failure in COVID-19. *Crit Care.* **2020**; 24: 320.

Shankar, A.H.; Prasad, A.S. Zinc and immune function: The biological basis of altered resistance to infection. *Am. J. Clin. Nutr.* **1998**, 68, 447S–463S.

Sharma, A.K.; Paramasivam, M.; Srinivasan, A.; Yadav, M.P.; Singh, T.P. Three-dimensional structure of mare diferric lactoferrin at 2.6 A resolution. *J. Mol. Biol.* **1999**, *289*, 303–317.

Shimazaki, K.; Tazume, T.; Uji, K.; Tanaka, M.; Kumura, H.; Mikawa, K.; Shimo-Oka, T. Properties of a heparin-binding peptide derived from bovine lactoferrin. *J. Dairy Sci.* **1998**, *81*, 2841–2849.

Shin, K.; Wakabayashi, H.; Yamauchi, K.; Teraguchi, S.; Tamura, Y.; Kurokawa, M.; Shiraki, K. Effects of orally administered bovine lactoferrin and lactoperoxidase on influenza virus infection in mice. *J. Med. Microbiol.* **2005**, *54*, 717–723.

Shin, K.; Wakabayashi, H.; Yamauchi, K.; Yaeshima, T.; Iwatsuki, K. Recombinant human intelectin binds bovine lactoferrin and its peptides. *Biol. Pharm. Bull.* **2008**, *31*, 1605–1608.

Siciliano, R.; Rega, B.; Marchetti, M.; Seganti, L.; Antonini, G.; Valenti, P. Bovine lactoferrin peptidic fragments involved in inhibition of herpes simplex virus type 1 infection. *Biochem. Biophys. Res. Commun.* **1999**, *264*, 19–23.

Singh, P.K.; Parsek, M.R.; Greenberg, E.P.; Welsh, M.J. A component of innate immunity prevents bacterial biofilm development. *Nature* **2002**, 417, 552–555.

Smith, D.J.; Anderson, G.J.; Bell, S.C.; Reid, D.W. Elevated metal concentrations in the CF airway correlate with cellular injury and disease severity. *J. Cyst. Fibros.* **2014**, 13, 289–295.

Sorensen, M.; Sorensen, S. The Proteins in Whey. *Compte rendu des Travaux du Laboratoire de Carlsberg Ser. Chim.* **1939**, *23*, 55–99.

Spear, P.G. Herpes simplex virus: receptors and ligands for cell entry. *Cell. Microbiol.* **2004**, *6*, 401–410.

Stallmann, S.; Hegemann, J.H. The *Chlamydia trachomatis* Ctad1 invasin exploits the human integrin ß1 receptor for host cell entry. *Cell. Microbiol.* **2015**.

Standiford, T.J.; Kunkel, S.L.; Lukacs, N.W.; Greenberger, M.J.; Danforth, J.M.; Kunkel, R.G.; Strieter, R.M. Macrophage inflammatory protein-1 alpha mediates lung leukocyte recruitment, lung capillary leak, and early mortality in murine endotoxemia. *J. Immunol.* **1995**, 155, 1515–1524.

Stites, S.W.; Walters, B.; O'Brien-Ladner, A.R.; Bailey, K.; Wesselius, L.J. Increased iron and ferritin content of sputum from patients with cystic fibrosis or chronic bronchitis. *Chest* **1998**, *114*, 814–819.

Su, S.; Wong, G.; Shi, W.; Liu, J.; Lai, A.C.; Zhou, J.; Liu, W.; Bi, Y.; Gao, G.F. Epidemiology, Genetic Recombination, and Pathogenesis of Coronaviruses. *Trends Microbiol.* **2016**, 24, 490–502.

Sun, X.-L.; Baker, H.M.; Shewry, S.C.; Jameson, G.B.; Baker, E.N. Structure of recombinant human lactoferrin expressed in Aspergillus awamori. *Acta Crystallographica Section D* **1999**, 55, 403–407.

Superti, F.; Siciliano, R.; Rega, B.; Giansanti, F.; Valenti, P.; Antonini, G. Involvement of bovine lactoferrin metal saturation, sialic acid and protein fragments in the inhibition of rotavirus infection. *Biochim. Biophys. Acta.* **2001**, *1528*, 107115.

Suzuki, Y.A.; Lopez, V.; Lönnerdal, B. Mammalian lactoferrin receptors: Structure and function. *Cell. Mol. Life Sci.***2005**, *62*, 2560–2575.

Suzuki, Y.A.; Shin, K.; Lönnerdal, B. Molecular cloning and functional expression of a human intestinal lactoferrin receptor. *Biochemistry* **2001**, *40*, 15771–15779.

Suzuki, Y.A.; Wong, H.; Ashida, K.Y.; Schryvers, A.B.; Lönnerdal, B. The N1 domain of human lactoferrin is required for internalization by Caco-2 cells and targeting to the nucleus. *Biochemistry* **2008**, *47*, 10915–10920.

Swart, P. j.; Kuipers, M. e.; Smit, C.; Pauwels, R.; De Béthune, M. p.; De Clercq, E.; Meijer, D. k. f.; Huisman, J. g. Antiviral Effects of Milk Proteins: Acylation Results in Polyanionic Compounds with Potent Activity against Human Immunodeficiency Virus Types 1 and 2 in Vitro. *AIDS Research and Human Retroviruses* **1996**, *12*, 769–775.

Tanaka, K.; Ikeda, M.; Nozaki, A.; Kato, N.; Tsuda, H.; Saito, S.; Sekihara, H. Lactoferrin inhibits hepatitis C virus viremia in patients with chronic hepatitis C: a pilot study. *Jpn. J. Cancer Res.* **1999**, *90*, 367–371.

Tang, N.; Li, D.; Wang, X.; Sun, Z. Abnormal coagulation parameters are associated with poor prognosis in patients with novel coronavirus pneumonia. *J. Thromb. Haemost.* **2020**, *18*, 844–847.

Thachil, J. What do monitoring platelet counts in COVID-19 teach us? *J. Thromb. Haemost.* **2020**.

Thomassen, E.A.; van Veen, H.A.; van Berkel, P.H.; Nuijens, J.H.; Abrahams, J.P. The protein structure of recombinant human lactoferrin produced in the milk of transgenic cows closely matches the structure of human milk-derived lactoferrin. *Transgenic Res.* **2005**, *14*, 397–405.

Thompson, A.B.; Bohling, T.; Payvandi, F.; Rennard, S.I. Lower respiratory tract lactoferrin and lysozyme arise primarily in the airways and are elevated in association with chronic bronchitis. *J. Lab. Clin. Med.* **1990**, *115*, 148–158.

Thompson, C.C.; Carabeo, R.A. An optimal method of iron starvation of the obligate intracellular pathogen, Chlamydia trachomatis. *Front. Microbiol.* **2011**, 2: 20.

Tian, X.; Li, C.; Huang, A.; Xia, S.; Lu, S.; Shi, Z.; Lu, L.; Jiang, S.; Yang, Z.; Wu, Y.; et al. Potent binding of 2019 novel coronavirus spike protein by a SARS coronavirus-specific human monoclonal antibody. *Emerg. Microbes Infect.* **2020**, 9, 382–385.

Tinari, A.; Pietrantoni, A.; Ammendolia, M.G.; Valenti, P.; Superti, F. Inhibitory activity of bovine lactoferrin against echovirus induced programmed cell death in vitro. *Int. J. Antimicrob. Agents* **2005**, *25*, 433–438.

Tomita, M.; Bellamy, W.; Takase, M.; Yamauchi, K.; Wakabayashi, K.; Kavase, K. Potent antibacterial peptides generated by pepsin of bovine lactoferrin. *J. Dairy Sci.* **1991**, *74*, 4137–4142.

Ueno, H.; Sato, T.; Yamamoto, S.; Tanaka, K.; Ohkawa, S.; Takagi, H.; Yokosuka, O.; Furuse, J.; Saito, H.; Sawaki, A.; et al. Randomized, double-blind, placebo-controlled trial of bovine lactoferrin in patients with chronic hepatitis C. *Cancer Sci.* **2006**, *97*, 1105–1110.

Valenti, P.; Antonini, G. Lactoferrin: An important host defence against microbial and viral attack. *Cell. Mol. Life Sci.* **2005**, *62*, 2576–2587.

Valenti, P.; Antonini, G.; Von Hunolstein, C.; Visca, P.; Orsi, N.; Antonini, E. Studies of the antimicrobial activity of ovotransferrin. *Int. J. Tissue React.* **1983**, *5*, 97–105.

Valenti, P.; Catizone, A.; Pantanella, F.; Frioni, A.; Natalizi, T.; Tendini, M.; Berlutti, F. Lactoferrin decreases inflammatory response by cystic fibrosis bronchial cells invaded with *Burkholderia cenocepacia* iron-modulated biofilm. *Int. J. Immunopathol. Pharmacol.* **2011**, *24*, 1057–1068.

Valenti, P.; Frioni, A.; Rossi, A.; Ranucci, S.; De Fino, I.; Cutone, A.; Rosa, L.; Bragonzi, A.; Berlutti, F. Aerosolized bovine lactoferrin reduces neutrophils and pro-inflammatory cytokines in mouse models of *Pseudomonas aeruginosa* lung infections. *Biochem. Cell. Biol.* **2017**, *95*, 41–47.

Valenti, P.; Rosa, L.; Capobianco, D.; Lepanto, M.S.; Schiavi, E.; Cutone, A.; Paesano, R.; Mastromarino, P. Role of Lactobacilli and Lactoferrin in the Mucosal Cervicovaginal Defense. *Front. Immunol.* **2018**, 9, 376.

Van der Kraan, M.I.; Groenink, J.; Nazmi, K.; Veerman, E.C.; Bolscher, J.G.; Nieuw Amerongen, A.V. Lactoferrampin: A novel antimicrobial peptide in the N1-domain of bovine lactoferrin. *Peptides* **2004**, *25*, 177–183.

van der Strate, B.W.; Beljaars, L.; Molema, G.; Harmsen, M.C.; Meijer, D.K. Antiviral activities of lactoferrin. *Antiviral Res.* **2001**, *52*, 225–239.

van Heeckeren, A.M. Murine models of chronic Pseudomonas aeruginosa lung infection. *Lab. Anim.* **2002**, 36, 291–312.

Vardhan, H.; Bhengraj, A.R.; Jha, R.; Singh Mittal, A. Chlamydia trachomatis alters iron-regulatory protein-1 binding capacity and modulates cellular iron homeostasis in HeLa-229 cells. *J Biomed Biotechnol.* **2009**; 2009:342032.

Verhaeghe, C.; Remouchamps, C.; Hennuy, B.; Vanderplasschen, A.; Chariot, A.; Tabruyn, S.P.; Oury, C.; Bours, V. Role of IKK and ERK pathways in intrinsic inflammation of cystic fibrosis airways. *Biochem. Pharmacol.* **2007**, 73, 1982–1994.

Vidya, P.; Smith, L.; Beaudoin, T.; Yau, Y.C.; Clark, S.; Coburn, B.; Guttman, D.S.; Hwang, D.M.; Waters, V. Chronic infection phenotypes of Pseudomonas aeruginosa are associated with failure of eradication in children with cystic fibrosis. *Eur. J. Clin. Microbiol. Infect. Dis.* **2016**, 35, 67–74.

Visca, P.; Berlutti, F.; Vittorioso, P.; Dalmastri, C.; Thaller, M.C.; Valenti, P. Growth and adsorption of *Streptococcus mutans* 6715–13 to hydroxyapatite in the presence of lactoferrin. *Med. Microbiol. Immunol.* **1989**, *178*, 69–79.

Vitetta, L.; Coulson, S.; Beck, S.L.; Gramotnev, H.; Du, S.; Lewis, S. The clinical efficacy of a bovine lactoferrin/whey protein Ig-rich fraction (Lf/IgF) for the common cold: a double blind randomized study. *Complement Ther Med* **2013**, *21*, 164–171.

Wakabayashi, H.; Oda, H.; Yamauchi, K.; Abe, F. Lactoferrin for prevention of common viral infections. *J. Infect. Chemother.* **2014**, *20*, 666–671.

Wandersman, C.; Stojiljkovic, I. Bacterial heme sources: The role of heme, hemoprotein receptors and hemophores. *Curr. Opin. Microbiol.* **2000**, *3*, 215–220.

Wang, H.-M.; Wu, C.; Jiang, Y.-Y.; Wang, W.-M.; Jin, H. Retinol and vitamin A metabolites accumulate through RBP4 and STRA6 changes in a psoriasis murine model. *Nutr. Metab.* **2020**, 17, 5–15.

Wang, Q.; Zhao, H.; Liu, L.-G.; Wang, Y.-B.; Zhang, T.; Li, M.-H.; Xu, Y.-L.; Gao, G.-J.; Xiong, H.-F.; Fan, Y.; et al. Pattern of liver injury in adult patients with COVID-19: a retrospective analysis of 105 patients. *Mil Med Res* **2020**, *7*, 28.

Waters, V.; Smyth, A. Cystic fibrosis microbiology: Advances in antimicrobial therapy. *J. Cyst. Fibros.* **2015**, 14, 551–560.
Wei, Z.; Nishimura, T.; Yoshida, S. Presence of a glycan at a potential N-glycosylation site, Asn-281, of bovine lactoferrin. *J. Dairy Sci.* **2000**, *83*, 683–689.
Weinberg, E.D. Iron withholding: A defense against viral infections. *BioMetals* **1996**, 9, 393–399.
Weinberg, E.D. The development of awareness of iron-withholding defense. *Perspect. Biol. Med.* **1993**, *36*, 215–221.
Weinstein, D.A.; Roy, C.N.; Fleming, M.D.; Loda, M.F.; Wolfsdorf, J.I.; Andrews, N.C. Inappropriate expression of hepcidin is associated with iron refractory anemia: Implications for the anemia of chronic disease. *Blood* **2002**, *100*, 3776–3781.
Wenstrom, K.D.; Andrews, W.W.; Tamura, T.; DuBard, M.B.; Johnston, K.E.; Hemstreet, G.P. Elevated amniotic fluid interleukin-6 levels at genetic amniocentesis predict subsequent pregnancy loss. *Am. J. Obstet. Gynecol.* **1996**, *175*, 830–833.
Wessling-Resnick, M. Crossing the Iron Gate: Why and How Transferrin Receptors Mediate Viral Entry. *Annu. Rev. Nutr.* **2018**, 38, 431–458.
Wessling-Resnick, M. Iron homeostasis and the inflammatory response. *Annu. Rev. Nutr.* **2010**, *30*, 105–122.
Willer Eda, M.; Lima Rde, L.; Giugliano, L.G. *In vitro* adhesion and invasion inhibition of *Shigella dysenteriae*, *Shigella flexneri and Shigella sonnei* clinical strains by human milk proteins. *BMC Microbiol.* **2004**, *4*, 18–25.
Williams, T.J.; Schneider, R.P.; Willcox, M.D. The effect of protein-coated contact lenses on the adhesion and viability of gram-negative bacteria. *Curr. Eye Res.* **2003**, *27*, 227–235.
Workowski, K.A., and Bolan, G.A. 2015. Sexually transmitted diseases treatment guidelines. *CDC, Morbidity and Mortality Weekly Report, Recommendations and Reports*, **2015** 64(RR-3): 1–137.
Wrackmeyer, U.; Hansen, G.H.; Seya, T.; Danielsen, E.M. Intelectin: A novel lipid raft-associated protein in the enterocyte brush border. *Biochemistry* **2006**, *45*, 9188–91897.
Wrapp, D.; Wang, N.; Corbett, K.S.; Goldsmith, J.A.; Hsieh, C.-L.; Abiona, O.; Graham, B.S.; McLellan, J.S. Cryo-EM Structure of the 2019-nCoV Spike in the Prefusion Conformation. *bioRxiv* **2020**.
Wrighting, D.M.; Andrews, N.C. Interleukin-6 induces hepcidin expression through STAT3. *Blood* **2006**, *108*, 3204–3209.
Wu, H.F.; Monroe, D.M.; Church, F.C. Characterization of the glycosaminoglycan-binding region of Lactoferrin. *Arch. Biochem. Biophys.* **1995**, *317*, 85–92.
Wu, Y.; Guo, C.; Tang, L.; Hong, Z.; Zhou, J.; Dong, X.; Yin, H.; Xiao, Q.; Tang, Y.; Qu, X.; et al. Prolonged presence of SARS-CoV-2 viral RNA in faecal samples. *Lancet Gastroenterol. Hepatol.* **2020**, 5, 434–435.
Wyrick, P.B. Chlamydia trachomatis persistence in vitro: an overview. *J. Infect. Dis.* **2010**, 201(Suppl. 2): S88–S95.
Xia JJ, Wang F, Jiang XN, et al. Serum iron levels are an independent predictor of in-hospital mortality of critically ill patients: a retrospective, single-institution study. *J Int Med Res.* **2019**; 47: 66- 75.
Xiao, J.P.; Yin, Y.X.; Gao, Y.F.; Lau, S.; Shen, F.; Zhao, M.; Chen, Q. The increased maternal serum levels of IL-6 are associated with the severity and onset of preeclampsia. *Cytokine* **2012**, *60*, 856–860.
Xiong, T.-Y.; Redwood, S.; Prendergast, B.D.; Chen, M. Coronaviruses and the cardiovascular system: Acute and long-term implications. *Eur. Hear. J.* **2020**, 41, 1798–1800.
Xu, Z.; Shi, L.; Wang, Y.; Zhang, J.; Huang, L.; Zhang, C.; Liu, S.; Zhao, P.; Liu, H.; Zhu, L.; et al. Pathological findings of COVID-19 associated with acute respiratory distress syndrome. *Lancet Respir Med* **2020**, *8*, 420–422.
Yang, F.; Haile, D.J.; Wang, X.; Dailey, L.A.; Stonehuerner, J.G.; Ghio A.J. Apical location of ferroportin 1 in airway epithelia and its role in iron detoxification in the lung, *Am. J. Physiol., Lung Cell. Mol. Physiol.* **2005**, 289 L14–L23.
Yen, M.-H.; Chiu, C.-H.; Huang, Y.-C.; Lin, T.-Y. Effects of lactoferrin-containing formula in the prevention of enterovirus and rotavirus infection and impact on serum cytokine levels: a randomized trial. *Chang Gung Med J* **2011**, *34*, 395–402.
Yi, M.; Kaneko, S.; Yu, D.Y.; Murakami, S. Hepatitis C virus envelope proteins bind lactoferrin. *J. Virol.* **1997**, *71*, 5997–6002.
Yu, T.; Guo, C.; Wang, J.; Hao, P.; Sui, S.; Chen, X.; Zhang, R.; Wang, P.; Yu, G.; Zhang, L.; et al. Comprehensive characterization of the site-specific N-glycosylation of wild-type and recombinant human lactoferrin expressed in the milk of transgenic cloned cattle. *Glycobiology* **2011**, *21*, 206–224.

Zaim, M.; Piselli, L.; Fioravanti, P.; Kanony-Truc, C. Efficacy and tolerability of a prolonged release ferrous sulphate formulation in iron deficiency anaemia: A non-inferiority controlled trial. *Eur. J. Nutr.* **2012**, *51*, 221–229.

Zhang, H.; Li, H.-B.; Lyu, J.-R.; Lei, X.-M.; Li, W.; Wu, G.; Lyu, J.; Dai, Z.-M. Specific ACE2 expression in small intestinal enterocytes may cause gastrointestinal symptoms and injury after 2019-nCoV infection. *Int. J. Infect. Dis.* **2020**, 96, 19–24.

Zhang, H.; Shang, W.; Liu, Q.; Zhang, X.; Zheng, M.; Yue, M. Clinical characteristics of 194 cases of COVID-19 in Huanggang and Taian, China. *Infection* **2020**.

Zhang, Y.; Lima, C.F.; Rodrigues, L.R. Anticancer effects of lactoferrin: Underlying mechanisms and future trends in cancer therapy. *Nutr. Rev.* **2014**, *72*, 763–773.

Zhao K, Huang J, Dai D, Feng Y, Liu L, Nie S. Serum iron level as a potential predictor of coronavirus disease 2019 severity and mortality: a retrospective study. *Open Forum Infect Dis.* **2020**; 7: 1- 8.

Zumerle, S.; Mathieu, J.R.; Delga, S.; Heinis, M.; Viatte, L.; Vaulont, S.; Peyssonnaux, C. Targeted disruption of hepcidin in the liver recapitulates the hemochromatotic phenotype. *Blood* **2014**, *123*, 3646–3650.

Zwirzitz, A.; Reiter, M.; Skrabana, R.; Ohradanova-Repic, A.; Majdic, O.; Gutekova, M.; Cehlar, O.; Petrovčíková, E.; Kutejova, E.; Stanek, G.; et al. Lactoferrin is a natural inhibitor of plasminogen activation. *J. Biol. Chem.* **2018**, *293*, 8600–8613.